STRUCTURING GOLD NANOPARTICLES USING DNA: TOWARDS SMART NANOASSEMBLIES AND FACILE BIOSENSORS

By

WEIAN ZHAO

B. Sc., Shandong University, China, 2000
M. Sc., Shandong University, China, 2003

A Thesis
Submitted to the School of Graduate Studies
In Partial Fulfillment of the Requirements
For the Degree
Doctor of Philosophy

McMaster University

STRUCTURING GOLD NANOPARTICLES USING DNA: TOWARDS SMART NANOASSEMBLIES AND FACILE BIOSENSORS

DOCTOR IN PHILOSOPHY (2008) McMaster University
(Chemistry) Hamilton, Ontario

Title: Structuring gold nanoparticles using DNA: towards smart nanoassemblies and facile biosensors

AUTHOR: Weian Zhao, M. Sc., B. Sc. (Shandong University, China)

SUPERVISORS: Dr. Michael A. Brook, Dr. Yingfu Li

NUMBER OF PAGES: XIX, 152

Abstract

This thesis has exploited the use of gold nanoparticles (AuNPs)/DNA conjugates towards 1) the development of simple colorimetric assays to monitor DNA functions and relevant biological processes, and 2) the control the nanoassembly of AuNPs using biomolecules and biological processes.

DNA has a number of attractive functions including specific biorecognition, catalysis and being manipulated by protein enzymes, etc. These characteristics were exploited to permit nanoassembly to be responsive to a specific stimulus and also ensure the specificity and precision in the construction of well-defined 3D nanostructures. Meanwhile, the assembly or disassembly of AuNPs, which results in distinct color changes due to the localized surface plasmon resonance, provides an excellent platform for the colorimetrically monitoring the DNA functions and the relevant biological processes.

We have specifically investigated how the surface charges, the length and conformations of surface-tethered DNA polymers affect the assembly of AuNPs. We found that the colloidal stability of AuNPs can be well-tuned by nucleotides (small charged molecules) with various binding affinity to AuNP surface and/or different number of negatively-charged phosphate groups. This relies on the fact that nucleotides can bind to AuNP surface via nucleobase-Au interaction, and negatively charged phosphates stabilize AuNPs via electrostatic repulsion. This investigation allowed us to monitor protein enzymatic reactions where nucleotides are modified by alkaline phosphatase and to control the growth of AuNPs using nucleotides as capping ligands.

We then investigated the effect of the length of DNA polymers on AuNP surface on AuNP colloidal stability. DNA-modified AuNPs are stabilized electrosterically at a relatively high salt concentration; the removal (or shortening) of the DNA molecules by enzymatic cleavage or the dissociation of DNA aptamers from AuNP surface upon binding to their target destabilizes AuNPs and results in AuNP aggregation. We attribute this to the loss of negatively-charged polymeric DNA molecules that initially served as colloidal stabilizers. This has been applied to the monitoring of enzyme (both protein enzyme and DNA enzyme) cleavage of DNA molecules, and DNA aptamer binding event to its target, respectively.

We also studied how DNA polymer conformational changes influence AuNP colloidal stability, which has been employed to monitor DNA aptamer folding events on the AuNP surfaces. We found that AuNPs to which folded aptamer/target complexes are attached are more stable towards salt induced aggregation than those tethered to unfolded aptamers. Experimental results suggested that the folded aptamers were more extended on the surface than the unfolded (but largely collapsed) aptamers in salt solution. The folded aptamers therefore provide higher stabilization effect on AuNPs from both the electrostatic and steric stabilization points of view.

Finally, we demonstrated the well-defined assembly of AuNPs using long (hundred nanometers to microns) single-stranded (ss) DNA molecules as template in a three-dimensional (3D) fashion. Specifically, these long ssDNA containing repeating units are generated by protein enzymatic reaction (DNA extension through rolling circle amplification) on AuNP surface. The resultant product provides a 3D-like scaffold that can be subsequently used for periodical assembly of complementary DNA-attached nanospecies.

We also expect that the facile colorimetric biosensing assays developed in this thesis work provide an attractive means to study biomolecular behaviors (e.g, biorecognition and conformational changes) on the surface, and to investigate other common DNA (or RNA) structural (e.g., triplex, G-quadruplex, hairpin, i-motif) and protein structural transitions.

Finally, this thesis work provides some novel and general strategies for the control of nanoassemblies by tuning surface charges and surface-tethered polymers. We expect these principles can also be applied in other AuNP-based sensing platforms that exploit interparticle interactions and in the construction of well-defined nanostructures which involves other types of nano-scaled materials (e.g., quantum dots, nanotubes, nanowires, etc).

To Zhilin Jin

Acknowledgements

I would like to express my sincere gratitude to my supervisors Dr. Michael A. Brook and Dr. Yingfu Li. I have learned tremendously from them not only in science but in all aspects of life.

I would also like to thank the members of my supervisory committee, Dr. John D. Brennan and Dr. Alex Adronov for their constructive suggestions for my research.

Moreover, I would like to thank all the colleagues in Dr. Brook and Dr. Li labs. They not only provided me insightful scientific suggestions but also made my life at McMaster enjoyable. Furthermore, I would like to thank the Department of Chemistry for providing me such a great learning environment and to all my friends at McMaster for the wonderful time we had together.

最后， 我把最诚挚的感谢献给我的家人：我的父母，弟弟和妻子。他们的关怀和陪伴是我一生奋斗的动力。

Table of Content

List of Figures

Chapter 1

Chapter 2

Chapter 3

Chapter 4

Chapter 5

Chapter 6

Chapter 7

Chapter 8

List of Tables

Chapter 6

Abbreviations

1D (or 2D, 3D)	one-dimensional (or two-dimensional, three-dimensional)
ADA	adenosine deaminase
ADO	adenosine
ADP	adenosine 5'-diphosphate
AFM	atomic force microscopy
AMP	adenosine 5'-monophosphate
ATP	adenosine 5'-triphosphate
AuNPs	gold nanoparticles
CIAP	calf intestine alkaline phosphatase
CTP	cytidine 5'-triphosphate
DAPI	4',6'-diamidino-2-phenylindole
dATP	deoxyadenosine 5'-triphosphate
dCTP	deoxycytidine 5'-triphosphate
ddH_2O	de-ionized water
dGTP	deoxyduanosine 5'-triphosphate
DLS	dynamic light scattering
DNA	deoxyribonucleic acid
DNase I	deoxyribonuclease I
DNAzyme	DNA enzyme
dNTPs	dATP, dTTP, dGTP and dCTP
dsDNA	double-stranded DNA
DTT	dithiothreitol
dTTP	deoxythymidine 5'-triphosphate
EHNA	erythro-9-(2-hydroxy-3-nonyl)adenine
EDTA	ethylene diamine tetraacetic acid
FCC	face-centered cubic
FFT	fast Fourier transform

GTP	guanosine 5'-triphosphate
$HAuCl_4$	hydrogen tetrachloroaurate (III)
HRTEM	high resolution transmission electron microscopy
K_d	dissociation constant
LSPR	localized surface plasmon resonance
MCE	mercaptoethanol
MCH	mercaptohexanol
mRNA	messenger RNA
MS	mass spectroscopy
$NaBH_4$	sodium boron hydride
Na_3VO_4	sodium orthovanadate
nt	nucleotide
ϕ29DNAP	ϕ29 DNA polymerase
PAGE	polyacrylamide gel electrophoresis
PNK	T4 polynucleotide kinase
RCA	rolling circle amplification
RNA	ribonucleic acid
SELEX	systematic evolution of ligands by exponential enrichment
ssDNA	single-stranded DNA
TEM	transmission electron microscopy
TTP	thymidine 5'-triphosphate
XPS	X-ray photoelectron spectroscopy
XRD	X-ray diffraction

Chapter 1: Introduction

1.1 Nanotechnology and nanobiotechnology

"Nanotechnology" is the science and technology of manipulating matter at the molecular and atomic level.[1] Nanotechnology has at least three integrated domains: construction of nanostructured devices from the "bottom up" or "top down" with molecular and atomic precision, unique physical properties that are tunable by controlling nanostructure size and shape, and various applications ranging from nanoelectronics in modern computers to biosensors in living cells.

"Nanobiotechnology" refers to the construction and application of nanostructured devices at the interface between nanotechnology and biological systems.[1] Nanobiotechnology has become one major (which may become dominant in the future[2]) branch in nanotechnology. There are at least two major reasons for this: (1) biological systems can help nanotechnology to realize the *precise* assembly of nanosized building blocks, taking advantage of the specificity of bio-recognition; (2) nanobiotechnology can find tremendous applications in diagnostic and biomedical areas, which may have real impact for life-changing developments.

In the following review, we discuss the unique properties of gold nanoparticles (AuNP), and of DNA, in order to provide a basis of discussion for the main subject of this thesis: harnessing the assembly of AuNP by DNA to better understand biological processes and, in a complementary manner, using biological elements to structure AuNP.

1.2 AuNPs

The assembly of nanosized building blocks, including nanoparticles, nanotubes and nanowires, is the foundation of nanotechnology. We chose to examine routes to structuring AuNPs mainly because of their unique physical properties, easy preparation routes and straightforward surface functionalization strategies.[3] While the study of colloidal phenomena and physical properties of AuNPs is over a century old, the exploitation of them as building blocks and signal transducers in nanobiotechnology is

much more recent. This section provides a brief introduction of AuNP preparation, surface chemistry, physical properties and applications in nanobiotechnology.

1.2.1 AuNP preparation

AuNPs are generally prepared by reducing Au (III) in the presence of capping ligands (Figure 1.1 A).[3] Capping ligands, which generally comprise AuNP surface binding tags (e.g., thiols, amines, phosphines, etc) and protecting moieties (e.g., polymers, charged moieties, polyelectrolytes) (Figure 1.1 B), are key ingredients in AuNP growth recipes. They not only protect AuNP against aggregation during growth, but often also play important role in controlling the AuNP size and shape.[3]

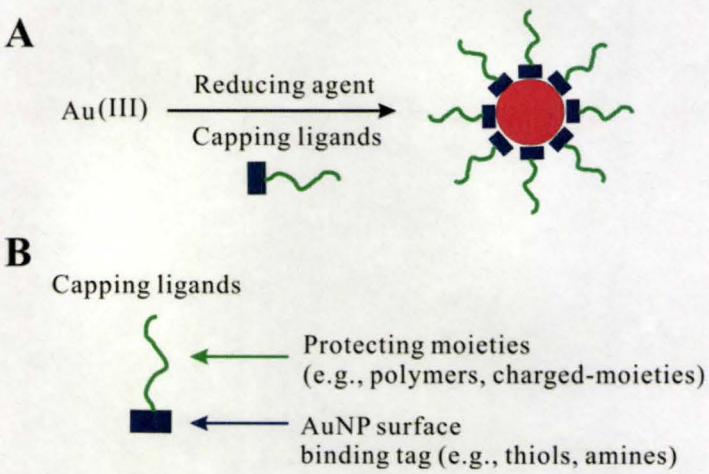

Figure 1.1 *(A) Schematic presentation of AuNP synthesis process, and (B) schematic structure of capping ligand used in the AuNP synthesis.*

One of the most popular routes for AuNP synthesis is the reduction of $HAuCl_4$ in water by trisodium citrate, which serves as both reducing agent and capping ligand.[4] The sizes of AuNP prepared by the citrate reduction approach can be tunable within the range of 10 – 150 nm by adjusting $HAuCl_4$/citrate molar ratio. The resultant citrate-capped AuNPs are stable in water at room temperature for a relatively long period of time (e.g., 6 months), but undergo rapid aggregation at elevated ionic strength (e.g., 50 mM NaCl)

where the surface charges carried by citrate ions are screened.[3] This may limit their direct use in biological applications, as salts are always included in assay buffers.

Another representative method for AuNP synthesis is the so-called "Brust-Schiffrin method".[5] It involves a two-phase (water-toluene) synthesis and uses alkanethiols as capping ligands to produce AuNPs with sizes between 1 – 5 nm. Briefly, $AuCl_4^-$ is transferred, using a phase-transfer reagent (e.g., tetraoctylammonium), from the water to toluene phase, where it is reduced by $NaBH_4$ in the presence of alkanethiol capping ligands such as dodecanethiol. The Brust-Schiffrin method provides a facile method for the preparation of highly monodisperse, thermally stabilized and (organic solvent) redispersible AuNPs. For biological applications, however, the AuNPs produced by this method may not be generally applicable because of the fact that these alkanethiol-capped AuNPs are generally not water-soluble or -dispersible. Furthermore, the use of organic solvents and organic capping ligands such as alkanethiols in this method is not environmentally friendly.

Therefore, there is a general need to develop "greener" or more environment- and bio-friendly routes for AuNP preparation. In particular, the resultant AuNPs should be water-soluble and stable at common salt-containing biological buffers for biological applications including biosensing, biolabeling and drug delivery. Towards this end, biomolecules such as amino acids have been applied as capping ligands in the preparation of AuNPs. For instance, AuNPs prepared using lysine as capping ligand are well-dispersed in water and stabilized electrostatically towards salt-induced aggregation.[6]

1.2.2 AuNP surface functionalization

Surface functionality can be introduced simultaneously during the AuNP synthesis step using, for example, functionalized thiols (Figure 1.2A), or by the subsequent surface functionalization steps.[3] Surface functionalization not only serves as a tool for altering such AuNP parameters as surface composition, stability, hydrophobicity and surface charge, and also provides surface functionalities for the subsequent reactions (or bio-recognition) towards specific applications.

Thanks to the strength and ease of formation of Au-S bonds, the adsorption of organosulfur molecules (thiols, disulfides, sulfides) on gold surfaces (both flat gold substrate and AuNPs) is probably the most straightforward surface functionalization technique available.[3] For AuNPs initially coated with a loose shell of ligands (e.g., citrate ions), organosulfur molecules can be spontaneously assembled onto AuNP surface, presumably accompanied with the displacement of citrate ions from the surface (Figure 1.2B).[3] For instance, thiol modified biomolecules such as DNA and proteins (with cysteine residues) can be conjugated to citrate-capped AuNPs through their thiol tags. For AuNPs initially capped by alkanethiols, functionalized organosulfur molecules can be introduced onto AuNP surfaces via a "ligand exchange" process (via displacement of one ligand by another) (Figure 1.2C).[3] This method is particularly useful to produce heterogeneous surfaces with different functionalities.

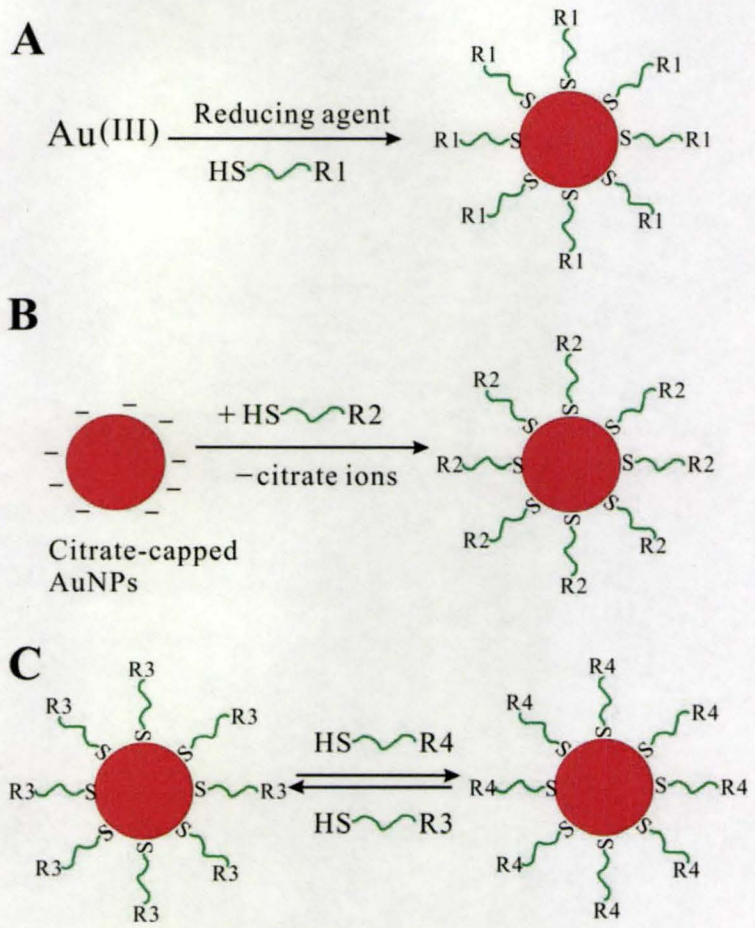

Figure 1.2. *Surface functionalization strategies of AuNPs. (A) Functionalities are introduced during AuNP preparation, (B) adsorption of thiol-containing molecules onto citrate-capped AuNPs, and (C) ligand exchange reaction using the displacement of one thiol-containing ligand for another. R1, R2, R3, R4 represent different functionalities.*

1.2.3 Physical properties: localized surface plasmon resonance

AuNPs have a number of fascinating physical properties including localized surface plasmon resonance (LSPR), fluorescence quenching and electronic properties.[3] We are particularly interested in the colors associated with LSPR due to the ability to use color change in applications such as colorimetric biosensors. Small AuNPs (normally 10-50 nm in diameter) in water or glass appear deep-red in color, a phenomenon that has fascinated people since ancient Roman times. The physical origin of this phenomenon is associated with the coherent oscillation of AuNP surface electrons (localized surface plasmon) induced by an incident electromagnetic field.[3] When visible light shines on AuNPs, the light of a resonant wavelength is absorbed by AuNPs to excite surface electron oscillation. For small AuNPs (e.g., 13 nm in diameter), green light is absorbed, corresponding to a strong absorption band (surface plasmon band) at ~ 520 nm in the visible light spectrum, and therefore AuNP solutions appear red in color (Figure 1.3, red line). As the AuNP size increases, the surface area/volume ratio, and thus the physical property-related surface effect, becomes smaller. Therefore, the energy required to excite surface electron oscillation is lower. Consequently, the surface plasmon band of larger AuNPs (e.g., 100 nm in diameter) undergoes a red-shift to longer wavelength at lower energy, and colloidal dispersions of such particles appear purple (or blue) in color.[3] This also explains the corresponding surface plasmon band shifts (red-shift) and color changes (red-to-purple) observed during aggregation processes of small AuNPs (Figure 1.3., blue line). When AuNPs aggregate, their surface plasmons combine (interparticle plasmon coupling), and the aggregates behave like single larger particles. The phenomenon that well-dispersed and aggregated AuNPs have different colors provides a great opportunity for the development of colorimetric biosensors (see Section 1.4.4).

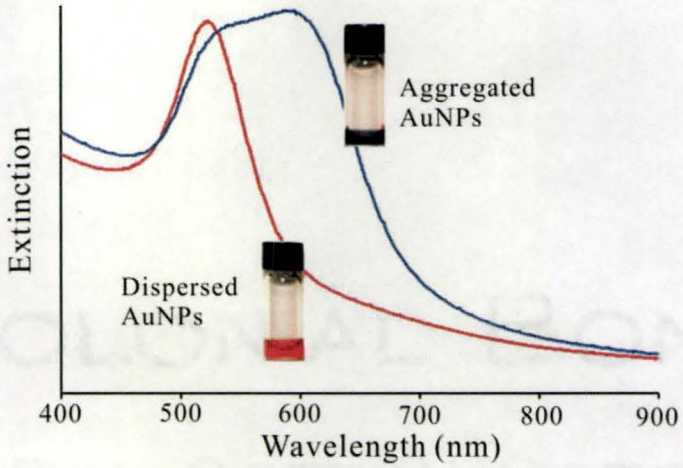

Figure 1.3. *SPB bands in the visible region and corresponding AuNP solutions for dispersed and aggregated AuNPs.*

1.2.4 Applications

AuNPs have a large variety of applications ranging from colloidal and surface chemistry, quantum physics, electronics and nonlinear optics, catalysis, to nanodevices and biology.[3,8,9] In nanobiotechnology, AuNPs are increasingly being applied for nanoassembly, biosensors, biolabeling and drug delivery, etc.[3,8,9] For instance, AuNPs are important building blocks towards the assembly of nano- (or micro-) devices. Of great interest is the programmable organization of AuNPs using biological "templates" such as DNA, protein and virus, etc.[3,8,9] With respect to biosensors, AuNPs can be adopted in a number of biosensing platforms which include colorimetric, light scattering, electrical and fluorescent biosensors.[3] Among these, the colorimetric sensors are particularly attractive due to 1) their simplicity, 2) the fact that the color signal can be observed by naked eye and therefore no sophisticated instruments are required, and 3) the extremely high extinction coefficients ($\geq$ 1000 times larger than those of organic dyes).[10] In 1997, Mirkin and co-workers pioneered the development of AuNP-based colorimetric biosensors for DNA detection (see Section 1.4.4).[11] Since then, similar assays have been developed for the detection of a variety of target analytes such as DNA, proteins, metal ions and small molecules.[8,9]

1.3 DNA and functional DNA

1.3.1 DNA and nucleotides

DNA is a biopolymer comprised of nucleotides (Figure 1.4, *left*) from constituents of nucleobase (Figure 1.4, *right*), sugar and phosphate groups. DNA is an anionic polymer at neutral pH due to negatively charged phosphate groups Nucleobases (adenine (A), thymine (T), guanine (G), cytosine(C)) are the recognition sites for DNA hybridization: the specific Watson-Crick hydrogen-bonding between nucleobases (A and T, G and C) and base-stacking interaction allow a single-stranded (ss) DNA to specifically recognize its "complementary strand" to form double-stranded (ds) DNA (or DNA duplex) (Figure 1.5).

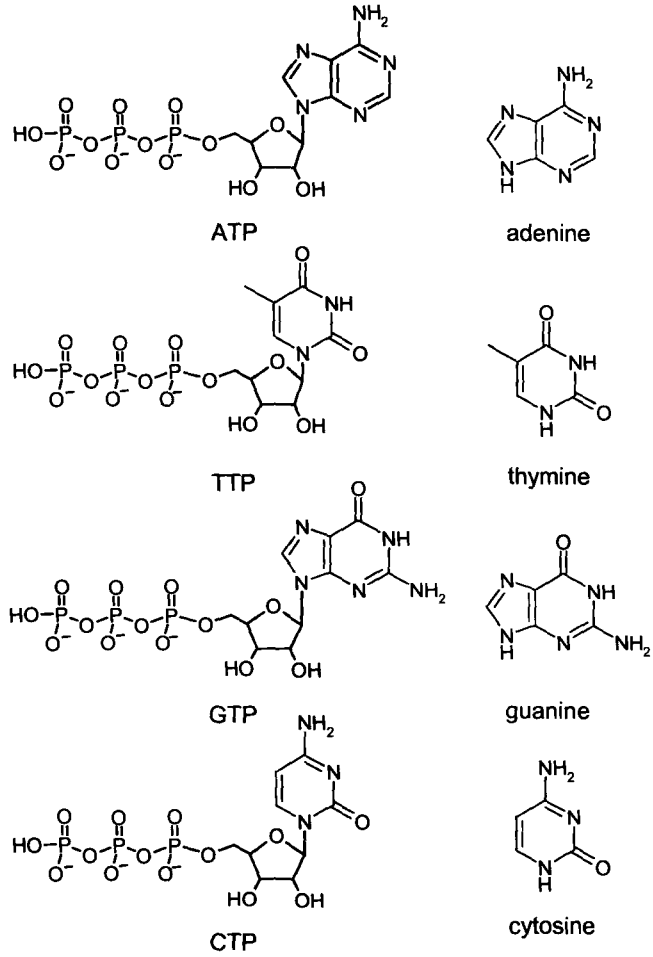

Figure 1.4. *Chemical structures of nucleotides (ATP: adenosine 5'-triphosphate, TTP: thymidine 5'-triphosphate, GTP: guanosine 5'-triphosphate, CTP: cytidine 5'-triphosphate) and nucleobases (adenine, thymine, guanine, cytosine) in DNA molecule.*

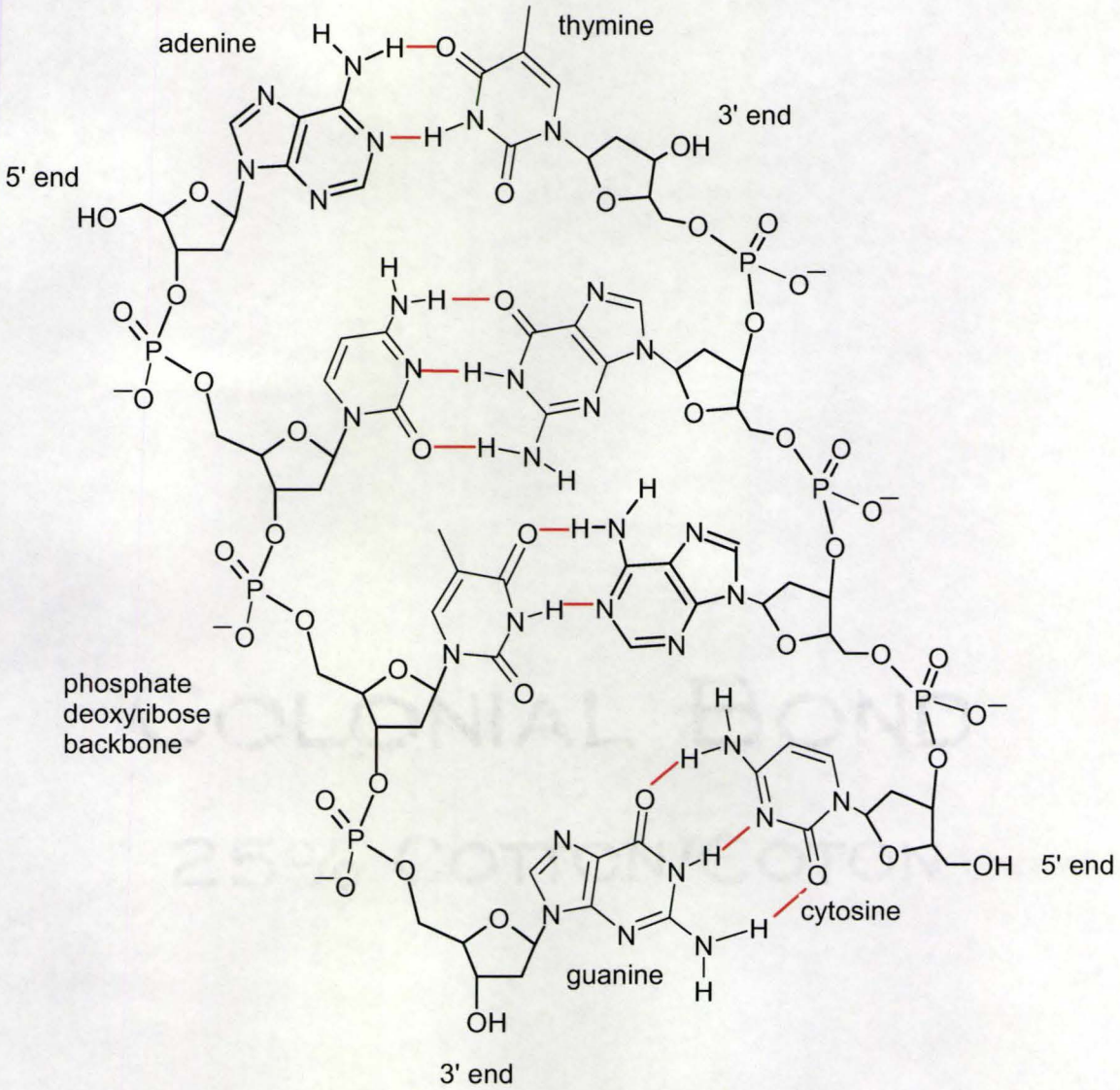

Figure 1.5. *Schematic illustration of DNA base-pairing. Red dashing lines represent hydrogen-bonding.*

DNA, a genetically encoded material, can be obtained *in vivo* through biosynthesis pathways. But for material scientist, short DNA polymers (or oligonucleotides) are more often synthesized chemically by DNA synthesizer. During

chemical synthesis, functional groups, such as thiols and amines, and other functionalities (e.g., fluorophores) can be introduced simultaneously. This provides great opportunities for DNA being manipulated as a "material" for *in vitro* applications such as surface-based bio-assays.

Enzymatic manipulation is another powerful tool for manipulating DNA molecules. For instance, DNA molecules can be cleaved, jointed, and extended by endonuclease, ligase, and polymerase, respectively (Figure 1.6). This, together with the specificity of DNA hybridization, its physicochemical stability and mechanical rigidity, makes DNA a highly suitable material that can be utilized as a building block in nanoassembly.[12] This so-called "DNA nanotechnology" employs DNA molecules as building blocks to construct well-organized nano- (or micro-) DNA structures which can further template the assembly of nanospecies to form more complex structures (Figure 1.7).[12,13]

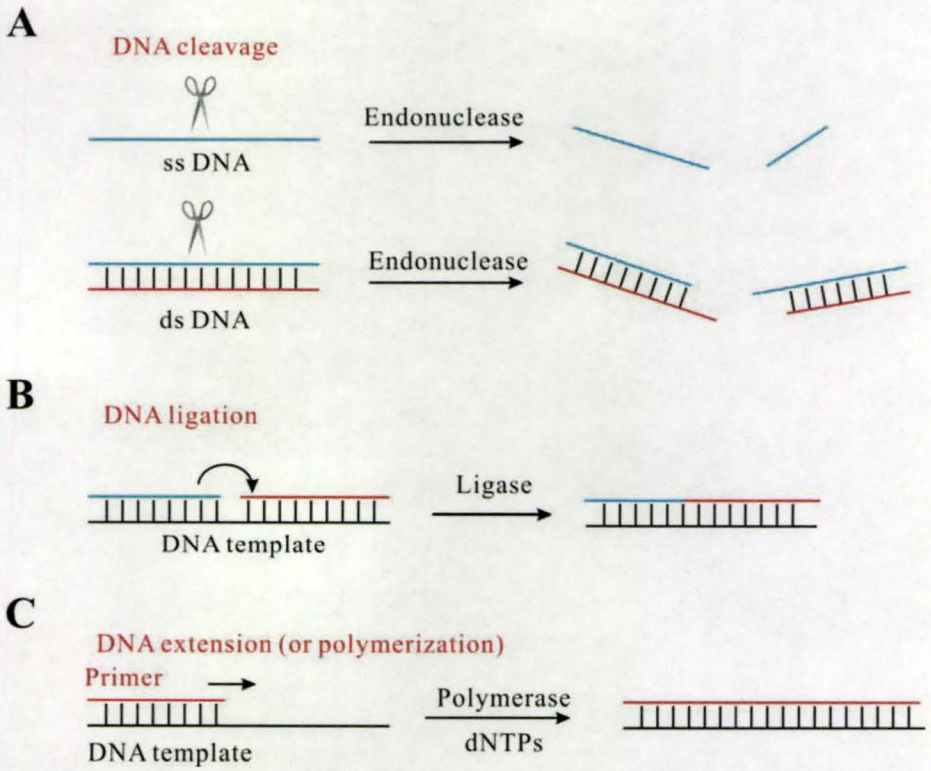

Figure 1.6. *Schematic representation of (A) DNA cleavage by endonuclease, (B) DNA ligation by DNA ligase, and (C) DNA extension by DNA polymerase in the presence of dNTPs (deoxynucleosides: dATP, dTTP, dGTP and dCTP), respectively.*

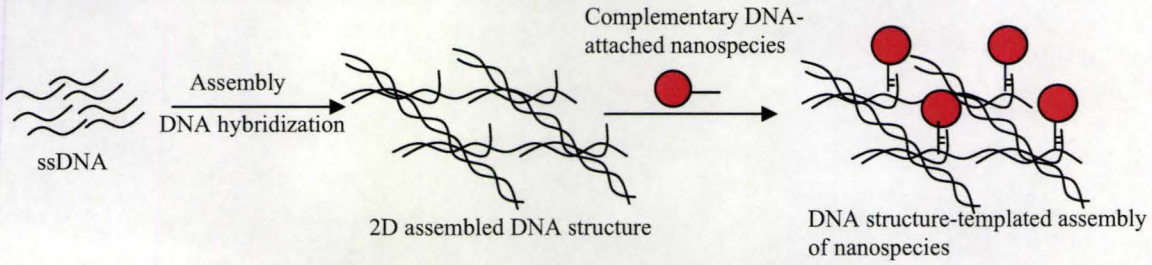

Figure 1.7. *A representative example in DNA nanotechnology: ssDNA are assembled via hybridization into a well-defined two-dimensional (2D) DNA nanostructure on which other nanospecies can be further assembled.*

1.3.2 Functional DNA

Recent years have also witnessed a dramatic increase of the study and use of DNA with certain "functions" other than hybridization with their complementary strands. Specifically, DNA can serve as a receptor (aptamer[14,15]) that recognizes non-nucleic acid targets such as proteins, small molecules and cells (Figure 1.8A), a process associated with aptamer conformational transition from loose random coil to rigid and compact structure. Some DNA molecules, defined as DNA enzymes,[14,15] also possess the capability of catalyzing chemical reactions such as the hydrolysis of phosphodiester bonds (Figure 1.8B). These functional nucleic acid molecules[15] exist *in vivo* and play significant roles in regulating biological functions such as gene expression.[14] Functional DNA can also be selected *in vitro* from a large random nucleic acid pool by SELEX (systematic evolution of ligands by exponential enrichment) (Figure 1.9).[16-18]

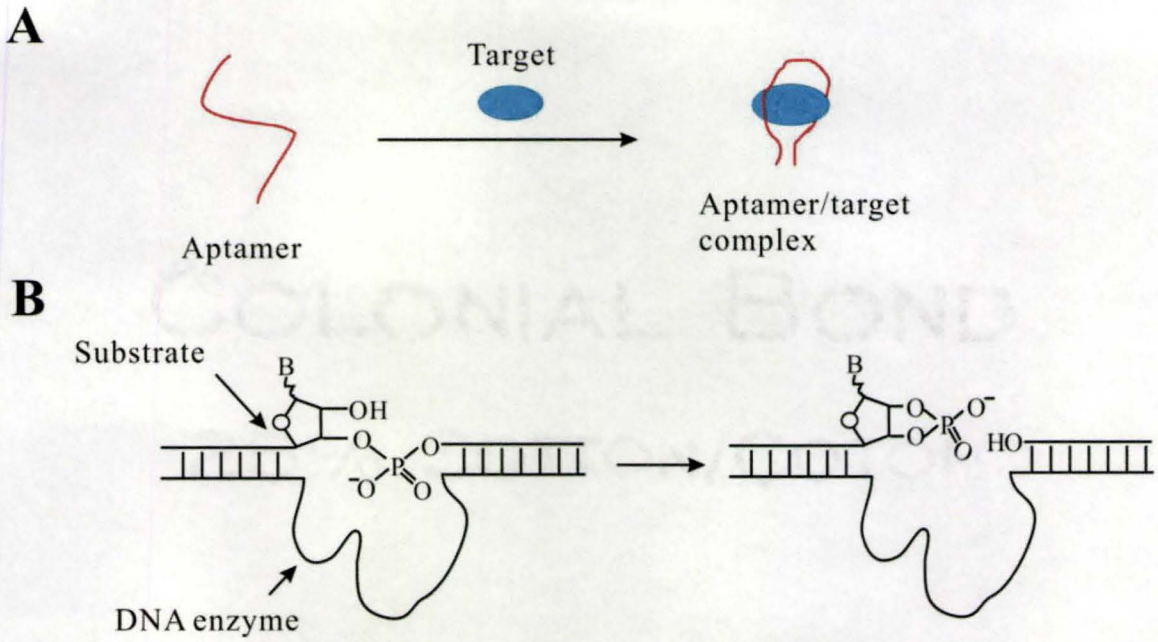

Figure 1.8. *Schematic illustration of (A) a DNA aptamer binds its target to form complex structure, and (B) DNA enzyme catalyzes a phosphodiester bond in a DNA substrate with a single RNA linkage (B represents a nucleobase).*

Since the development of the SELEX technique a decade ago, many funtional DNA have been identified and these molecules have demonstrated great potential of being used as drugs in therapeutics.[14] For example, a selected aptamer can bind to a protein and inhibit its activity *in vivo*.[14] DNA enzymes can regulate gene expression by cleaving a messenger RNA (mRNA).[14] Moreover, as a recognition element that can specifically bind to both its complementary DNA strand and non-nucleic target, DNA aptamers or enzymes can also be readily adopted into a variety of biosensing platforms.[15] For instance, Nutiu and Li previously developed a fluoresence-based ATP sensor based on a "structure-switching" aptamer (Figure 1.10A, see figure legend for detailed description).[19] Using a similar signal transducing mechanism, Lu and co-workers have applied DNA enzyme called "8-17" for Pb^{2+} detection (Figure 1.10B).[20]

Meanwhile, functional DNA has quickly become an important player in nanobiotechnology.[21] Taking advantage of its specific recognition nature, DNA aptamers, in conjugation with nanoparticles (e.g., polymers and quantum dots), have found great utility in biolabeling and drug delivery fields.[22] Function DNA can also be applied as

building blocks to control the assembly/disassembly of nanospecies. For instance, Liu and Lu have applied ATP aptamer or Pb^{2+}-mediated DNA enzyme (with its substrate) to assemble AuNP into aggregates that can be subsquently dissociated by the addition of ATP or Pb^{2+} (Figure 1.11).[23,24] Significantly, the color change associated with these processes can be used to detect the presence of ATP or Pb^{2+} (see Section 1.4.4 for more details).

In addition to the advantages shared with normal DNA, functional DNA is particularly attractive in nanobiotechnology due to the fact that species for many targets can be obtained by the powerful SELEX approach. With respect to biosensor applications, this greatly expands the detection scope of functional DNA-based assays. Also importantly, functional DNA that possess dual functions (target recognition and signal generation) can be directly selected by *in vitro* evolution,[25] which makes it possible that the obtained functional DNA function at their optimized performance for a specific task.

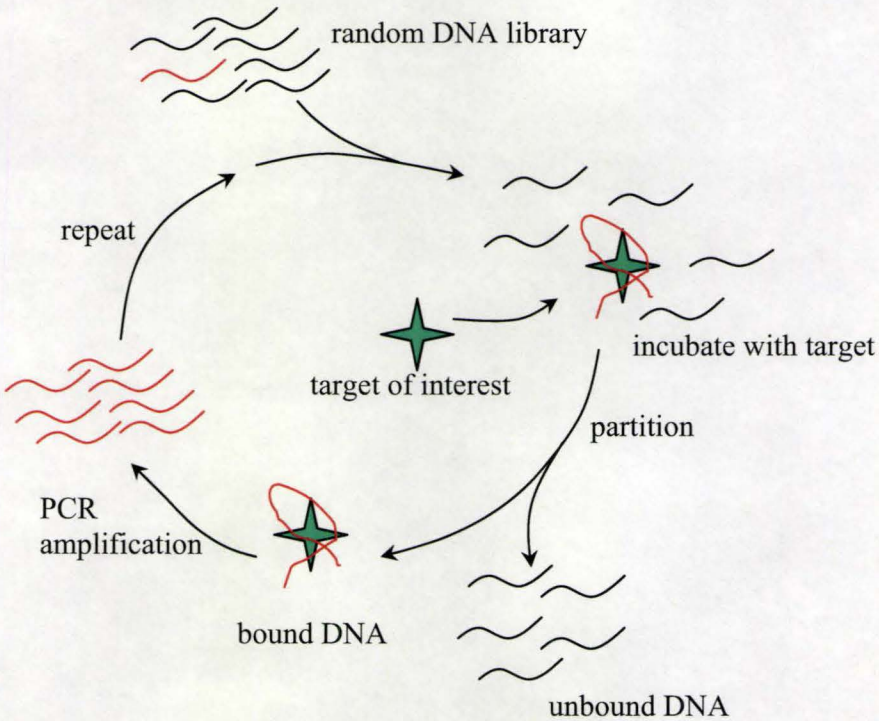

Figure 1.9. *Schematic illustration of in vitro selection of aptamer for a specific target using SELEX.*

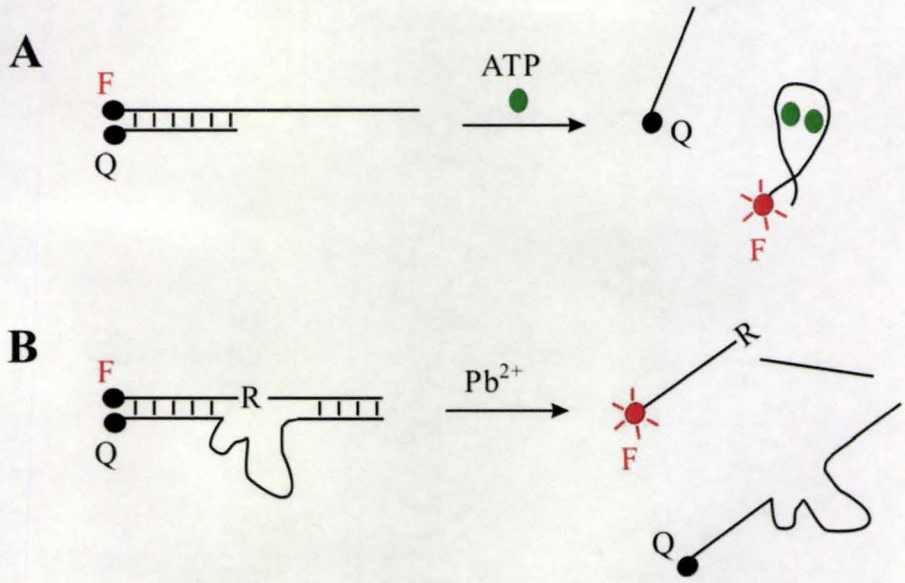

Figure 1.10. *Schematic presentation of fluorescence sensors using (A) ATP structure-switching aptamer[19] and (B) Pb^{2+} mediated DNA enzyme.[20] In both constructions, fluorophore (F) and quencher (Q) are initially at close proximity where fluorescence signal is significantly quenched. Upon addition of target (ATP or Pb^{2+}), the dissociation of aptamer (or DNA enzyme) with its complementary strand separate F and Q, which generates a fluorescence signal.*

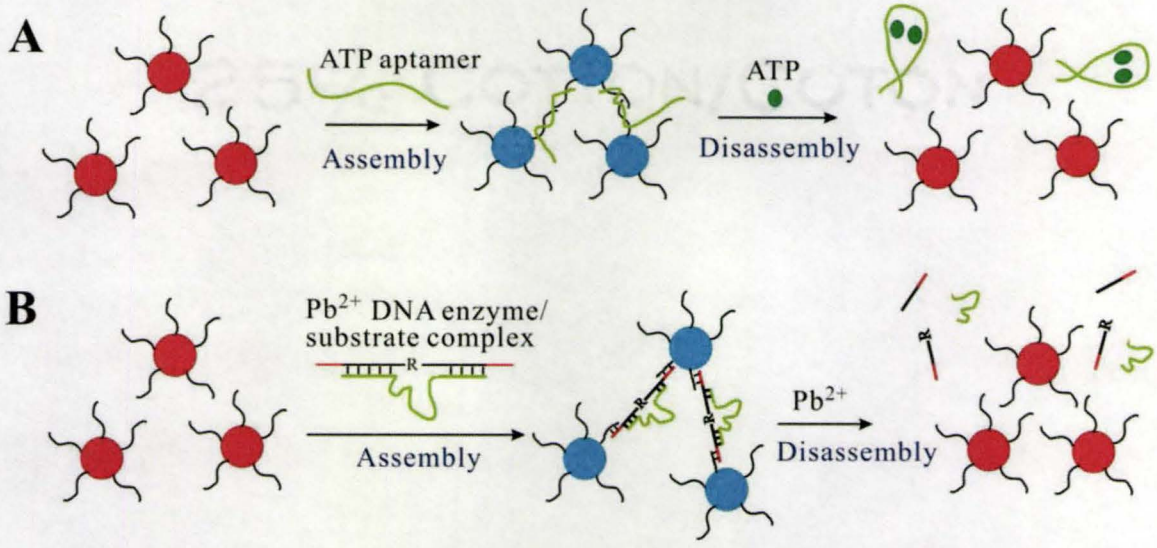

Figure 1.11. *Functional DNA (aptamer and DNA enzyme) is used for assembly and disassembly of AuNPs in the development of colorimetric biosensors. (A) ATP aptamer is used as crosslinker to bridge complementary DNA-modified AuNPs (assembly).[24] The addition of ATP causes the dissociation of aptamer from their complementary strands*

and therefore the disassembly of AuNP aggregates. (B) A similar strategy has been applied using a Pb^{2+} mediated DNA enzyme.[23] Here, the DNA enzyme and its hybridized DNA substrate serve as the crosslinker to assemble AuNPs. The addition of Pb^{2+} triggers the cleavage of substrate (crosslinker) by DNA enzyme, which results in the disassembly of AuNP aggregate. In both cases, a red-to-blue (or blue-to-red) color transition is associated with the AuNP assembly (or disassembly).

1.4 AuNP/DNA conjugates

It is not a surprise that AuNP and DNA have been married in nanobiotechnology. By their nature, AuNPs are highly suitable building blocks in nanoassemblies and signal-transducers for biosensors; DNA ensures the precision and specificity required by programmable nanoassemblies, biosensing and biolabeling. Indeed, AuNP/DNA conjugates have demonstrated great potential in the construction of well-organized nanostructures, colorimetric biosensors, *in vivo* biolabeling, drug discovery and delivery. This section provides a brief background of the preparation of AuNP/DNA conjugates, interactions between AuNP and DNA, their colloidal properties and applications with respect to nanoassembly and colorimetric biosensors.

1.4.1 Preparation of AuNP/DNA conjugates

AuNP/DNA conjugates are normally prepared using citrate-capped AuNPs and thiol-modified DNA based on Au-S chemistry.[3] Thiol-modified DNA is commercially available and is generally disulfide protected (e.g., DNA–S–S–C_6OH) to prevent dimerization between DNA molecules. The disulfide protected DNA can be used as such or reduced by, for example, dithiothreitol (DTT), to generate a free thiol group before being loaded onto a AuNP surface. Thiol-modified DNA can spontaneously assemble onto citrate-capped AuNP surface upon mixing (*Step one*, Figure 1.12), a process where a weakly bound ligand (citrate ion) is displaced by strongly binding ligand (thiol).[26] Note that de-ionized (dd) H_2O is normally used for the first step reaction and salt-containing buffer should be avoided as citrate-capped AuNPs are not stable at high ionic strength ($\geq$ 50 mM NaCl).[3] The number of DNA molecules on a AuNP surface (graft density) reaches its first plateau in a few hours and the further assembly becomes difficult due to

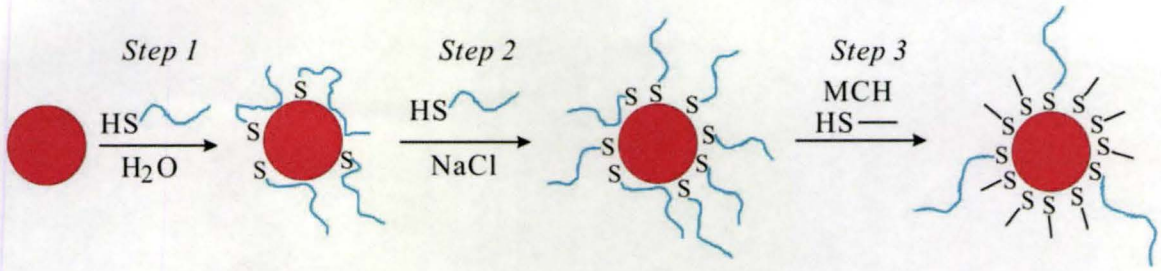

Figure 1.12. *The preparation of DNA-modified AuNPs. See main text in Section 1.4.1 for details.*

the electrostatic repulsion between negatively charged DNA molecules on AuNP surface and those in solution.[26] To minimize such electrostatic repulsion and load more DNA, a salt solution (e.g., 300 mM NaCl) is applied at this stage (*Step 2*, Figure 1.12), where the pre-loaded DNA molecules (negatively charged polymers) are sufficient to stabilize AuNP at salt solution via a combination of electrostatic and steric stabilization (see Section 1.4.3 for details). It is also interesting to note that the DNA conformation on the surface changes during the coupling reaction.[26,27] In *Step 1*, nucleobases on DNA backbone may "nonspecifically" adsorb onto AuNP surface via ligand-metal interaction (see Section 1.4.2 for more details) as there is much free space available on the surface. This makes DNA adopt a "flat conformation" on the AuNP surface and, consequently, less accessible for the subsequent biomolecular recognition.[26,27] In *Step 2*, the addition of salt facilitates the further loading of DNA, a process in which thiols on incoming DNA molecules break Au-nucleobase interaction by forming stronger Au-S interaction. Consequently, DNA adopts a more extended (into solution) conformation on AuNP surface.[26,27] The maximum DNA graft density for AuNPs of, for example, 13 nm in diameter is ~ 150 – 200 strands per AuNP. It was found, however, that not all DNA probes on the surface are equally accessible to hybridization with their complementary strands. Indeed, the typical hybridization efficiency is ~ 20 – 40 %.[28,29] This is presumably because the steric hindrance and electrostatic repulsion, resulting from neighboring DNA molecules, inhibit the DNA recognition with its complementary strand.[29] To improve the hybridization efficiency of DNA probe on AuNP surface, a

mercaptohexanol (MCH) treatment are often conducted (*Step 3*, Figure 1.12). MCH treatment is a ligand exchange process where MCH displaces the nonspecifically bound (e.g., via Au-nucleobase) and some of specifically bound (Au-S) DNA from AuNP surface.[28,29] As a result, 1) more DNA adopts the extended conformation on the surface, and 2) DNA surface graft density decreases, which reduces the repulsive effect from neighboring DNA molecules. Both of these effects make DNA more accessible to bind to its targets.[28,29] Indeed, the hybridization efficiency of DNA probes, after MCH treatment, can reach $\geq$ 90 %.[10] Note that MCH treatment can also be used to tune (or decrease) the colloidal stability of DNA-modified AuNPs (see Section 1.4.3) by removing negatively charged DNA molecules (colloidal stabilizers) from AuNPs.[10]

1.4.2 Interactions between AuNP and DNA (and nucleotides)

Apart from the Au-S interaction between thiol-modified DNA and AuNP, DNA (with and without thiol) can also interact with AuNP surfaces through Au-nucleobase interactions.[26,30,31] This was initially a surprise, particularly considering the electrostatic repulsive force between negatively-charged AuNP (due to citrate ions) and negatively-charged DNA backbone. It turned out that ssDNA can strongly adsorb onto AuNPs via the ligand-metal interactions between nucleobases (with amine and/or carbonyl groups) and AuNP surface.[26] The involvement of nucleobases in such process is demonstrated by the fact that dsDNA in which nucleobases are occupied by the complementary strand showed little affinity to AuNP surface.[32] The interactions between nucleobases and gold surfaces have been demonstrated by both qualitative and quantitative experiments.[30,31] However, the exact mechanism of nucleobase adsorption and the resulting geometry on AuNP surfaces remain largely unknown due to their complex nature.

"Nonspecific" binding was traditionally treated as a "serious issue" for surface-based bioassays due to the fact that nonspecifically adsorbed DNA probes become less accessible to their targets. However, this phenomenon has recently been applied for DNA immobilization[33] and biosensor development[32] (see Section 1.4.4 for details).

1.4.3 Colloidal chemistry of AuNP/DNA conjugates

AuNP colloidal properties such as stability and aggregation are key aspects in nanoassembly and biosensing applications of AuNPs and AuNP/DNA conjugates. This section briefly discusses the basics of colloidal stabilization and aggregation (Figure 1.13), particularly for DNA-modified AuNPs.

As-prepared AuNPs (Section 1.2.1) are often stabilized against van der Waals attraction induced aggregation by surface-tethered capping ligands. For instance, AuNPs prepared by the classic citrate reduction method[4] are stabilized in water by charged citrate ions on the surface. The stability of AuNPs can be further controlled to an exceptional degree by introducing colloidal stabilizers (see below) onto these as-prepared AuNPs via chemical grafting methods (e.g., Au-thiol, Au-amine), electrostatic adsorption and physical adsorption, etc. Common colloidal stabilizers include small charged species, polymers, and charged-polymers (polyelectrolytes) that stabilize the colloidal particles through electrostatic, steric, and electrosteric (a combination of electrostatic and steric) stabilizations, respectively (Figure 1.13A).

With respect to electrostatic stabilization (Figure 1.13A), the surface charges, together with the counterions in the medium, form a repulsive electric double layer that stabilizes colloids against van der Waals attractive forces.[36] A characteristic feature of the electrostatic repulsion force is its high sensitivity to the bulk ionic strength: the electrostatic repulsion force diminishes significantly at high salt concentration where the electric double layer is highly suppressed.[36] This explains why citrate-capped AuNPs are only stabilized in water but undergo aggregation at elevated salt concentrations (e.g. 50 mM NaCl).[3]

In the case of steric stabilization[36,37] (Figure 1.13A), macromolecules grafted on colloid surfaces in a good solvent (steric stabilization diminishes with decreasing solubility) impart a polymeric barrier that prevents colloids from coming close enough such for van der Waals attractive forces to dominate.[36,37] Essentially, the penetration of polymer chains on colloids when they approach each other results in a loss of polymer configurational entropy, which makes the aggregation process disfavored.[36,37] Steric

stabilization is much less sensitive towards ionic strength than electrostatic stabilization. Rather, the macromolecule molecular weight and surface graft density are more important factors. In general, thicker polymer layers and higher graft densities lead to more effective steric stabilization effecting.[36,37]

Electrosteric stabilization provided by surface-tethered charged polymers (Figure 1.13A) is probably the most effective strategy to stabilize colloidal particles.[36,37] DNA (negatively charged polymers)-modified AuNPs represent an excellent example of such systems. It is found that DNA-modified AuNPs with high DNA graft density remain stabilized even at very high salt concentrations (e.g., 300 mM $MgCl_2$). Steric stabilization is expected to play a major role in stabilizing AuNPs at such salt concentrations where electrostatic repulsion is significantly diminished.[36]

To aggregate DNA-modified AuNPs, one can use an "inter-particle crosslinking" mechanism (Figure 1.13B), where AuNPs are bridged together via a complementary DNA crosslinker taking advantage of DNA hybridization. The bonding formation in inter-particle crosslinking process yields an enthalpic benefit, which overcomes the electrostatic and steric repulsion forces.[36]

Alternatively, DNA-modified AuNP aggregation can be achieved by reducing electrostatic and steric repulsion forces through, for instance, the addition of salt or removal of charged and polymeric DNA moieties. The aggregation induced by such means is referred to as "non-crosslinking aggregation" (Figure 1.13B).[35,36]

Although the colloidal properties of DNA-modified AuNPs follow the general rules developed for polyelectrolyte-modified colloids, the real situation is much more complex due to the potential DNA inter- and intra-biomolecular interactions (e.g., hydrogen bonding). In particular, the effect of the molecular recognitions between AuNPs bound ssDNA molecules and their targets on the colloidal stabilities of AuNPs is difficult to predict.[35,36]

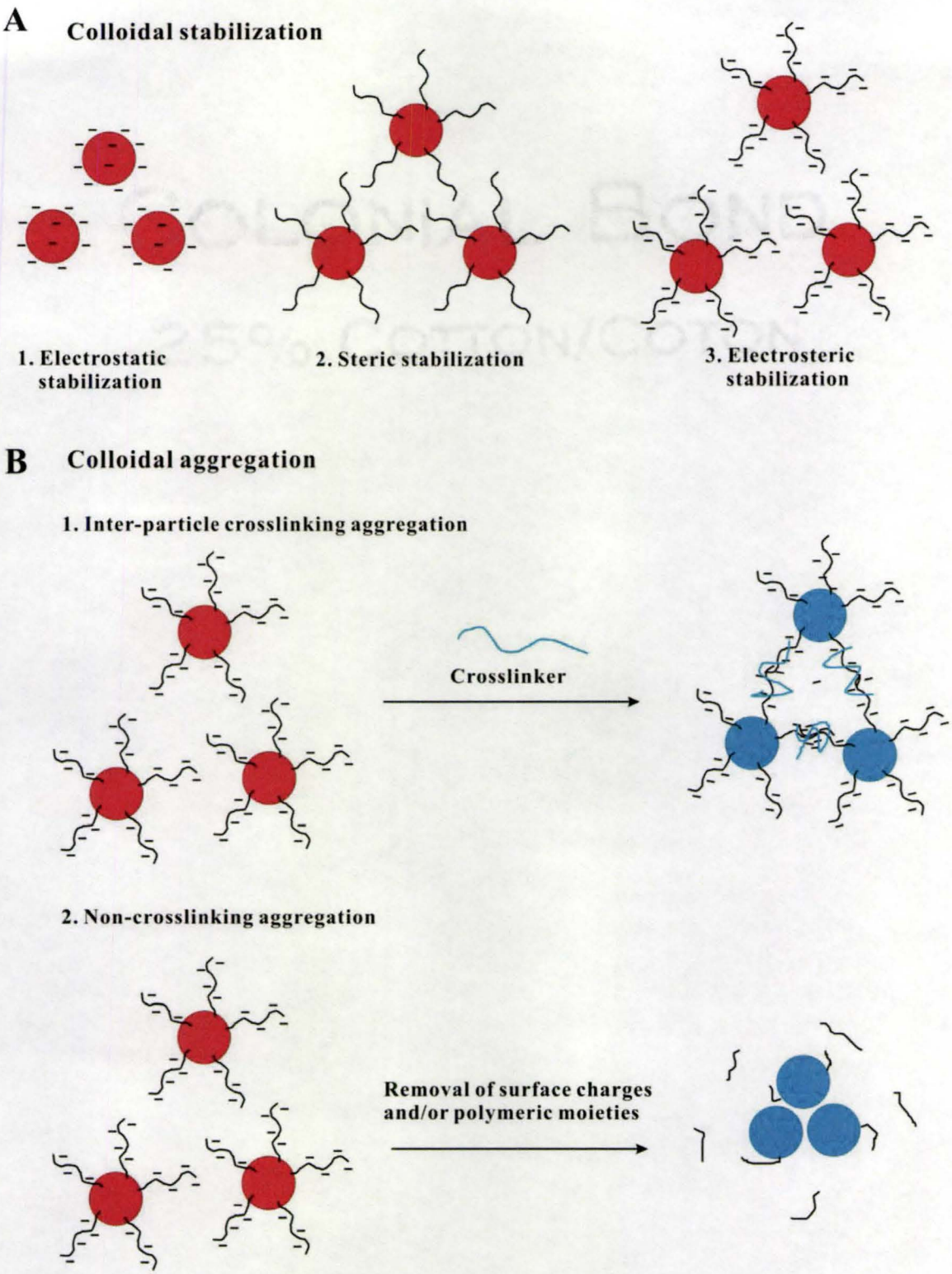

Figure 1.13. *Schematic representation of colloidal stabilization and aggregation. (A) colloids can be stabilized by 1. small charged molecules or ions, 2. surface grafted*

polymers, and 3 surface grafted charged polymers through electrostatic, steric and electrosteric stabilization, respectively. (B) Colloidal aggregation can be induced by 1. inter-particle crosslinking or 2. removing surface charges and/or polymeric moieties.

1.4.4 Applications of AuNP/DNA conjugates

The organization of DNA-modified AuNPs taking advantage of DNA hybridization (Figure 1.7) is one of the best examples to demonstrate the power and versatility of biomolecule-directed self-assembly. Indeed, DNA nanotechnology holds great potential for the programmable construction of future nanodevices.[12] Meanwhile, due to the unique LSPR of AuNPs, the assembly of such nanostructures has numerous applications in biosensors.[3,8]

As mentioned previously in Section 1.2.3, AuNP solutions appear as different colors in their dispersed and aggregated states. Therefore, colorimetric biosensors can be designed for the detection of biological events (or analytes) that trigger the aggregation of AuNPs (or redispersion of AuNP aggregate). Mirkin and co-workers pioneered the development of AuNP-based colorimetric biosensors.[11] In their work (Figure 1.14A), DNA-modified AuNPs are assembled into aggregates, accompanied by a red-to-blue color change, in the presence of the complementary DNA target. The redispersion of pre-formed AuNP aggregates, which leads to a blue-to-red color transition, can also be used for the design of colorimetric biosensors.[23,24] As shown in Figure 1.11, Liu and Lu have used this strategy to construct adenosine and Pb^{2+} sensors. Specifically, the AuNP aggregates were first prepared by crosslinking DNA-modified AuNPs using structure-switching DNA aptamers (or DNA enzyme substrate).[23,24] The addition of target adenosine molecules (or Pb^{2+}) removes crosslinkers by dissociating the aptamers (or cleaving DNA substrate), which results in the dispersion of aggregates and therefore a blue-to-red color change.[23,24]

The aggregation in these assays is essentially induced by the "inter-particle crosslinking (or bridging)" mechanism (Figure 1.13B) using DNA crosslinkers. Since Mirkin's pioneering work, biosensors using a similar aggregation mechanism have been developed for the detection of a variety of substances including DNA, protein, small

molecules and metal ions.[8,38,39] A conceivable drawback of inter-particle crosslinking aggregation is that a crosslinker (the target in many cases) is required to possess at least two binding sites in order to crosslink AuNPs. This may limit the generality of this assay. Moreover, for the inter-particle crosslinking of DNA-modified AuNPs with its complementary DNA crosslinker, it is known to be a relatively slow process: it generally requires a few hours (e.g., 2 h) to form the assembled aggregates.[11] Furthermore, the assays[23,24] where the AuNP aggregates are first prepared and then dissociated in the presence of target also suffers from 1) the extra steps required to form aggregates, 2) difficulties of handling unstable aggregates due to precipitation and potential dissociation, and 3) that the biomolecules embedded insides aggregates appear less accessible for the biomolecular recognition.[23,24]

In addition to inter-particle crosslinking, the colloidal aggregation can also be tuned by a number of other factors such as surface charges or surface-grafted polymers (Figure 1.13B, *non-crosslinking aggregation*).[36] This can also be applied as a highly useful tool to manipulate AuNP aggregation and to develop colorimetric biosensors. For instance, Maeda and co-workers found that ssDNA-modified AuNPs are more stable toward salt-induced aggregation than those after the hybridization of its complementary DNA strands (i.e., dsDNA-modified AuNPs) (Figure 1.14B).[35] While the precise mechanism was not fully understood, the authors attributed this to the entropic loss associated with the formation of a rigid DNA duplex. Moreover, Rothberg and colleagues have also developed AuNP-based colorimetric biosensor for DNA detection, taking advantage of the fact that ssDNA can adsorb onto citrate-capped AuNPs via Au-nucleobase interactions and stabilize AuNPs against salt-induced aggregation whereas dsDNA does not possess the same effect (Figure 1.14C).[32] In the "non-crosslinking aggregation" mechanism (Figure 1.13B), AuNP aggregation is driven by van der Waals attraction after interparticle repulsive forces (e.g., electrostatic and steric repulsion) are significantly diminished. Non-crosslinking aggregation has a few advantages over inter-particle crosslinking mechanism. First, it does not require the targets to have at least two binding sites in order to crosslink the AuNPs. Second, the aggregation induced by non-

crosslinking mechanism is very rapid (normally from seconds to a few minutes).[10,35] This is presumably due to the nature of non-crosslinking aggregation: once the inter-particle repulsive forces are significantly reduced, the attractive forces (van der Waals) dominate to result in rapid aggregation.[35] By contrast, in the inter-particle crosslinking system, the aggregation is mainly driven by random collisions between nanoparticles with relatively slow Brownian motion.[35] Third, compared with the biomolecules entrapped inside of the aggregates in the assays where the color change is based on the redispersion of AuNP aggregates, the biomolecules on AuNP surface in non-crosslinking aggregation systems are presumably more accessible for the bio-recognition events.[10] Nevertheless, in non-crosslinking aggregation systems, biomolecular interactions may not be performed at the optimized conditions (e.g., salt concentration) since a specific salt concentration is required to modulate the AuNP stability and aggregation.[10] Therefore, one may need to either choose a salt that has no effect on the biomolecular activity or seek a compromise between biomolecular performance and AuNP stability at a specific salt concentration.[10]

1.5 Summary and Challenges

AuNP/DNA conjugates have recently been a subject of great interest due mainly to its potential in the programmable assembly of well-defined nanostructures and colorimetric biosensors.

AuNPs with their unique physical properties are excellent building blocks for the construction of nano- (or micro-) structured materials. However, the precise and controllable assembly of AuNPs, particularly in response to a specific stimulus and/or in a periodic three-dimensional (3D) fashion, still remains a challenge. Most previous AuNP-based colorimetric bioassays use an inter-particle crosslinking aggregation mechanism; the assembly and disassembly of AuNPs by modulating AuNP colloidal properties (e.g., surface charges and surface-tethered polymers) in a non-crosslinking aggregation fashion have not been fully exploited.

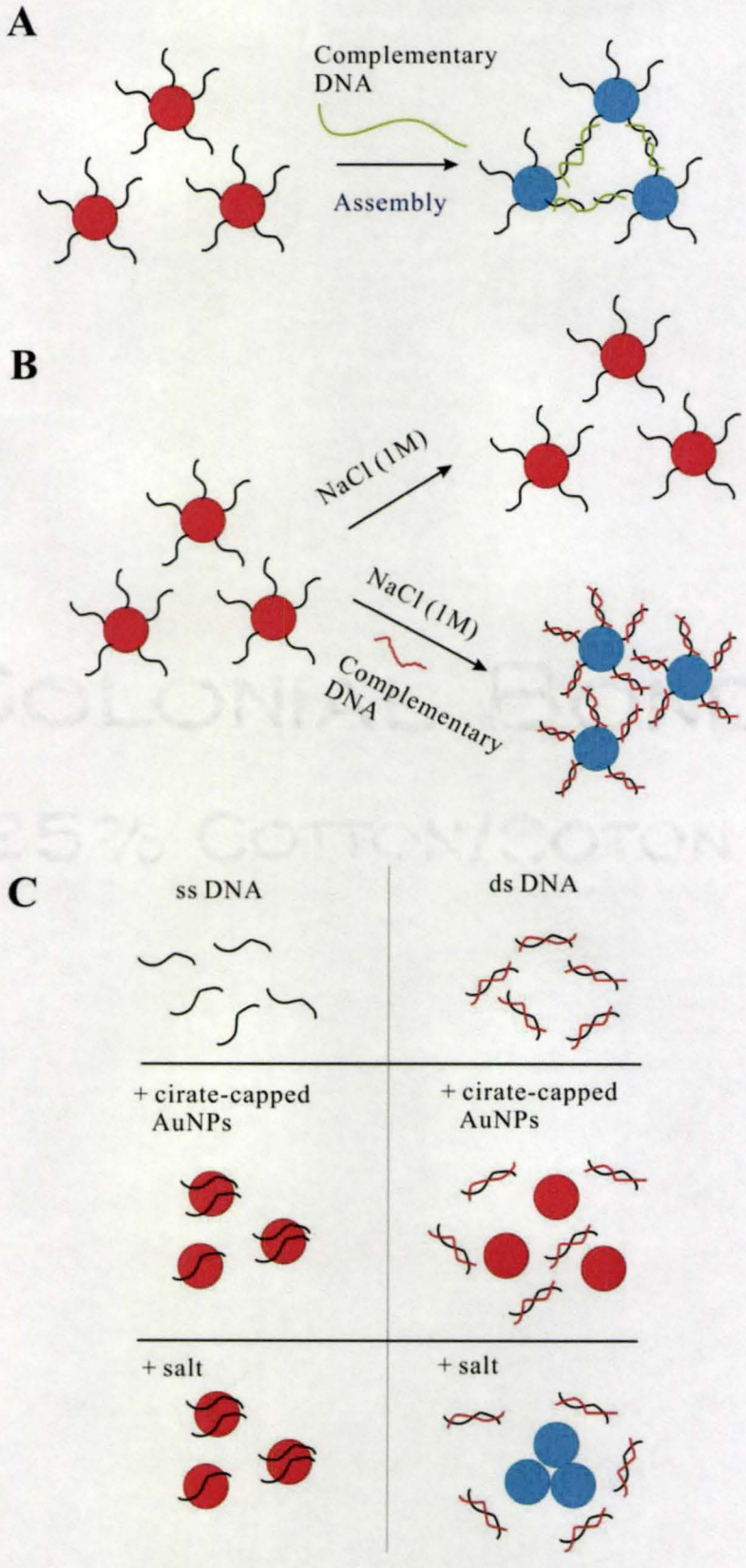
A
Complementary DNA
Assembly
B
NaCl (1M)
NaCl (1M)
Complementary DNA
C
ss DNA
ds DNA
+ cirate-capped AuNPs
+ cirate-capped AuNPs
+ salt
+ salt

Figure 1.14. *(A) Inter-particle crosslinking aggregation of DNA-modified AuNPs using a complementary DNA target that serves as a crosslinker. Red-to-blue color change indicates the presence of target DNA.*[11] *(B) ssDNA-modified AuNPs are stable at 1 M NaCl due to the stabilization provided by surface-grafted DNA molecules. By contrast, the formation of dsDNA by hybridization causes the decrease of AuNP colloidal stability towards salt-induced aggregation and a red-to-blue color change. This is presumably due to the entropic penalty resulted from the conformational transition from flexible ssDNA to rigid dsDNA.*[35] *(C) The design of colorimetric biosensors based on the different affinity of ssDNA and dsDNA on AuNP surface. ssDNA can bind to AuNP surface and stabilize AuNPs against salt-induced aggregation whereas dsDNA does not. This phenomenon has been applied to detect the complementary DNA target of a ssDNA.*[32]

DNA has multiple functions: DNA is widely known for its hybridization with the complementary strand, which has also been exploited as a tool to guide nanoassemblies. In particular, the fact that DNA molecules can be manipulated by a number of enzymatic reactions offers extra advantages of using DNA as a material. More recently, DNA molecules with novel functions have been discovered: DNA aptamers and enzymes can specifically recognize non-nucleic targets and catalyze chemical reactions, respectively. These functional DNA molecules largely extend the detection scope of DNA-based biosensors from targeting only nucleic acid targets to many other non-nucleic acid targets. Therefore, the development of facile method to monitor these DNA functions becomes important with respect both to understanding these functional DNA behaviors and developing biosensors standpoints.

Our hypothesis was that the combination of AuNP and DNA would benefit both sides towards the above-mentioned aspects: the color changes associated with AuNP assembly (or disassembly) can be used as a simple tool to monitor the DNA functions (e.g., DNA aptamer binding and folding, DNA enzyme catalysis), and DNA-involved biological processes (e.g., protein enzymatic manipulation of DNA molecules), which will eventually lead to the development of facile colorimetric biosensors; function DNA molecules which specifically recognize a target allow the DNA-guided nanoassembly to be responsive to a certain stimulus. Furthermore, the specificity of DNA recognition, together with the powerful enzymatic manipulation reactions, should offer opportunities to construct well-defined 3D nano-assembled structures.

1.6 Thesis objective and outline

The objective of this thesis work is therefore aimed to 1) develop facile colorimetric AuNP assays to monitor DNA function and DNA-involved biological processes, and simultaneously construct prototypes of biosensors. Specifically, the investigated functions and the relevant biological processes include DNA aptamer binding and folding upon complexing with its target, DNA enzyme catalysis and protein enzymatic manipulation of DNA molecules; 2) control the assembly of AuNPs using (functional) DNA towards stimuli-responsive assembly and construction of well-defined 3D structures. In particular, this is addressed by modulating AuNP colloidal parameters including surface charges, the length and conformations of surface-tethered DNA polymers. The thesis projects are outlined as follows.

Chapter 2: Simple and rapid colorimetric enzyme sensing assays using non-crosslinking gold nanoparticle aggregation. In this chapter, we investigated how the interaction of small nucleotide molecules, the DNA monomers, with citrate-capped AuNPs affects AuNP colloidal stabilities through tuning surface charge properties of AuNPs, and how that is applied to monitor enzymatic reactions where nucleotides are modified by protein enzymes.

Chapter 3: Highly stabilized nucleotide-capped small gold nanoparticles with tunable size. In this chapter, talking advantage of the fact that nucleotides can interact with AuNPs and then modulate AuNP colloidal stabilities, we exploited the use of nucleotides as capping ligands to control the growth of AuNP crystals. These nucleotide-capped AuNPs possess tunable sizes and have narrow monodispersities. Moreover, they are water-soluble and highly stable towards salt-induced aggregation.

Chapter 4: Enzymatic cleavage of nucleic acid on gold nanoparticle: a generic platform for facile biosensors. In this chapter, the AuNP colloidal stability and aggregation is tuned by the length of DNA polymers on AuNP surfaces: long DNA molecules stabilize AuNPs electrosterically whereas the removal (or shortening) of such polymers by enzymatic cleavage destabilizes AuNPs. This was applied to monitor DNA enzyme catalysis and protein enzyme manipulation reactions of DNA molecules.

Chapter 5: Simple and rapid colorimetric biosensors based on DNA aptamer and non-crosslinking gold nanoparticle aggregation. The controlled assembly of AuNPs by the length of surface-tethered DNA polymers was further exploited to monitor DNA aptamer binding to its target. Instead of removing DNA by enzymatic cleavage (chapter 4), the DNA aptamers are switched off from AuNP surface upon binding its target.

Chapter 6: DNA aptamer folding on gold nanoparticle: from colloid chemistry to biosensors. This work investigated the DNA aptamer folding with its target on AuNP surfaces, and how this polymer conformational change affects AuNP colloidal stability and aggregation. Strikingly, we discovered a unique colloidal stabilization effect associated with aptamer folding: AuNPs to which folded aptamer structures are attached are more stable towards salt induced aggregation than those tethered with unfolded aptamers. Therefore, distinct AuNP aggregation and redispersion stages can be readily operated by controlling aptamer folding and unfolding states. Meanwhile, this allows us to easily monitor DNA aptamer folding events on AuNP surfaces by the color changes arising from the different AuNP assembly stages.

Chapter 7: DNA polymerization on gold nanoparticles through rolling circle amplification: towards novel scaffolds for three-dimensional periodic nanoassemblies. This work attempted to control the nanoassembly in a well-defined 3D fashion. AuNPs attached with long (typically hundreds of nanometers to microns) DNA polymers containing repetitive units were obtained by performing an enzymatic extension reaction of a short DNA primer attached to the AuNP core. This 3D structure serves as a scaffold on which complementary DNA-attached nanospecies can be assembled periodically.

Chapter 8: Conclusions. This chapter summarizes the major achievements of this thesis.

Appendix: Ph.D. publication list.

1.7 References

(1) Vo-Dinh, Tuan. *Nanotechnology in Biology and Medicine: Methods, Devices, and Applications.* Abingdon : Taylor & Francis Ltd, **2007**.

(2) Ritchie, R. *Materials today*, **2005**, 8, 72.

(3) Daniel, M.-C.; Astruc, D. *Chem. Rev.* **2004**, 104, 293.

(4) Turkevitch, J.; Stevenson, P. C.; Hillier, J. *Discuss. Faraday Soc.* **1951**, *11*, 55.

(5) Brust, M.; Walker, M.; Bethell, D.; Schiffrin, D. J.; Whyman, R. J. *J. Chem. Soc., Chem. Commun.* **1994**, 801.

(6) Selvakannan, P.; Mandal, S.; Phadtare, S.; Pasricha, R.; Sastry, R. *Langmuir*, **2003,** 19, 3545.

(7) Mie, G. *Ann. Phys.* **1908**, 25, 377.

(8) Rosi, N. L.; Mirkin, C. A. *Chem. Rev.* **2005**, *105*, 1547.

(9) Günter, S. *Nanoparticles: from theory to application.* Weinheim : Wiley-VCH, c**2004**.

(10) Zhao, W.; Chiuman, W.; Brook, M. A.; Li, Y. *ChemBioChem* **2007**, *8*, 727.

(11) Elghanian, R.; Storhoff, J. J.; Mucic, R. C.; Letsinger, R. L.; Mirkin, C. A. *Science* **1997**, *277*, 1078.

(12) Seeman, N. C. *Trends. Biotechnol.* **1999**, *17*, 437.

(13) Pinto, Y. Y.; Le, J. D.; Seeman, N. C.; Musier-Forsyth, K.; Taton, T. A.; Kiehl, R. A. *Nano Lett.* **2005**, *5*, 2399.

(14) Eckstein F. *Expert Opin Biol Ther.* **2007,** 7, 1021.

(15) Navani, N. K.; Li, Y. *Curr. Opin. Chem. Biol.* **2006**, *10*, 272.

(16) Ellington, A. D.; Szostak, J. W. *Nature* **1990**, 346, 818.

(17) Joyce, G. F. *Gene*, **1989**, 82, 83.

(18) Tuerk, C.; Gold, L. *Science* **1990**, 249, 505.

(19) Nutiu, R.; Li, Y. *J. Am. Chem. Soc.* **2003**, *125*, 4771.

(20) Liu, J.; Lu, Y. *J. Am. Chem. Soc.* **2000**, 122**,** 10466.

(21) Famulok, M.; Mayer, G. *Nature* **2006**, 439, 666.

(22) Farokhzad, O. C.; Karp, J. M.; Langer, R. *Expert. Opin. Drug. Deliv.* **2006,** 3, 311.

(23) Liu, J.; Lu, Y. *J. Am. Chem. Soc.*, **2005**, 127**,** 12677.

(24) Liu, J.; Lu, Y. *Angew. Chem. Int. Ed.* **2006**, 45**,** 90.

(25) Nutiu, R.; Li, Y. *Angew. Chem. Int. Ed.* **2005**, 44, 5464.

(26) Storhoff, J. J.; Elghanian, R.; Mirkin, C. A.; Letsinger, R. L. *Langmuir,* **2002**, 18, 6666.

(27) Parak, W. J.; Pellegrino, T.; Micheel, C. M.; Gerion, D.; Williams, S. C.; Alivisatos, A. P. *Nano Lett.* **2003**, 3, 33.

(28) Park, S.; Brown, K. A.; Hamad-Schifferli, K. *Nano Lett.* **2004**, 4, 1925.

(29) Huang, E.; Satjapipat, M.; Han, S.; Zhou, F. *Langmuir*, **2001**, 17, 1215.

(30) Ostblom, M.; Liedberg, B.; Demers, L. M.; Mirkin, C. A. *J. Phys. Chem. B.* **2005**, 109, 15150.

(31) Kimura-Suda, H.; Petrovykh, D. Y.; Tarlov, M. J.; Whitman, L. J. *J. Am. Chem. Soc.* **2003**, 125, 9014.

(32) Li, H.; Rothberg, L. *Proc. Natl. Acad. Sci. USA* **2004**, 101, 14036.

(33) Opdahl, A.; Petrovykh, D. Y.; Kimura-Suda, H.; Tarlov, M. J.; Whitman, L. J. *Proc. Natl. Acad. Sci. USA* **2007**, 104, 9.

(34) Zheng, M.; Jagota, A.; Strano, M. S.; Santos, A. P.; Barone, P.; Chou, S. G.; Diner, B. A.; Dresselhaus, M. S.; McLean, R. S.; Onoa, G. B.; Samsonidze, G. G.; Semke, E. D.; Usrey, M.; Walls, D. J. *Science*, **2003**, 302, 1545.

(35) Sato, K.; Hosokawa, K.; Maeda, M. *J. Am. Chem. Soc.* **2003**, *125*, 8102.

(36) Zhao, W.; Chiuman, W.; Lam, J. C. F.; McManus, S. A.; Chen, W.; Cui, Y.; Pelton, R.; Brook, M. A.; Li, Y. *J. Am. Chem. Soc.*, **2008**, *130*, 3610.

(37) Napper, D. H. *Polymeric stabilization of collodial dispersions*; Academic Press: London, **1983**.

(38) Liu, J.; Lu, Y. *Acc. Chem. Res.* **2007**, 40, 315.

(39) Katz, E.; Willner, I. *Angew. Chem. Int. Ed.* **2004**, *43*, 6042.

Chapter 2: Simple and rapid colorimetric enzyme sensing assays using non-crosslinking gold nanoparticle aggregation

The following chapter was published in Chemical Communications under the citation:

Weian Zhao, William Chiuman, Jeffrey C. F. Lam, Michael A. Brook, Yingfu Li. Simple and rapid colorimetric enzyme sensing assays using non-crosslinking gold nanoparticle aggregation. *Chem. Commun.*, 2007, 3729-3711.

I was responsible for all data collection and analysis. William Chiuman provided helpful suggestions on enzyme assays and helped with the calculation of the enzymatic reaction rate. Jeffrey C. F. Lam helped in the UV-Visible spectroscopy experiments. I wrote the first draft of the manuscript and Dr. Brook and Dr. Li provided editorial input to generate the final draft of the paper.

2.1 Abstract

Non-crosslinking gold nanoparticle (AuNP) aggregation induced by the loss (or screen) of surface charges is applied for enzymatic activity sensing and potentially inhibitor screening.

2.2 Introduction

AuNP-based colorimetric assay has been recently used for the detection of various substances,[1] based on the unique phenomenon that well-dispersed AuNP solution is red in color whereas aggregated AuNPs appear a blue (or purple) color.[2] The major advantage of AuNP-based assays is that molecular recognition events can be transformed into color changes, which can be observed by the naked eye, and therefore no sophisticated instruments are required.[1] Moreover, because of the extremely high extinction coefficients of AuNPs, AuNP-based assays could provide sensitivity comparable to (or even higher than) conventional analytical methods such as fluorescence assays.[1b] Mirkin and co-workers pioneered the study of AuNP-based colorimetric biosensors where they used oligonucleotide-modified AuNPs to detect a target complementary DNA molecule.[1a] Recently, AuNP-based assays have also been applied for the detection of other targets such as metal ions,[1b] proteins,[1d–i] and small molecules.[1j] The sensing of enzymatic activity and study of enzyme inhibitor using AuNP-based assay have also been developed.[3–5] For instance, Brust and co-workers developed an elegant assay to identify kinase inhibitors taking advantage of the fact that kinase modified AuNP can undergo inter-particle crosslinking to form aggregates and therefore generate a red-to-blue color change.[3a] Guarise and coworkers demonstrated that a short peptide, which contains a cysteine group at both ends, can effectively crosslink AuNP leading to AuNP aggregation.[4] They then developed an assay to detect protease that can cleave that peptide. Most recently, Choi and coworkers extended this concept to a phosphate group containing peptide substrate.[5] They showed that the substrate charge properties, controlled by a phosphatase, can affect the peptide crosslinking of AuNP, and thus the AuNP aggregation and color change.[5]

In all aforementioned assays, AuNP aggregation is induced by inter-particle crosslinking such as DNA hybridization,[1a,b] antibody-antigen interactions,[1e] and peptide bridging with two binding tags.[4,5] However, this crosslinking AuNP aggregation is limited to the use of crosslinkers that possess at least two binding tags in order to bridge AuNP together. To meet this criterion, the crosslinkers (e.g. peptide with two binding tags to AuNP) sometimes have to be carefully designed and synthsized.[5,6] Moreover, AuNP aggregation induced by inter-particle crosslinking is a relatively slow process: it sometimes takes a few hours to observe the aggregation-induced color change.[1a]

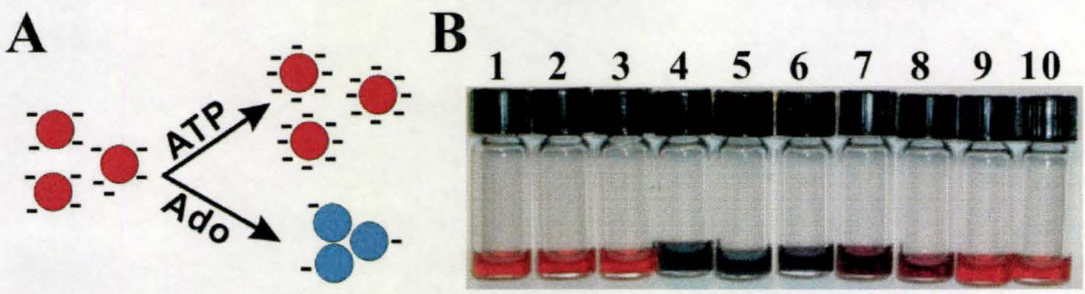

Figure. 2.1. *(A) Schematic illustration of the differential impact of ATP and adenosine (Ado) on AuNP stability. (B) Photographs of AuNP solutions containing 60 μM ATP, ADP, AMP, inosine, and adenosine (vials 1-5, respectively). Vial 6-10 are the AuNP solutions containing 30, 20, 10, 5, and 2.5 μM adenosine, respectively. Photographs were taken 1 min after mixing AuNP with a relevant compound.*

It is well known that colloidal stability can also be adjusted by modifying surface charges which affect electrostatic stabilization, and that aggregation can be induced due to the loss (or screening) of surface charges.[7] In this communication we exploited this "noncrosslinking" aggregation phenomenon[8] to develop colorimetric assays for sensing enzymatic activities. We speculate that if the substrate and product of an enzymatic reaction differently affect the AuNP stability by changing their electrophoretic properties, such a reaction can be monitored colorimetrically using AuNPs and the enzymatic activity can therefore be determined.

Enzymatic reactions concerning nucleoside triphosphates as substrates, specifically nucleotide dephosphorylation by alkaline phosphatase and DNA polymerization by DNA polymerase, were chosen as model systems due to their vital

importance in molecular biology.[9] It is known that nucleobases can bind to citrate-capped AuNPs with the displacement of weakly bound citrate ions via metal–ligand interactions.[10] The adsorption of highly charged nucleotides or uncharged nucleosides should then further stabilize AuNPs or cause their aggregation, respectively, due to the gain or loss of surface charges (Fig. 2.1(A)). We found that the AuNPs capped by adenosine 5'-triphosphate (ATP), adenosine 5'-diphosphate (ADP), or adenosine 5'-monophosphate (AMP) were much more stable than bare AuNP (see Supplementary Information (SI)). The stability of AuNPs followed the order AuNP/ATP > AuNP/ADP > AuNP/AMP > bare AuNP. This is further confirmed by surface charge measurements: the zeta potentials of ATP-adsorbed AuNPs and bare AuNPs are -32.36 ± 1.43 mV and -24.98 ± 1.54 mV, respectively. This clearly illustrates the direct relationship between the concentration of negatively charged phosphates on AuNP surface and colloidal stability. In contrast, the adsorption of uncharged nucleosides (e.g. adenosine and inosine) caused AuNP aggregation, indicated by an instant red-to-blue color change (Fig. 2.1(B)).

We then sought to take advantage of the observed noncrosslinking AuNP aggregation phenomenon to develop a simple colorimetric assay for monitoring an enzymatic dephosphorylation reaction where ATP was converted into adenosine by calf intestine alkaline phosphatase (CIAP) (Fig. 2.2(A)). The development of simple, quick and inexpensive assays to monitor dephosphorylation or phosphorylation reactions is technically challenging because the loss or gain of nucleotide phosphate group(s) cannot be easily distinguished by conventional spectroscopic methods. For instance, the substrate (ATP) and the product (adenosine) in CIAP-mediated dephosphorylation reactions have essentially identical absorption spectra (see SI, Fig. S2.2(A)).

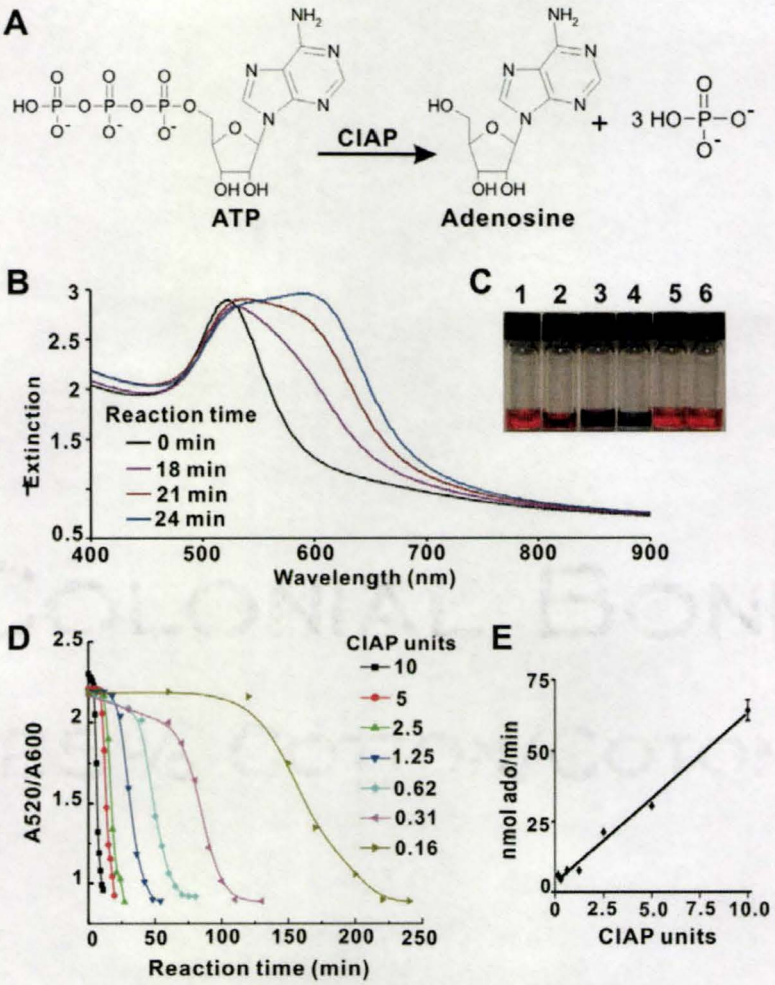

Figure. 2.2*. (A) Conversion of ATP into adenosine by CIAP. (B) UV-Vis spectra of AuNP solutions after addition of ATP-CIAP mixture incubated at indicated time points. (C) Photographs of AuNP solutions after addition of ATP-CIAP mixture incubated for 0, 18, 21 and 24 min (vials 1-4, respectively). Vials 5 and 6 were the AuNP solutions with addition of the mixture (incubated for 24 min) where ATP or CIAP was omitted, respectively. This control experiment showed that CIAP itself does not cause AuNP aggregation.[13] (D) A520/A600 vs. enzymatic reaction time for the indicated CIAP concentrations. (E) The amount of substrate processed per minute vs. CIAP concentration (units/20 μL reaction solution).*

2.3 Results and discussion

In our AuNP-based assay, a typical reaction mixture (20-μL) containing 10 mM ATP, 10 mM $MgCl_2$, 10 mM Tris-HCl (pH 7.5), and 2.5 units (~ 250 nM) of CIAP. To monitor the reaction, 1 μL of the mixture was taken out at a given reaction time, diluted

100 times by H_2O,[11] and then added to 200 μL AuNP solution (14 nM). The UV-Vis adsorption spectra were recorded 1 min after mixing. As expected, with the increase of reaction time, the adsorption of the mixture (originally peaked at ~ 520 nm) broadened and shifted to longer wavelength (Fig. 2.2(B)), while the color of the solution changed progressively from red to blue (Fig. 2.2(C)), indicating the AuNP aggregation during the conversion of ATP to adenosine.

To estimate the percentage of ATP converted, a calibration curve relating the ratio of A520/A600 as a function of ATP/adenosine molar ratio (in the absence of CIAP) was developed (see SI, Fig. S2.3). By fitting the A520/A600 value calculated from Fig. 2.2(B) at a certain reaction time, one can easily estimate how far the reaction has progressed.

To quantify the enzyme activities, reactions with various amounts of CIAP were performed and the adsorption spectra are given in Fig. S2.4 in SI. The A520/A600 ratios as a function of enzymatic reaction time are plotted in Fig. 2.2(D); the amount of substrate processed per minute (see SI for calculations) as a function of CIAP units is shown in Fig. 2.2(E). A linear relationship was obtained, which strongly suggests that this assay can be applied to quantify the effective enzyme activities. The typical detection limit of CIAP in the current study is ~ 0.16 units/20 μL (~ 16 nM).[12]

Notably, this assay can be further used to study enzyme inhibitors. Sodium orthovanadate (Na_3VO_4), a well known inhibitor for CIAP,[14] is used in our proof-of-concept experiment. It was found that 2 mM of Na_3VO_4 (note that, under investigated conditions, Na_3VO_4 itself does not stabilize or aggregate AuNPs) completely inhibited CIAP (1.25 units/20 μL) activity, as there is no significant spectra shift (Fig. 2.3(A)) or color change (data not shown) in the AuNP test. The titration of inhibitor concentration showed that, at the investigated enzyme concentration (1.25 units/20 μL), the detectable inhibitor concentration is ~ 300 μM or above (Fig. 2.3(B)). Note that the detectable inhibitor concentration is highly dependent on the enzyme concentration used for the reaction, that is, less inhibitor is required for effective inhibition when enzyme with lower concentration is used (data not shown).

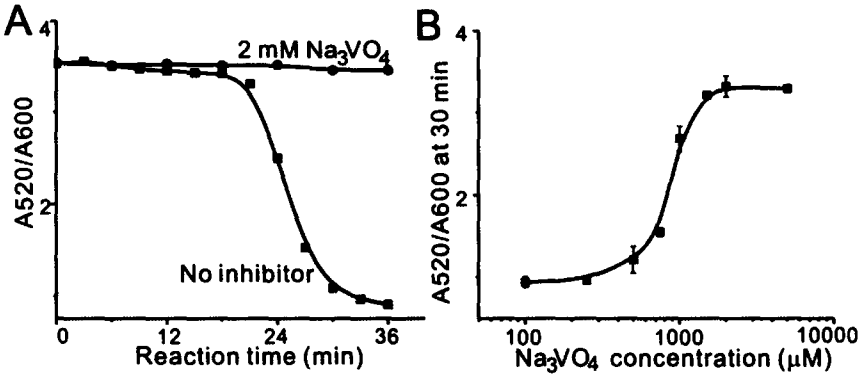

Figure. 2.3. *(A) A520/A600 calculated from UV-Vis spectra in the AuNP test as a function of enzymatic reaction time. The enzymatic reaction was conduct with 2 mM Na_3VO_4 inhibitor and without inhibitor. (B) A520/A600 of the sample which underwent 30 min enzymatic reaction time is plotted as a function of Na_3VO_4 concentration.*

We reasoned that the concept illustrated above could also be adapted to other enzymatic reactions where substrates and products impact differently on the AuNP stability. To provide a second demonstration, we applied the same method to monitor an enzymatic reaction known as "rolling circle amplification" where dNTPs (dATP, dTTP, dGTP and dCTP) are converted to a long single-stranded DNA (ssDNA) by phi29 DNA polymerase.[15] We anticipated that dNTPs would bind AuNP more effectively than the long ssDNA product because of the steric hindrance and large secondary structures formed in long ssDNA,[8b] and that dNTPs would stabilize AuNP more effectively than the long ssDNA. Since dNTPs and the long ssDNA product both stabilize AuNPs (although to different extents), the assay was performed at a specific salt concentration where dNTP/AuNP is stable whereas long ssDNA/AuNP would aggregate.[16] The results are shown in Fig. S2.5 in SI. Briefly, the AuNP solution mixed with the reaction mixture that either excluded or contained DNA polymerase was red and blue in color, respectively. The red-to-blue color change indicated that AuNP aggregation occurred as dNTPs were made into long ssDNA by phi29 DNA polymerase.

2.4 Conclusion

In conclusion, we have demonstrated simple and rapid enzyme sensing assays using the principle of non-crosslinking AuNP aggregation. The use of AuNP is advantageous, particularly for the enzymatic reactions that cannot be easily monitored by traditional spectroscopic techniques, due to its simplicity and the colorimetric detection nature. Moreover, compared to the crosslinking AuNP aggregation, this non-crosslinking aggregation induced by a change of the electrophoretic properties of AuNPs is generally faster (the AuNP test assay in the present study was completed in 1 min).[8] In the non-crosslinking system, the aggregation is driven by the London/van der Waals attractive force between the nanoparticles.[8c] Once the electrostatic repulsion is significantly reduced due to the loss (or screen) of surface charges, the attractive forces dominate, leading to a rapid aggregation. In contrast, in the crosslinking system, the aggregation is mainly driven by random collisions between nanoparticles with relatively slow Brownian motion.[8c] Furthermore, this approach is conceptually simpler than the crosslinking system and, in principle, can be applied to any target molecules which can affect the electrophoretic properties of AuNPs, whereas in the crosslinking aggregation process, the crosslinker has to carry at least two binding tags in order to bring AuNP into close proximity. We speculate that our assay can be adapted to other charged substrates such as DNA oligonucleotides, amino acids and peptides, and that similar assays could be easily developed to detect and quantify other enzymes including ligases, endonucleases, proteases, etc. Nevertheless, nonspecific aggregation of bare AuNP could be a potential issue for the use of this assay in more complex matrices (rather than pure buffers) and therefore a pre-purification step might be required in some specific cases. Finally, since the interaction between nucleobases and AuNP is quite complicated and has been the subject of extensive debate,[10] we hope this work will provide insight into the nature of the interaction between DNA (or nucleotides, nucleosides) and AuNPs.

2.5 Acknowledgement

The authors wish to thank the Natural Sciences and Engineering Research Council of Canada (NSERC) and Sentinel Bioactive Paper Network for financial support. Y. L. holds a Canada Research Chair.

2.6 Notes and references

1. (a) R. Elghanian, J. J. Storhoff, R. C. Mucic, R. L. Letsinger, C. A. Mirkin, *Science*, 1997, 277, 1078. (b) J. Liu, Y. Lu, *J. Am. Chem. Soc.* 2003, 125, 6642. (c) J. Liu, Y. Lu, *Angew. Chem. Int. Ed.* 2005, 45, 90. (d) V. Pavlov, Y. Xiao, B. Shlyahovsky, I. Willner, *J. Am. Chem. Soc.*, 2004, 126, 11768. (e) C. Tsai, T. Yu, C. Chen, *Chem. Commun.*, 2005, 4273. (f) C. Huang, Y. Huang, Z. Cao, W. Tan, H. Chang, *Anal. Chem.* 2005, 77, 5735. (g) J. Li, X. Chu, Y. Liu, J. Jiang, Z. He, Z. Zhang, G. Shen, R. Yu, *Nucleic Acids Res.* 2005, 33, e168. h) J. M. Nam, K. J. Jang, J. T. Groves, *Nat. Protoc.*, 2007, 2, 1438. i) R. Baron, B. Willner, I. Willner, *Chem. Commun.*, 2007, 323. j) Z. Wu, S. Zhang, M. Guo, C. Chen, G. Shen, R. Yu, *Anal. Chim. Acta.* 2007, 584, 122.

2. G. Mie, *Ann. Phys.* 1908, 25, 377.

3. a) Z. Wang, R. Lévy, D. G. Fernig, M. Brust, *J. Am. Chem. Soc.* 2006, 128, 2214. b) X. Xu, M. Han, C. A. Mirkin, *Angew. Chem. Int. Ed.*, 2007, 46, 3468.

4. C. Guarise, L, Pasquato, V. De Filippis, P. Scrimin, *Proc. Natl. Acad. Sci. USA* 2006, 103, 3978.

5. Y. Choi, N. Ho, C. Tung, *Angew. Chem. Int. Ed*, 2007, 46, 707.

6. R. Levy, N. T. Thanh, R. C. Doty, I. Hussain, R. J. Nichols, D. J. Schiffrin, M. Brust, D. G. Fernig. *J. Am. Chem. Soc.*, 2004, 126, 10076.

7. E. A. Hauser, *Colloidal phenomena: an introduction to the science of colloids.* New York; London: McGraw-Hill, 1939.

8. (a) W. Zhao, W. Chiuman, M. A. Brook, Y. Li, *Chembiochem.* 2007, 8, 727. (b) H. Li, L. Rothberg, *Proc. Natl. Acad. Sci. USA* 2004, 101, 14036. (c) K. Sato, K. Hosokawa, M. Maeda, *J. Am. Chem. Soc.* 2003, 125, 8102. (d) L. Wang, X. Liu, X. Hu, S. Song, *Chem. Commun.* 2006, 2, 3780.

9. R. F. Weaver, *Molecular Biology*, McGraw-Hill College, 2002.

10. (a) J. J. Storhoff, R. Elghanian, C. A. Mirkin, R. L. Letsinger, *Langmuir*, 2002, 18, 6666. (b) A. Gourishankar, S. Shuka, K. N. Ganesh, M. Sastry, *J. Am. Chem. Soc.* 2004, 126, 13186. (c) H. Kimura-Suda, D. Y. Petrovykh, M. J. Tarlov, L. J. Whitman, *J. Am. Chem. Soc.* 2003, 125, 9014. (d) M. Cardenas, J. Barauskas, K. Schillen, J. L. Brennan, M. Brust, T. Nylander, *Langmuir* 2006, 22, 3294. (e) W. Zhao, F. Gonzaga, Y. Li, M. A. Brook, *Adv. Mater.* 2007, 19, 1766.

11. The initial purpose of this dilution is to minimize the effect of local salt concentration increase on the AuNP stability when reaction sample solution is added into AuNP solution. However, our subsequent study showed that the undiluted reaction solution could also be directly added to AuNP solution without causing significant AuNP stability change (see SI, Fig. S2.2).

12. The lower CIAP concentration (e.g. 0.05 units/20 μL) could also be detectable, but a longer reaction time (e.g. 12 h) was required to ensure enough ATP had been converted into adenosine to get a quick color change (1 min) in the subsequent AuNP test.

13. Control experiments where the AuNP stability with or without CIAP were accessed by gradually adding NaCl solution (1 M) to AuNP solution showed that CIAP did not stabilize AuNP either under studied conditions.

14. I. R. Gibbons, M. P. Cosson, J. A. Evans, B. H. Gibbons, B. Houck, K. H. Martinson, W. S. Sale, W. Y. Tang, *Proc. Natl. Acad. Sci. USA* 1978, 75, 2220.

15. (a) A. Fire, S. Xu, *Proc. Natl. Acad. Sci. USA* 1995, 92, 4641. (b) D. Liu, S. L. Daubendiek, M. A. Zillman, K. Ryan, E. T. Kool, *J. Am. Chem. Soc.* 1996, 118, 1587.

16. Theoretically, there is a possibility that AuNPs are bridged by RCA product (or H-bonds between DNA molecule-adsorbed AuNPs). However, we think this is a minor contribution to AuNP aggregation in our assay given the fact that this type of interparticle crosslinking process is known as a relatively slow process (for example, see ref. 1a, 8c). Considering the AuNP aggregation (or color change) in our assay was completed in 1 min, we believe this aggregation is induced by the loss (or screen) of surface charges.

2.7 Supplementary Information

Experimental

Materials

Calf intestine alkaline phosphatase (CIAP), phi29 DNA polymerase, and dNTPs (dATP, dCTP, dTTP, and dGTP) were purchased from MBI Fermentas. ATP and other reagents were obtained from Sigma. DNA oligonucleotides used in this study were obtained from Central Facility, McMaster University. H_2O was doubly deionized and autoclaved before use. 13 nm gold nanoparticles (AuNP) were prepared according to reported procedures[1] and the final concentration was estimated to be about 14 nM using UV-Vis spectrometric measurements based on an extinction coefficient of ~ 2.7×10^8 M^{-1} cm^{-1} at λ 520 nm for 13 nm particles.[1]

Study of AuNP stability in the presence of ATP, ADP, AMP, adenosine and Inosine

100 μL of ATP (or ADP, AMP, adenosine and inosine) solution (18 nmol, 180 μM) was added to 200 μL of AuNP solution (14 nM) in a 2-mL glass vial, and the photographs, as shown in Fig. 2.1B vials 1-5, were taken in 1 min following the mixing. To further investigate the impact of adenosine concentration on AuNP stability, the same assay was performed with adenosine in different concentrations (90, 60, 30, 15, and 7.5 μM), and the results are shown in Fig. 2.1B vials 6-10, respectively.

We found that ATP, ADP and AMP all stabilize AuNP. To investigate the relative stability of AuNP/ATP, AuNP/ADP, and AuNP/AMP solutions, NaCl (5 M) was gradually added to the above solutions. The color change was first observed in AuNP/AMP solution, then AuNP/ADP, and finally AuNP/ATP, indicating that the AuNP stability follows the order of AuNP/ATP > AuNP/ADP > AuNP/AMP. In the present work, AuNP/ATP, AuNP/ADP, AuNP/AMP, and bare AuNP solution were found to be unstable (color change in 1 min) at NaCl concentration of ≥ 320 mM, ≥ 250 mM, ≥ 170 mM, and ≥ 50 mM, respectively.

The zeta potential of the nanoparticles were measured at room temperature by using a ZetaPlus (Brookhaven Instruments Corporation, Holtsville, NY). The reported values were based on 5 measurements with 15 cycles for each sample.

Development of calibration curve for determining the percentage conversion of ATP

ATP and adenosine with various molar ratios were mixed in a total concentration of 10 mM in 20 μL Tris-HCl (10 mM, pH 7.5), $MgCl_2$ (10 mM) (1× reaction buffer). 1 μL of the mixture was diluted 100 times by ddH_2O and added into 200 μL AuNP (14 nM). UV-Vis adsorption spectra were recorded after 1 min following the mixing, and shown in Fig. S2.3A. The ratio of extinction at 520 and 600 nm (A520/A600) were plotted as a function of ATP/adenosine molar ratio, as shown in Fig. S2.3B.

Assay of sensing CIAP

20 μL of enzymatic reaction solution contained ATP (200 nmol, 10 mM), 1× reaction buffer, and various amounts of CIAP (from 10 units to 0.16 units, one unit is defined as the amount of enzyme required to catalyze the hydrolysis of 1 μmol of 4-nitrophenyl phosphate per minute at 37 °C in 1 M diethanolamine, 10.9 mM 4-nitrophenyl phosphate, 0.5 mM $MgCl_2$ (pH 9.8)). 1 μL of reaction mixture was taken at given reaction times, diluted 100 times by ddH_2O and added into 200 μL AuNP (14 nM). UV-Vis adsorption spectra were measured after 1 min following the mixing, as shown in Fig. S2.4. A520/A600 was plotted as a function of reaction time and shown in Fig. 2.2D. The amount of ATP converted to adenosine per minute for different CIAP units added to the reaction was approximated by the following procedures: (1) Two data points were taken closest to the inflection point for each curve in Fig. 2.2D; (2) converted into nmol adenosine ($200 - ((A_{520}/A_{600} - \text{lowest } A_{520}/A_{600}) \div \text{maximum } \Delta\ A_{520}/A_{600}) \times 200$); (3) then divided by the difference in the amount of adenosine produced over the two concerned time points by the time. It is important to note that the y axis in Fig. 2.2E, the amount of ATP converted to adenosine per minute, was not intended to represent the real reaction rate. Rather, it was only used to quantify the enzymatic activities.

Enzymatic inhibition assay was conducted as follows: CIAP (1.25 units) was pre-incubated with desirable amount of Na_3VO_4 in 20 μL reaction buffer for 10 min. ATP (final concentration 10 mM) was then added to the mixture and the reaction was performed at 37 °C. At certain given reaction time, 1 μL of reaction mixture was taken, then diluted 100 times by ddH_2O and finally added into 200 μL AuNP (14 nM). UV-Vis spectra were taken and A520/A600 was calculated. The A520/A600 was plotted as a function of enzymatic reaction time and the data was shown in Fig. 2.3A. For the inhibitor concentration assay, the enzymatic reactions with different amount of inhibitor were performed for 30 min, and 1 μL of reaction solution was then taken for the AuNP test.

Assay of sensing phi29 DNA polymerase

20 μL of enzymatic reaction solution contained dNTPs (2 mM dGTP, 3 mM dATP, 0.6 mM dCTP, and 0.7 mM dTTP), phi29 DNA polymerase (40 units, one unit is defined as the amount of enzyme required to catalyze the incorporation of 0.5 pmol of dCTP into a polynucleotide fraction in 10 min at 30°C), primer (5'-GGCGAAGACAGGTGCTTAGTC, 20 pmol, 1 μM), circular template (5'-TGTCTTCGCCTTCTTGTTTCCTTTCCTTGAAACTTCTTCCTTTCTTTCTTTCGAC TAAGCACC, 20 pmol, 1 μM) (for the synthesis of circular template, see ref. 2), 1 × reaction buffer (33 mM Tris-acetate (pH 7.9 at 37°C), 10 mM Mg-acetate, 66 mM K-acetate, 1% (v/v) Tween 20). The reaction was performed at 37 °C. 1 μL of the reaction mixture was taken at certain reaction time, and added to 99 μL NaCl solution (75 mM). This resulting mixture was then added to 200 μL AuNP solution (14 nM). UV-Vis adsorption spectra were measured after 1 min following mixing, as shown in Fig. S2.5.

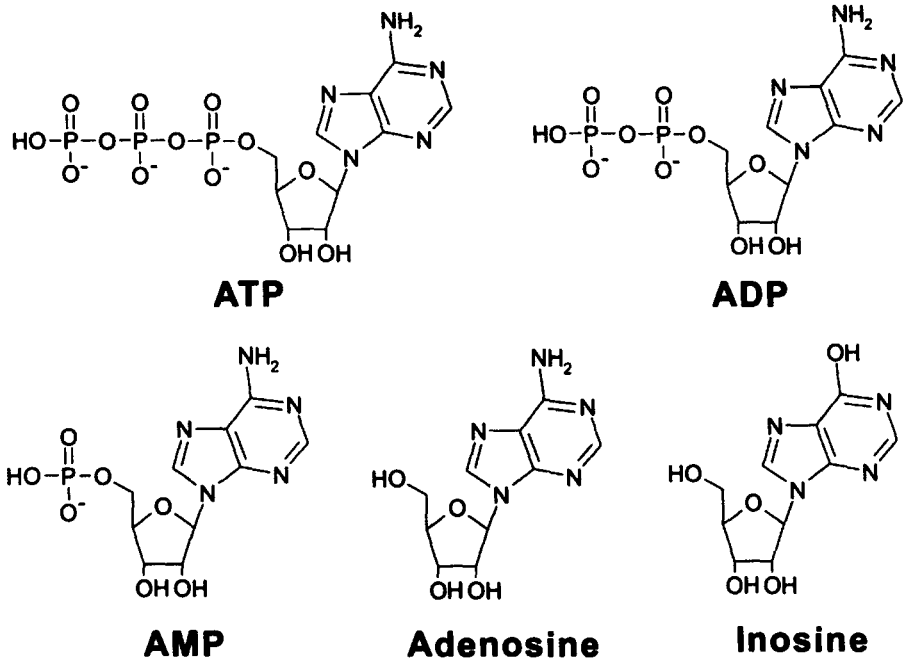

Figure. S2.1. *Chemical structures of ATP, ADP, AMP, adenosine and inosine.*

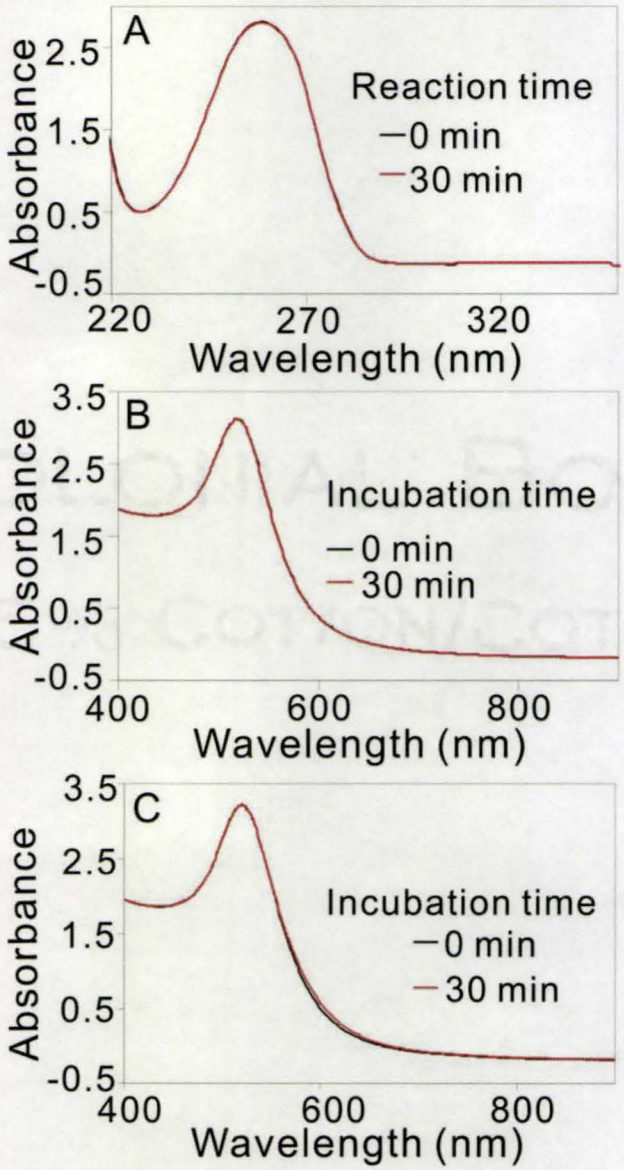

Figure. S2.2*. (A) UV-Vis spectroscopy monitoring CIAP reaction without AuNPs. There was no difference in the spectra between ATP (substrate) and adenosine (product). The reaction contained ATP (180 μM), CIAP (0.66 units/20 μL) and 1× reaction buffer. (B) The effect of 1× reaction buffer on AuNP stability. 1 μL of 1× reaction buffer (Tris-HCl (10 mM, pH 7.5), $MgCl_2$ (10 mM)) was added to AuNP solution (200 μL, 14 nM) without any dilution. Black and red curves are the UV-Vis spectra of the mixture after 0 and 30 min incubation time, respectively. The data indicate that 1× reaction buffer, without any dilution, has no effect on AuNP stability. (C) The effect of CIAP on AuNP stability. 1 μL of CIAP solution (CIAP: 0.125 units, Tris-HCl (10 mM, pH 7.5), $MgCl_2$ (10 mM)) was added to AuNP solution (200 μL, 14 nM) without any dilution. Black and red curves are the UV-Vis spectra of the mixture after 0 and 30 min incubation time, respectively. It*

indicates that CIAP, without any dilution, has little effect on AuNP stability after 30-min incubation. Given that the color was read after 1 min following addition of the reaction mixture to AuNP solution in our assay, we expect that the buffer and enzyme have little effect on the AuNP stability, that is, one can directly add the reaction solution to AuNP for detection without any dilution.

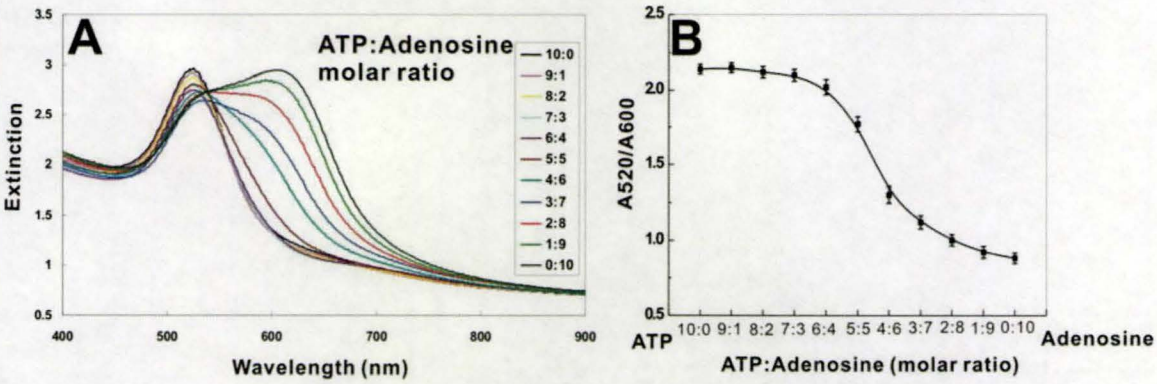

***Figure. S2.3**. (A) Representative UV-Vis spectra of AuNP solutions with various amounts of ATP and adenosine. All spectra were recorded after 1 min following the addition of ATP and adenosine mixture to AuNP solution. (B) The A520/A600 ratios are plotted as a function of ATP and adenosine molar ratios.*

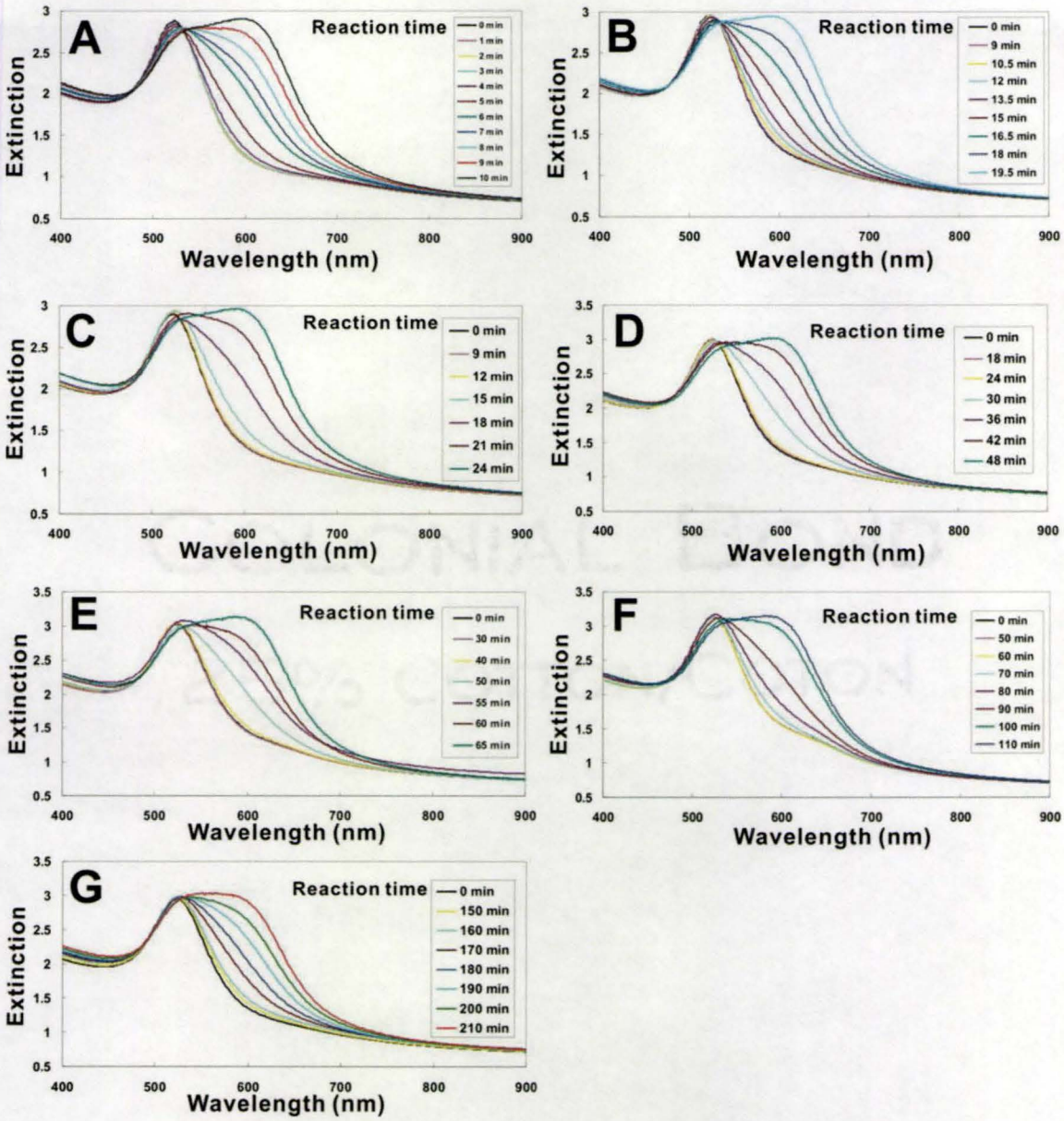

Figure. S2.4. *Representative UV-Vis spectra of AuNP solution after addition of CIAP-ATP reaction solution with 10 (A), 5 (B), 2.5 (C) 1.25 (D), 0.625 (E), 0.31 (F), and 0.16 (G) units of CIAP (in 20 μL reaction volume) at different reaction times. All spectra were recorded after 1 min following addition of the relevant reaction mixture to AuNP solution. Note that the spectra which overlap with the spectrum at 0 min reaction time are not shown for clarity.*

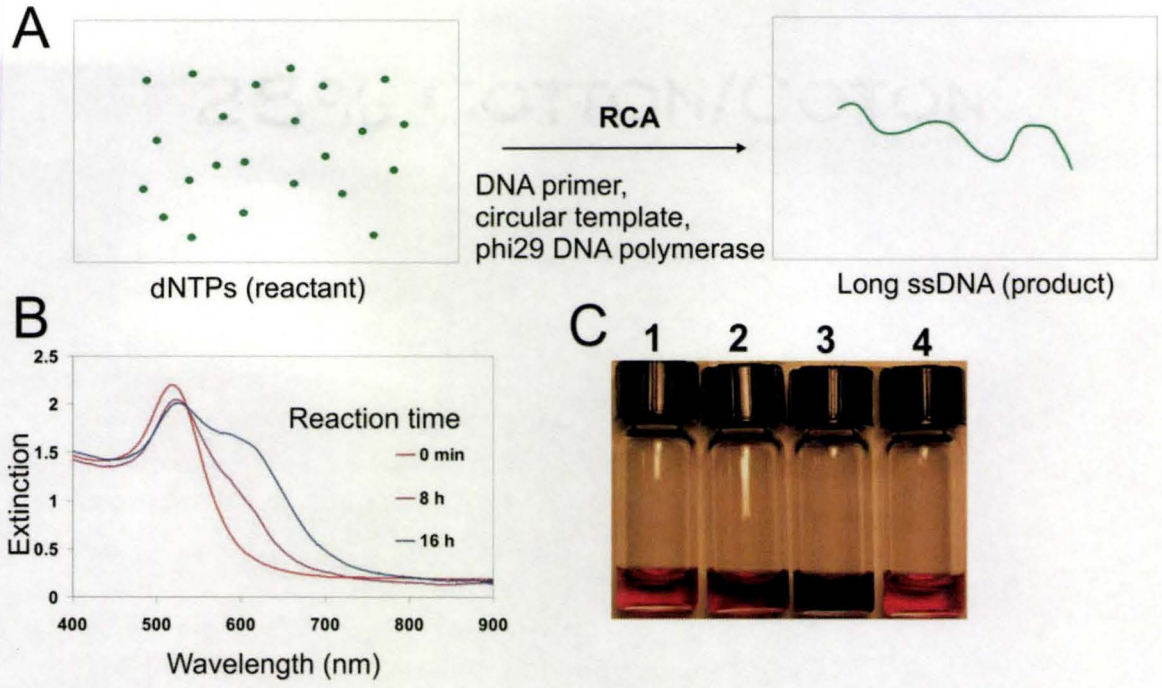

Figure. S2.5*. (A) DNA polymerization via rolling circle amplification (RCA): dNTPs (reactant) are converted into long ssDNAs (product). See ref. 3 and 4 for more detailed information of RCA. (B) Representative UV-Vis spectra of AuNP solution after addition of phi29 enzymatic reaction mixtures taken at different reaction time. (C) Photographs of AuNP solutions after the addition of phi29 enzymatic reaction solutions with reaction times at 0 (vial 1), 8 h (vial 2) and 16 h (vial 3), respectively. Vial 4 was the AuNP solution after addition of a control enzymatic reaction solution quenched at 90 °C for 10 min right after the addition of phi29 DNA polymerase. The control reaction was conducted for 16 h.*

References

(1) R. Jin, G. Wu, Z. Li, C. A. Mirkin, G. C. Schatz, *J. Am. Chem. Soc.* 2003, **125**, 1643.

(2) W. Zhao, Y. Gao, S. A. Kandadai, M. A. Brook, Y. Li, *Angew. Chem. Int. Ed.* 2006, **45**, 2409.

(3) A. Fire, S. Xu, *Proc. Natl. Acad. Sci. USA* 1995, **92**, 4641.

(4) D. Liu, S. L. Daubendiek, M. A. Zillman, K. Ryan, E. T. Kool, *J. Am. Chem. Soc.* 1996, **118**, 1587.

Chapter 3: Highly Stabilized Nucleotide-capped Small Gold Nanoparticles with Tunable Size

The following chapter was published in Advanced Materials under the citation:

Weian Zhao, Ferdinand Gonzaga, Yingfu Li, Michael A. Brook. Highly stabilized nucleotide-capped small gold nanoparticles with tunable size. *Adv. Mater.* 2007, 19, 1766-1771.

I was responsible for all data collection and analysis. Dr. Ferdinand Gonzaga provided helpful suggestions in the project design and data collection. I wrote the first draft of the manuscript and Dr. Brook and Dr. Li provided editorial input to generate the final draft of the paper.

3.1 Introduction

Gold nanoparticles (AuNPs) have attracted considerable attention in recent years due to their various applications in nano- and biotechnology.[1] In particular, small AuNPs (d < 5 nm) are of great interest for use in certain nanodevices,[2a] biosensors,[2b] and biolabels.[2c] While a number of approaches have been developed to prepare AuNPs,[3,4] the synthesis of stabilized small AuNPs, particularly with tunable size and controllable morphology still faces challenges.[4] This is partially due to the fact that small nanocrystals tend to aggregate due to van der Waals attraction.[5]

Capping ligands such as alkanethiols,[3,4a,b,6] phosphines,[7] amines,[8] and polymers[4c,9] are typically used during nanocrystal growth processes to protect nanocrystals against aggregation. For instance, the classical method reported by Brust et al.,[3a] which involves a two-phase synthesis, and uses alkanethiols to produce AuNPs with sizes between 1-5 nm. More recently, Hussain et al. successfully prepared AuNPs in the 1-4 nm range using thiol-tethered polymeric ligands.[3b] Remarkably, precise size control and monodispersity were achieved in their study. However, most of these organic capping ligands, particularly alkanethiols, are arguably toxic,[8b] and the use of organic solvents in most of these synthetic approaches also raises environmental issues: there is a general need to develop "greener" or more environmentally and bio-friendly routes to prepare AuNPs.[10] Moreover, these organic layer-protected AuNPs suffer from poor water solubility or water instability which significantly limits their use in biological applications.[10a,b] Herein, we report a facile and more environmentally friendly route to synthesize water-soluble small AuNPs ($d \approx 2$ nm − 5 nm) using nucleotides as capping ligands. Significantly, these nucleotide-capped AuNPs have precisely controlled sizes, and are highly stabilized against salt-induced aggregation.

It is well known that nucleic acids interact with metal ions through nucleobases and the phosphodiester backbone.[11] Both DNA and RNA have been used as scaffolds for metal-nanoparticle deposition, a process that can be potentially applied to 1-D nanoelectronics.[12] These efforts suggest that nucleotides, the monomers of nucleic acids, could be effective ligands to prepare metal nanocrystals. Indeed, Kelley and co-workers

recently reported that guanosine 5′-triphosphate (GTP) played an important role in their semiconductor PbS growth.[13] We also recently demonstrated that nucleotides can effectively adsorb onto AuNP surfaces and thus stabilize AuNPs by electrostatic repulsion.[14] The chemical structure of nucleotides suggests that they could be effective capping ligands in metallic nanoparticle formation processes: nucleobases (e.g., adenine, thymine, guanine, and cytosine) bind to metallic nanoparticle surface due to the interaction between functional groups (amines and carbonyls) in nucleobases and the metal surface;[15] the negatively charged phosphate group stabilizes the nanoparticle against aggregation during its growth phase through electrostatic repulsion. To verify this hypothesis, we set out to investigate the influence of the presence of nucleotides on AuNP formation.

3.2 Results and discussion

In a typical AuNP synthesis reaction (details are provided in the Experimental Section), $HAuCl_4$ (10 mM, 60 μL) and adenosine 5′-triphosphate (ATP) (10 mM, 60 μL) were added into 2.75 mL of double-deionized water (ddH_2O) in a glass vial, and the mixture was incubated at room temperature for 30 min. Freshly prepared $NaBH_4$ (100 mM, 100 μL) was then quickly added, and the vial was vigorously shaken for 10 s. An orange color appeared immediately upon the addition of $NaBH_4$, indicating the formation of AuNP.[4] The color of the solution changed gradually from orange to red over 2 h, after which there was no further color change, indicating the AuNP growth was complete within 2 h. This was further confirmed by a kinetic study using UV-Vis spectroscopy (see Supplementary Information, S. Fig. 3.1) which showed that there was no significant spectral shift after 2 h. The as-prepared AuNPs were characterized by transmission electron microscopy (TEM), high resolution transmission electron microscopy (HRTEM), UV-Vis spectroscopy, X-ray photoelectron spectroscopy (XPS), and X-ray diffraction (XRD).

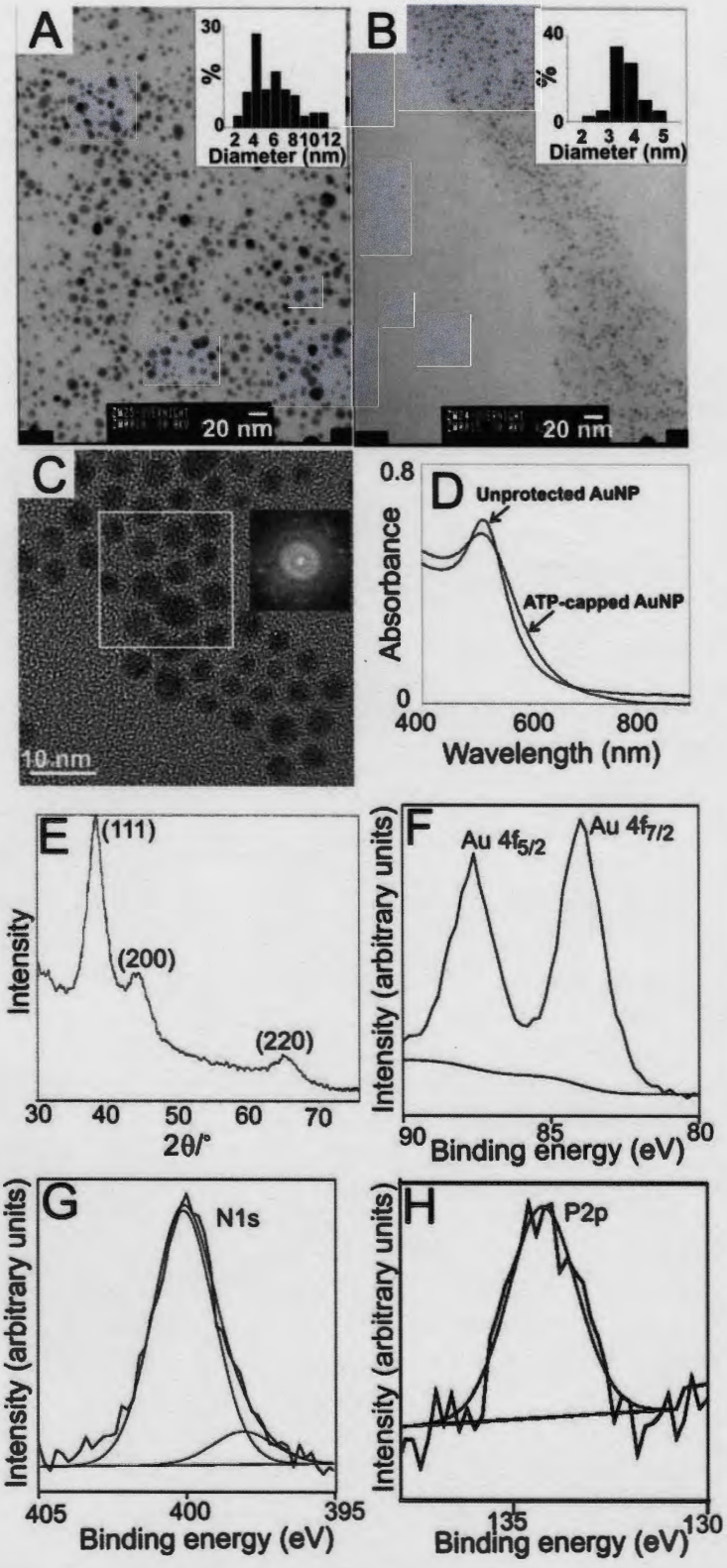

Figure 3.1. *(A) Representative TEM image of AuNP prepared in the absence of ATP. The average size is 7.85 ± 2.31 nm. Scale bar = 20 nm. (B) and (C) are representative TEM*

and HRTEM images, respectively, of ATP-capped AuNPs. Scale bar is 20 nm in (B) and 10 nm in (C), respectively. The molar ratio of $HAuCl_4$:ATP:$NaBH_4$ in this experiment is 1:1:16.7. The size of this ATP-capped AuNP is 3.75 ± 0.60 nm. The insets in (A) and (B) are size distributions. The inset in (C) shows the corresponding fast Fourier transform (FFT) of the selected area. The discrete dots in FFT pattern illustrate the crystalline nature of these as-prepared AuNPs. (D) UV-Vis absorption spectra of AuNP solution prepared in the presence or absence of ATP. (E) XRD pattern of ATP-capped AuNP. (F), (G), and (H) are XPS spectra of ATP-capped AuNPs, which correspond to Au, N and P, respectively.

AuNPs prepared by the reduction of $HAuCl_4$ using $NaBH_4$ in the absence of nucleobases were used as controls. The representative TEM image (Fig. 3.1A) reveals that these "unprotected" AuNPs are roughly spherical with an average diameter of 7.85 ± 2.31 nm (note that in this study the standard deviation of AuNP size was calculated based on more than 200 particles in the TEM images). Higher magnification TEM images for each sample in Fig. 3.1A, B and Fig. 3.2A-D are provided in the Supplementary Information, see S. Fig. 3.2). In some cases, elongated or fused particles were also observed (data not shown). By contrast, TEM images of the ATP-capped AuNPs displayed well-distributed spherical nanocrystals with much smaller sizes and improved dispersity (3.75 ± 0.60 nm) (Fig. 3.1B & C). This indicates that ATP played an essential role in controlling the AuNP size and morphology, presumably because the binding of ATP, which has negatively charged phosphate groups, on the AuNP surface prevented small nanoparticles from aggregating during the growth process (see below for more detailed discussion of the mechanism). UV-Vis spectroscopy of ATP-capped AuNP (Fig. 3.1D) showed a small and broadened surface plasmon band around 510 nm, which is characteristic for small spherical AuNPs.[4] It is known that the SPR band decreases and broadens with decreasing AuNP size and is undetectable for very small AuNPs (diameter < 2 nm), which can be interpreted as an indication of the quantum size effects (i.e., the loss of bulk Au character during the transition from bulky Au to small "quantum-sized" Au cluster).[4a,f] Compared to the spectrum of "unprotected" AuNPs (Fig. 3.1D), which has a much sharper and more intense band at about 515 nm, this blue shifted and broadened surface plasmon band of the ATP-capped AuNP further confirmed that smaller

nanocrystals were formed.[4d] HRTEM (Fig. 3.1C) and XRD (Fig. 3.1E) results reveal the crystalline nature (face-centered cubic (fcc) structure) of the ATP-capped AuNPs. XPS spectra (Fig. 3.1F) clearly showed two peaks centered at binding energies of 83.9 and 87.6 eV, which correspond to the Au $4f_{7/2}$ peak and Au $4f_{5/2}$ peak, respectively, indicating the formation of the metal AuNP.[8b] XPS data (see Supplementary Information S. Fig. 3.3) also confirmed that there was no free gold ions left after the reduction process. The binding of ATP to AuNP is demonstrated by the presence of N1s and P2p at binding energies of 400.1 and 134.2 eV, respectively (Fig. 3.1G, H).[16] To estimate how much of the capping agent initially added is finally bound to the AuNPs, we used UV-Vis

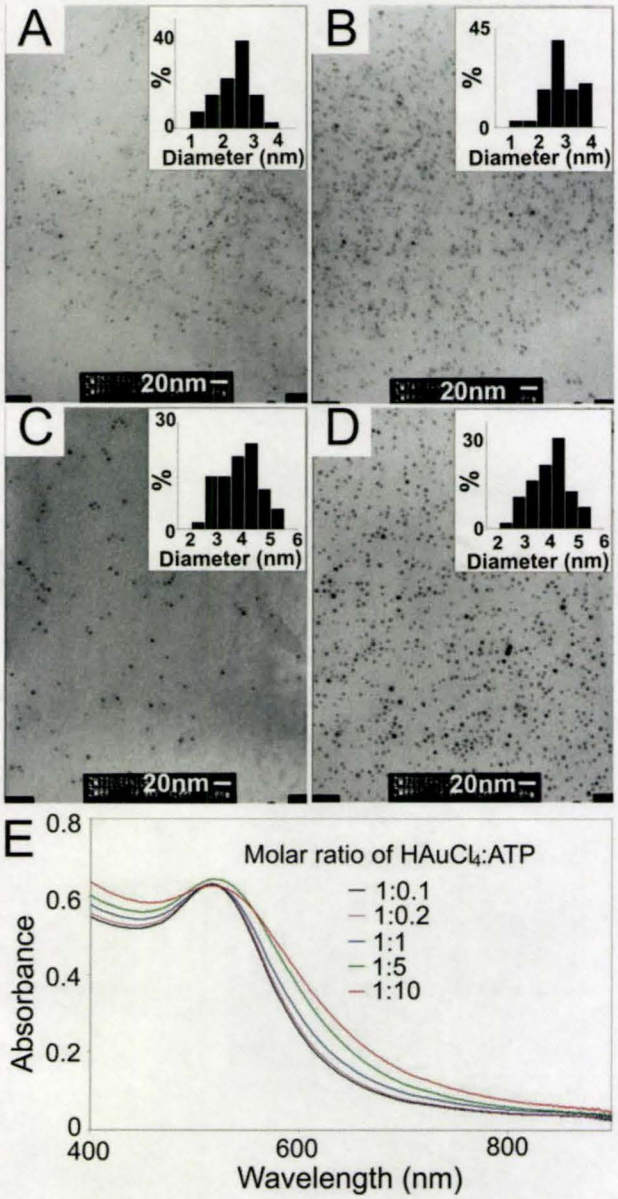

Figure 3.2. *Representative TEM images of ATP-capped AuNPs prepared with the $HAuCl_4$:ATP molar ratio of 1:10 (A), 1:5 (B), 1:0.2 (C) and 1:0.1 (D), respectively. The insets are size distributions. The one with $HAuCl_4$:ATP molar ratio of 1:1 was given in Fig. 3.1B. Scale bar = 20 nm. The average sizes of these AuNPs are 2.73 ± 0.53 nm (A), 3.12 ± 0.58 nm (B), 4.23 ± 0.63 nm (C), and 4.54 ± 0.67 nm (D), respectively. (E) UV-Vis spectra of ATP-capped AuNP solutions which are prepared with various $HAuCl_4$:ATP molar ratios.*

spectroscopy to measure the amount of ATP in the supernatant solution after AuNP formation and centrifugation. It was found that there were about 79 ATP molecules on each 3.75 nm AuNP.

Previous studies suggested that the size and shape of AuNPs can be controlled by varying the molar ratio of $HAuCl_4$, ligands, and/or reducing agents.[7-9] We therefore investigated the impact of the amount of ATP and $NaBH_4$ on the AuNP size and shape. As the molar ratio of $HAuCl_4$:ATP decreases, the size of the AuNP decreases (e.g., 2.73 ± 0.53 nm for ATP:$HAuCl_4$ = 10:1), as shown in the TEM images (Fig. 3.2A-D). This is further confirmed by UV-Vis adsorption spectra (Fig. 3.2E) which showed that the surface plasmon band became less distinct as more ATP was added, indicating that AuNPs with smaller sizes were formed.[4d,9a] The AuNPs prepared in the presence of more ATP also showed a better control of size dispersity. These observations are consistent with the previous finding that the availability of more ligands generally yielded smaller AuNPs with narrower monodispersities.[4d,9a]

The experiments where the $NaBH_4$:$HAuCl_4$ molar ratios were varied indicated that the $NaBH_4$:$HAuCl_4$ molar ratio required to produce monodisperse spherical AuNP ranged from 15 to 20. When less or more $NaBH_4$ was added, poorly size-controlled (e.g., fused or elongated) particles were observed in TEM images (see Supplementary Information S. Fig. 3.4). It has been previously demonstrated that insufficient reducing agent results in a slower crystal growth process leading to difficulties in controlling the crystal size and morphology.[17] Similarly, it is generally understood that the use of higher reducing agent concentrations generally produce nanocrystals with smaller sizes and more controlled morphology.[16] In light of these reports, it was surprising, in the current study, to show that an excess of reducing agents also yielded poorly controlled AuNPs.

Although this observation is not yet fully understood, we attribute it to the fact that excess $NaBH_4$[18] resulted in such a rapid crystal growth process that the ATP ligand may no longer effectively stabilize the growing particles: the rate of generation of Au surface area during particle synthesis may exceed the rate at which ATP can stabilize the growing surface under these conditions.

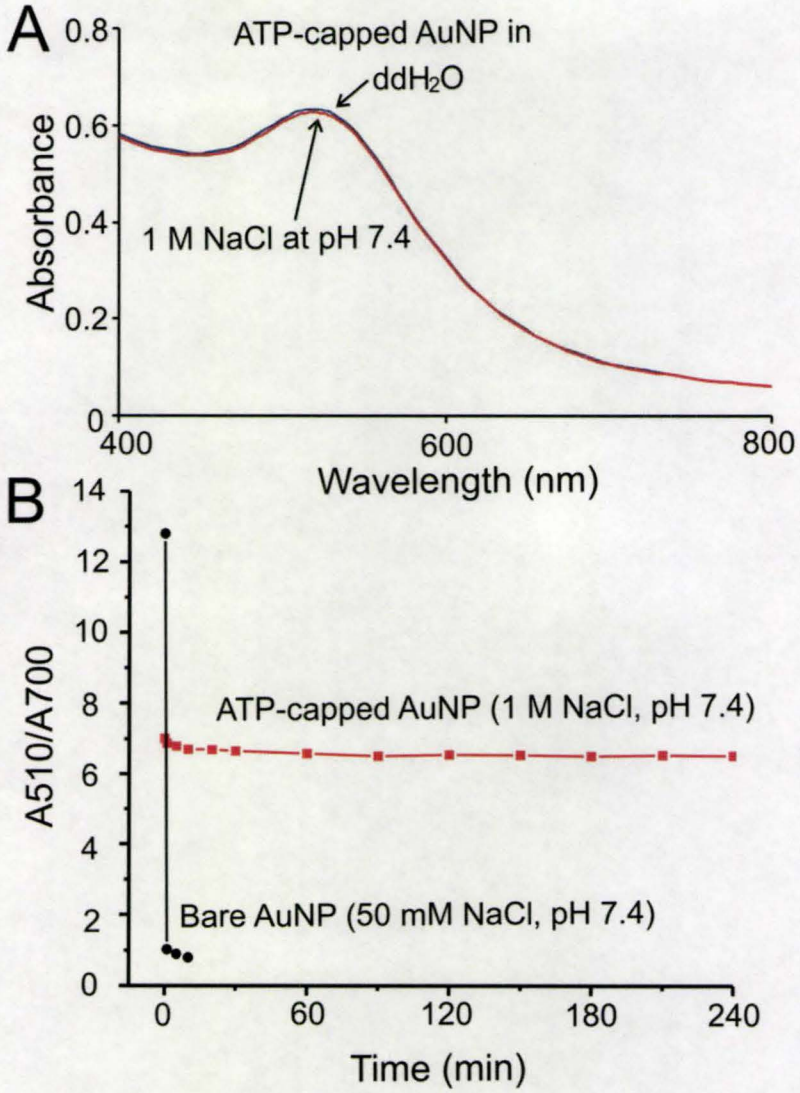

***Figure 3.3**. (A) UV-Vis spectra of ATP-capped AuNP in ddH_2O (blue curve) and in 1 M NaCl at 20 mM phosphate buffer saline (pH 7.4) (red curve). The spectra were taken 1 h after the mixing of AuNP with salt solution. Note that the SPR band of ATP-capped AuNPs under the investigated salt concentration decreased slightly over a few hours. (B)*

A510/A700 was used to monitor the stability and aggregation stage of ATP-capped AuNPs (red line) and bare AuNPs (black line) over a longer period of time.

Other fascinating properties of these small ATP-capped AuNPs include their water solubility and extremely high stability toward salt-induced aggregation. Most of AuNPs produced by conventional methods (e.g., alkanethiol-capped AuNPs) show poor solubility in water.[5,10a-b] Although efforts have been made to generate water-soluble AuNPs, the as-prepared AuNPs are normally unstable in water at high salt concentrations.[10b] For instance, AuNPs prepared according to the classical citrate or $NaBH_4$ reduction methods in the absence of ligands aggregate and precipitate at about 50 mM NaCl. This largely limits the broad use of AuNPs, particularly in biological applications where most of the assays are performed in the presence of buffers and salts (e.g., 300 mM NaCl). In the present work, the ATP-capped AuNP was found to be highly stable at high salt concentrations as evidenced by the fact that there is no color change or significant UV-Vis spectral shift when salt concentrations are increased up to at least 1 M NaCl at pH 7.4 (Fig. 3.3A). To further determine the stability of ATP-capped AuNPs over longer periods of time, we monitored the absorbance ratio at 510 nm and 700 nm (A510/A700),[19] which was previously used to follow AuNP aggregation. As shown in Fig. 3.3B, the ATP-capped AuNPs are stable for at least a few hours at 1 M NaCl (pH 7.4). This extremely high stability of ATP-capped AuNP may be due to the fact that negatively charged phosphate groups prevent particle against aggregation via the electrostatic repulsion. This proposal is supported by the fact that these ATP-capped AuNPs migrate through an agarose gel toward the positive anode (data not shown). The zeta potential of ATP-capped AuNP is about -19.81 ± 2.75 mV whereas the zeta potential of AuNP prepared without nucleotides is only about -5.34 ± 2.73 mV. These stability studies of nucleotide-capped AuNPs and bare AuNPs confirmed that nucleotides have higher binding affinity to AuNP than that of BH_4^-, and nucleotides are indeed the stabilizing ligands during the growth of AuNPs (see below for more detailed discussion of mechanism). Importantly, these stable AuNPs should be "ready-to-use" for biological

purpose (e.g., biolabeling and bioimaging) without further surface modifications or ligand exchange reactions.

While the exact mechanism of AuNP formation in the presence of ATP is still not completely understood due to the complex nature of AuNP and nucleotide interactions,[15] we speculate that the binding of ATP on AuNP surface during the crystal growth process results in highly negatively charged nanoparticles due to the presence of phosphate groups. The AuNPs are thus stabilized or protected against the interparticle fusion or aggregation. This mechanism is further supported by the experiments where different nucleotides (i.e., GTP, cytidine 5′-triphosphate (CTP) and thymidine 5′-triphosphate (TTP)) or adenosine bearing different numbers of phosphate groups (i.e., adenosine 5′-diphosphate (ADP), adenosine 5′-monophosphate (AMP) and adenosine) are used as ligands in the AuNP formation process.

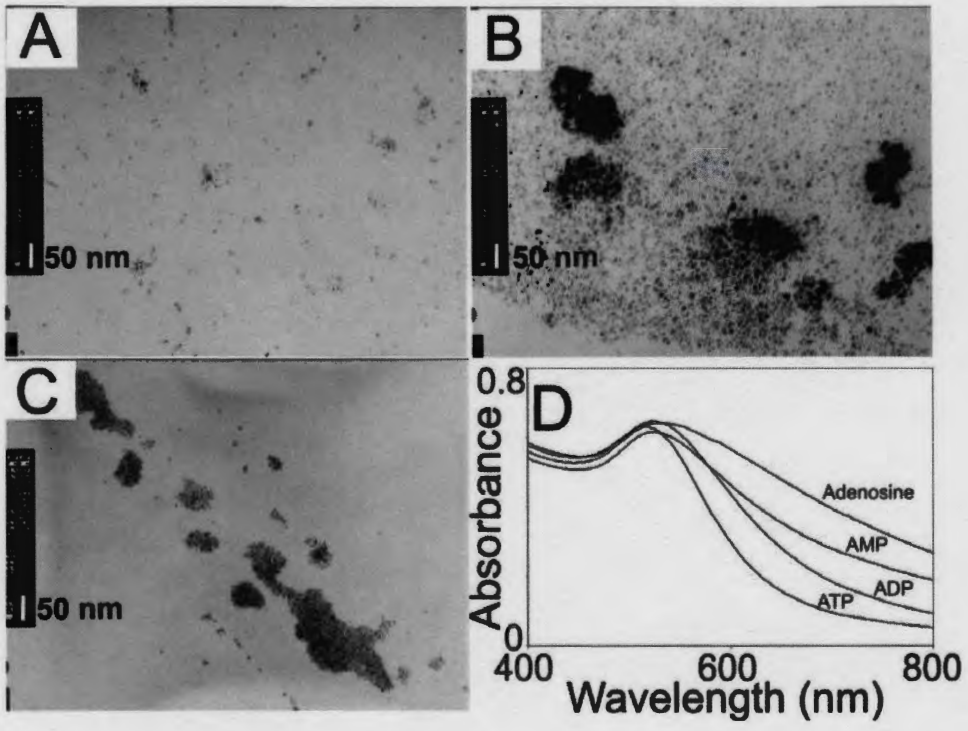

Figure 3.4. *Representative TEM images of AuNPs prepared using ADP (A), AMP (B) and adenosine (C) as capping ligands. Scale bar = 50 nm. (D) UV-Vis spectra of AuNPs prepared using ATP, ADP, AMP or adenosine as ligands. The molar ratio $HAuCl_4$:ligand:$NaBH_4$ using in these experiments was 1:1:16.7.*

Mirkin and co-workers systematically studied the interactions between nucleosides and citrate-capped AuNPs.[15a,b] Their results revealed that adenosine, cytidine, guanosine and thymidine can all bind to AuNP surfaces because the functional groups (e.g., amines and carbonyls) in these nucleosides can coordinate to the metal surface:[15] thymidine was found to have a much lower binding affinity to AuNP surface than the other three nucleosides.[15b] In the present work, we found that all four nucleotides (ATP, GTP, CTP and TTP) yield significantly smaller AuNPs with narrower monodispersity when compared with AuNPs prepared in the absence of ligands (see Supplementary Information, S. Fig. 3.5). Based on the TEM studies, the efficiency of nucleotides in controlling AuNP size and monodispersity in the present study follows the sequence: ATP > CTP > GTP > TTP, indicating that these nucleotides have different affinities to AuNP, which is consistent with the previous study.[15c] Compared to the other three nucleotides, TTP is the least effective ligand to control AuNP growth, as shown by the formation of relatively larger and more polydisperse AuNP when TTP was used as a ligand (see Supplementary Information, S. Fig. 3.5A). A stability study of these nucleotide-capped AuNPs further confirmed that TTP has a much lower binding affinity to AuNP surface than ATP, GTP and CTP: ATP- (or GTP-, CTP-) capped AuNPs are stable at > 1 M NaCl whereas TTP-capped AuNPs aggregate at about 250 mM NaCl. These results, which are in agreement with previous studies,[15] together with the XPS data, strongly suggest that the nucleotides interact with AuNP surfaces through nucleobases during the AuNP growth process. We further speculated that the nucleotides absorbed on the AuNP surface then became the stabilizing ligands: the negatively charged phosphate groups prevented these small particles from aggregating during the growth process.

To further verify this point, experiments were conducted in which adenosines carrying different numbers of phosphate groups were used as capping ligands. As the number of phosphate groups decreases (i.e., from ATP to ADP, AMP and adenosine), more aggregated or fused AuNPs are produced, as shown by TEM images (Fig. 3.4A-C). The AuNP aggregation was also corroborated well with the UV-Vis spectral data (Fig.

3.4D), which shows that the surface plasmon band becomes broader as the number of the phosphate group in the ligands decreases. These results indicate that negatively charged phosphate groups play important roles in protecting AuNPs against aggregation during the crystal growth process and, therefore, in controlling the size and morphology of AuNPs.

3.3 Conclusion

In summary, we present a facile method to prepare highly stabilized water-soluble AuNPs that have precisely and easily tunable sizes that range from 2 to 5 nm, and narrow monodispersity, which provides great opportunities to use these nucleotide-capped AuNPs as novel building blocks for bioconjugation, nanodevices, biosensors and biolabels. The reaction is performed in water at room temperature, and AuNP growth is completed quite rapidly (~2 h). The approach is thus more convenient and environmentally friendly when compared with conventional synthetic approaches. Finally, this work should also provide insight into the nature of the interaction between nucleotide (or nucleic acid) and AuNPs, and thus facilitate the further research where nucleic acids and AuNPs are used for nanoassemblies and biosensing.

3.4 Experimental

Typical synthesis of nucleotide-capped AuNPs: $HAuCl_4$ (10 mM, 60 μL, Sigma) and ATP (or TTP, CTP, GTP, ADP, AMP, and adenosine) (10 mM, 60 μL, Sigma) were added into 2.75 mL ddH_2O in a 4-mL glass vial, and the mixture was incubated at room temperature for 30 min. Freshly prepared $NaBH_4$ solution (100 mM, 100 μL, Sigma) was then quickly added, and the vial was vigorously shaken for 10 s. The reaction was left at room temperature for at least 3 h to ensure the completion of AuNP growth. The final $HAuCl_4$ concentration and reaction volume were fixed at 250 μM and 2.97 mL, respectively, for the experiments where [$HAuCl_4$]:[nucleotide] or [$HAuCl_4$]:[$NaBH_4$] were varied.

Characterization: The (HR)TEM sample was prepared by dropping AuNP solution (4 μL) onto a carbon-coated copper grid. After 1 min, the solution was wicked from the edge of the grid with a piece of filter paper. The TEM and HRTEM images were measured with a JEOL 1200 EX and Philips CM12 transmission electron microscope, respectively. UV-Vis adsorption spectra were measured using a Cary 100 UV-Vis spectrophotometer. For XPS and XRD experiments, samples were prepared as follows: AuNPs were precipitated by centrifugation at 45,000 *rpm* for 30 min. The pellet can be easily redispersed in ddH_2O (1 mL). The solution was centrifuged again and redispersed in ddH_2O for XPS experiments or dried at room temperature under vacuum for 3 days for XRD experiments. For XPS experiment, a few drops of AuNP solutions were put on a glass substrate and dried in air. XPS experiments were conducted on a Leybold Max 200, magnesium anode nonmonochromatic source spectrometer. Peak positions were internally referenced to the C1s peak at 285.0 eV. XRD was performed using a X-ray diffractometer with Cu Kα radiation (wavelength $\lambda = 0.154$ nm) operated at 40 kV and 40 mA. Zeta potentials of AuNPs were measured at room temperature using a ZetaPlus (Brookhaven Instruments Corporation). The reported values were based on 10 measurements with 15 cycles for each sample.

3.5 Acknowledgement

This work was supported by the Natural Sciences and Engineering Research Council of Canada (NSERC), Sentinel: The Canadian Research Network on Bioactive Paper, and the Canadian Institutes for Health Research (CIHR). Y.L. holds a Canada Research Chair.

3.6 References

[1] a) M.-C. Daniel, D. Astruc, *Chem. Rev.* **2004**, 104, 293; b) N. L. Rosi, C. A. Mirkin, *Chem. Rev.* **2005**, 105, 1547; c) E. Katz, I. Willner, *Angew. Chem. Int. Ed.* **2004**, 43, 6042; d) W. Zhao, Y. Gao, S. A. Kandadai, M. A. Brook, Y. Li, *Angew. Chem. Int. Ed.* **2006**, 45, 2409; e) D. Kisailus, M. Najarian, J. C. Weaver, D. E. Morse, *Adv. Mater.*

2005, 17, 1234; f) X. He, H. Liu, Y. Li, S. Wang, Y. Li, N. Wang, J. Xiao, X. Xu, D. Zhu, *Adv. Mater.* **2005**, 17, 2811.

[2] a) R. P. Andres, T. Bein, M. Dorogi, S. Feng, J. I. Henderson, C. P. Kubiak, W. Mahoney, R. G. Osifchin, R. Reifenberger, *Science*, **1996**, 272, 1323; b) B. Dubertret, M. Calame, A. J. Libchaber, *Nat. Biotechnol.* **2001**, 19, 365; c) G. B. Birrell, K. K. Hedberg, O. H. J. Griffith, *Histochem. Cytochem.* **1987**, 35, 843.

[3] a) M. Brust, M. Walker, D. Bethell, D. J. Schiffrin, R. Whyman, *J. Chem. Soc., Chem. Commun.* **1994**, 801; b) I. Hussain, S. Graham, Z. Wang, B. Tan, D. C. Sherrington, S. P. Rannard, A. I. Cooper, M. Brust. *J. Am. Chem. Soc.*, **2005**, 127, 16398.

[4] a) M. J. Hostetler, J. E. Wingate, C. –J. Zhong, J. E. Harris, R. W. Vachet, M. R. Clark, J. D. Londono, S. J. Green, J. J. Stokes, G. D. Wignall, G. L. Glish, M. D. Porter, N. D. Evans, R. W. Murray. *Langmuir*, **1998**, 14, 17; b) T. Yonezawa, K. Yasui, N. Kimizuka, *Langmuir*, **2001**, 17, 271; c) K. Fsumi, A. Suzuki, A. Yamahira, K. Torigoe, *Langmuir*, **2000**, 16, 2604; d) Y. Liu, K. B. Male, P. Bouvrette, J. H. T. Luong, *Chem. Mater.* **2003**, 15, 4172; e) T. Sakai, P. Alexandridis, *Langmuir*, **2004**, 20, 8426. f) M. M. Alvarez, J. T. Khoury, T. G. Schaaff, M. N. Shafigullin, I. Vezmar, R. L. Whetten, *J. Phys. Chem. B* **1997**, 101, 3706.

[5] S. K. Bhargava, J. M. Booth, S. Agrawal, P. Coloe, G. Kar, *Langmuir*, **2005**, 21, 5949.

[6] M. Kimura, S. Kobayashi, T. Kuroda, K. Hanabusa, H. Shirai, *Adv. Mater.* **2004**, 16, 335.

[7] a) W. W. Weare, S. M. Reed, M. G. Warner, J. E. Hutchison, *J. Am. Chem. Soc.* 2000, 122, 12890; b) M. Green, P. O'Brien, *Chem. Commun.* **2000**, 183; c) M. Tamura, H. Fujihara, *J. Am. Chem. Soc.* **2003**, 125, 15742.

[8] a) D. V. Leff, L. Brandt, J. R. Heath, *Langmuir*, **1996**, 12, 4723; b) S. R. Isaacs, E. C. Cutler, J. Park, T. R. Lee, Y. Shon, *Langmuir*, **2005**, 21, 5689; c) L. O. Brown, J. E. Hutchison, *J. Am. Chem. Soc.* **1999**, 121, 882; d) A. Kumar, S. Mandal, P. R. Selvakannan, R. Pasricha, A. B. Mandale, M. Sastry, *Langmuir*, **2003**, 19, 6277; e) N. R. Jana, L. Gearheart, C. J. Murphy, *Langmuir*, **2001**, 17, 6782.

[9] a) R. G. Shimmin, A. B. Schoch, P. V. Braun, *Langmuir*, **2004**, 20, 5613; b) K. Esumi, T. Hosoya, A. Suzuki, K. Torigoe, *Langmuir*, **2000**, 16, 2978; c) T. Teranishi, I. Kiyokawa, M. Miyahe, *Adv. Mater.* **1998**, 10, 596.

[10] a) P. Selvakannan, S. Mandal, S. Phadtare, R. Pasricha, M. Sastry, *Langmuir*, **2003**, 19, 3545; b) R. Lévy, N. T. K. Thanh, R. C. Doty, I. Hussain, R. J. Nichols, D. J. Schiffrin, M. Brust, D. G. Fernig, *J. Am. Chem. Soc.* **2004**, 126, 10076; c) L. Gardea-Torresdey, J. G. Parsons, E. Gomez, J. Peralta-Videa, H. E. Troiani, P. Santiago, M. Jose Yacaman, *Nano Lett.* **2002**, 2, 397; d) M. Zayats, R. Baron, I. Popov, I. Willner, *Nano Lett.* **2005**, 5, 21.

[11] G. M. Blackburn, M. J. Gait, in *Nucleic Acids in Chemistry and Biology*, Oxford University Press, Oxford, **1990**.

[12] a) E. Braun, Y. Eichen, U. Sivan, G. Ben-Yoseph, *Nature*, **1998**, 391, 775; b) R. M. Stoltenberg, A. T. Wolley, *Biomed. Microdev.* **2004**, 6, 105; c) N. Ma, C. J. Dooley, S. O. Kelley, *J. Am. Chem. Soc.* **2006**, 128, 12598.

[13] S. Hinds, B. J. Taft, L. Levina, V. Sukhovatkin, C. J. Dooley, M. D. Roy, D. D. MacNeil, E. H. Sargent, S. O. Kelley, *J. Am. Chem. Soc.* **2006**, 128, 64.

[14] W. Zhao, W. Chiuman, J. C. F. Lam, M. A. Brook, Y. Li, *Chem. Commun.*, **2007**, 3729.

[15] a) M. Ostblom, B. Liedberg, L. M. Demers, C. A. Mirkin, *J. Phys. Chem. B.* **2005**, 109, 15150; b) J. J. Storhoff, R. Elghanian, C. A. Mirkin, R. L. Letsinger, *Langmuir,* **2002**, 18, 6666; c) H. Kimura-Suda, D. Y. Petrovykh, M. J. Tarlov, L. J. Whitman, *J. Am. Chem. Soc.* **2003**, 125, 9014.

[16] D. Y. Petrovykh, H. Kimura-Suda, L. J. Whitman, M. J. Tarlov, *J. Am. Chem. Soc.* **2003**, 125, 5219.

[17] L. Pei, K. Mori, M. Adachi, *Langmuir*, **2004**, 20, 7837.

[18] Mass spectroscopy spectra (see Supporting Information, S. Fig. 3.6) suggest that $NaBH_4$ has no significant effect (or damage) on nucleotide under the investigated conditions.

[19] a) J. Liu, Y. Lu. *Angew. Chem. Int. Ed.* **2006**, 45, 90; b) J. Liu, Y. Lu, *Adv. Mater.* **2006**, 18, 1667.

3.7 Supplementary Information

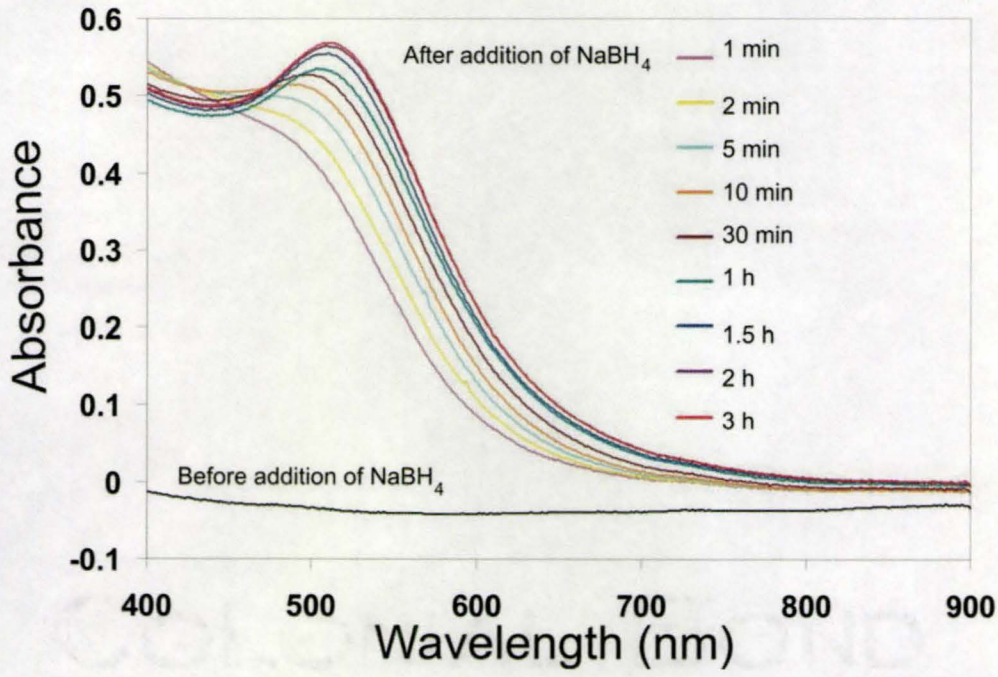

***S. Fig. 3.1**. Kinetic study of AuNP growth in the presence of ATP. Molar ratio of $HAuCl_4$:ATP:$NaBH_4$ in this experiment was 1:1:16.7.*

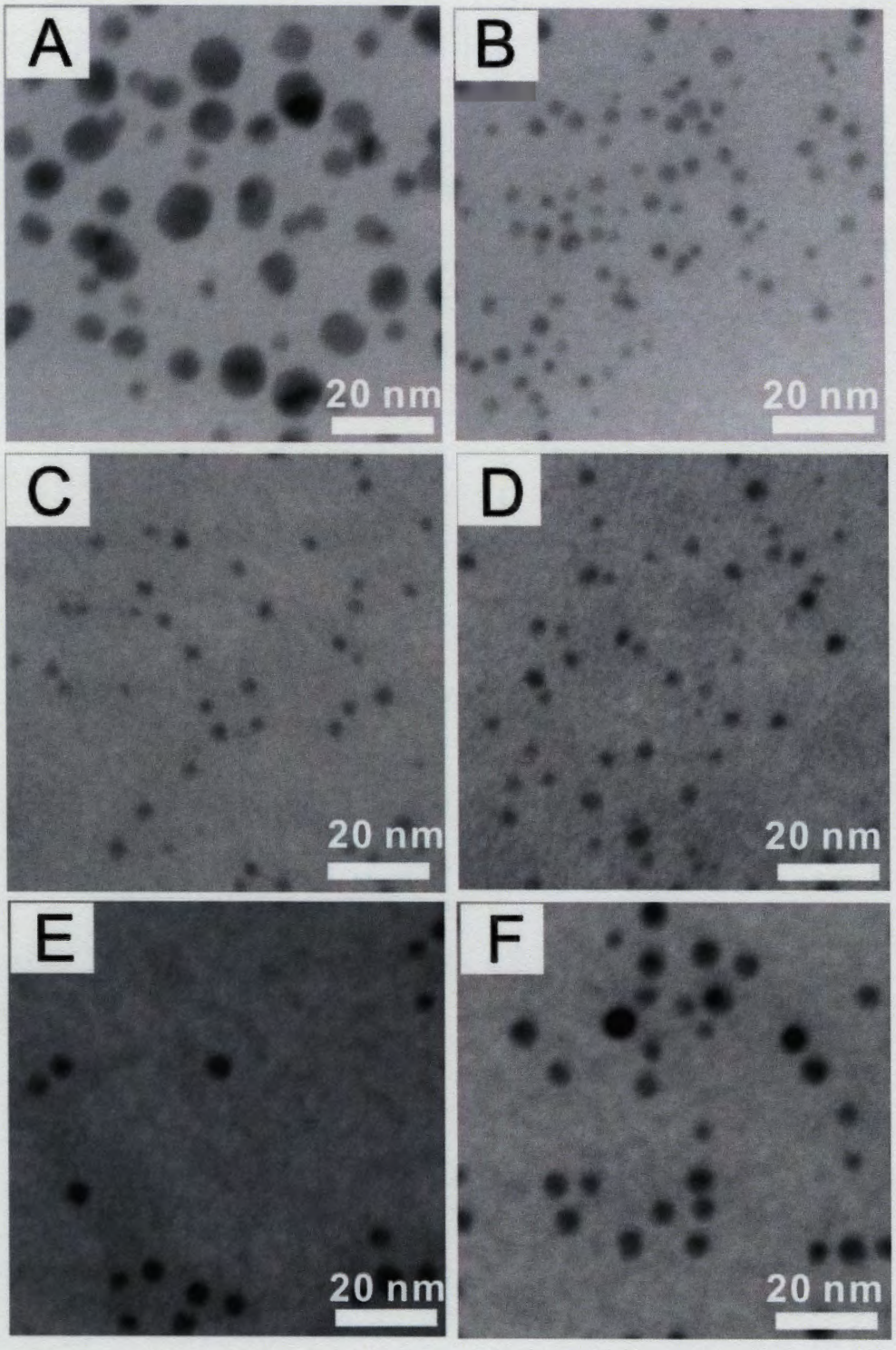

***S. Fig. 3.2**. Higher magnification TEM images for samples in Fig. 3.1A (A), 3.1B (B), 3.2A (C), 3.2B (D), 3.2C (E) and 3.2D (F) of the main text, respectively.*

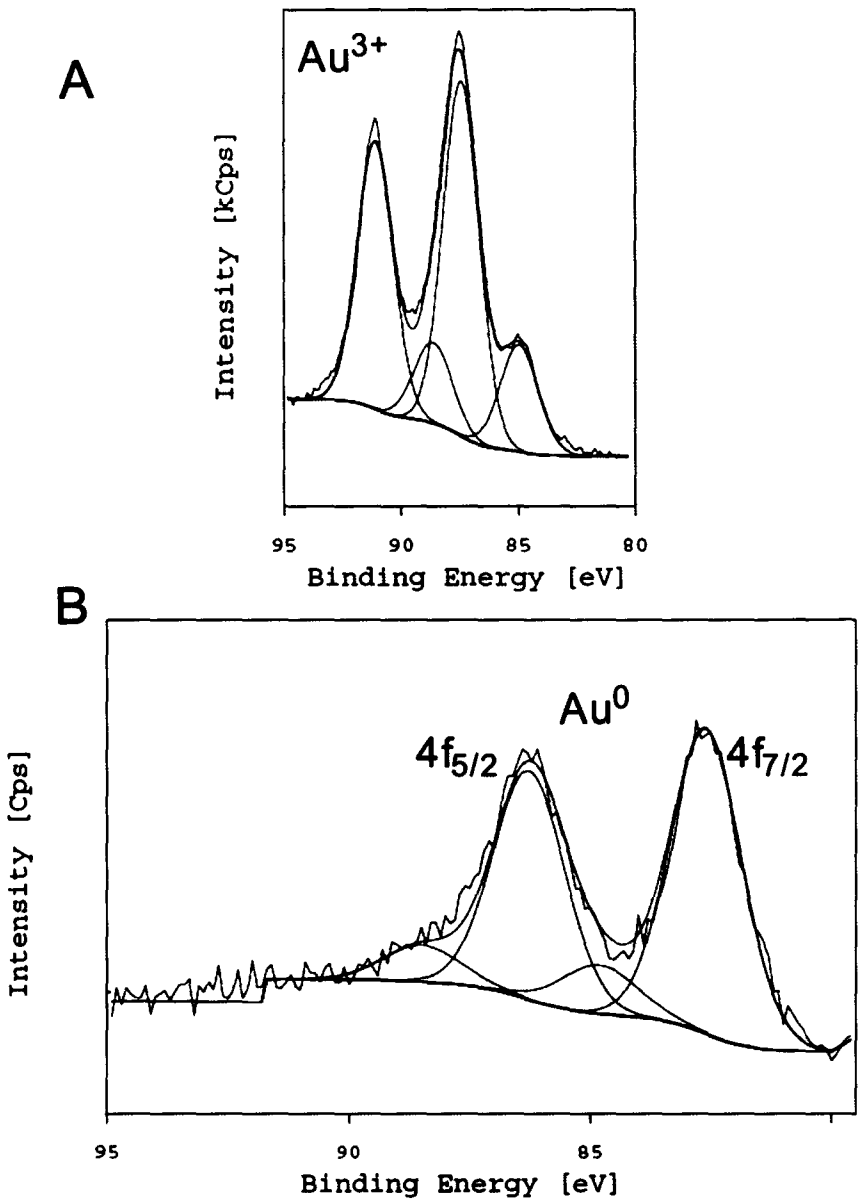

S. Fig. 3.3. *High resolution XPS survey of Au 4f of (A) Au^{3+} before reduction and (B) Au^{0} after reduction. The samples before and after reduction were directly dropped onto a glass substrate and recorded by XPS spectrometer. After reduction (B), the characteristic peak at higher binding energy for ionic Au disappeared. Instead, Au^{0} 4f doublet ($4f_{7/2}$ and $4f_{5/2}$) dominates.[8b] Note that the tiny components in (B) may be due to charge transfers from gold to the nucleotide binding ends (for example, see J. Phys. Chem. B, 2006, 110, 16812).*

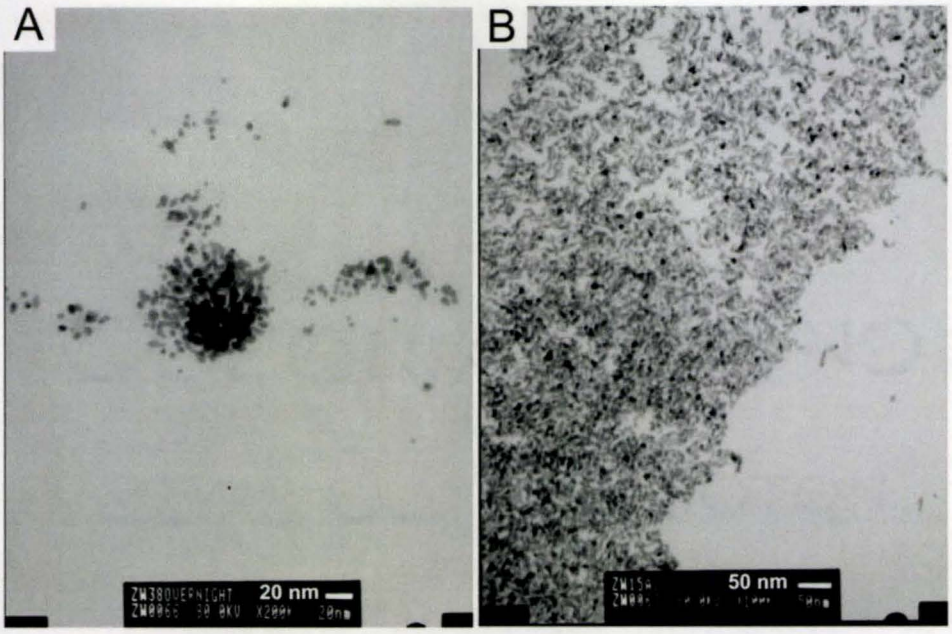

S. Fig. 3.4. *Representative TEM images for ATP-capped AuNPs prepared with the $HAuCl_4$:$NaBH_4$ molar ratio of 1:10 (A) and 1:25 (B), respectively. $HAuCl_4$:ATP molar ratio was 1:10 in these experiments. Scale bar is 20 nm in (A) and 50 nm in (B), respectively.*

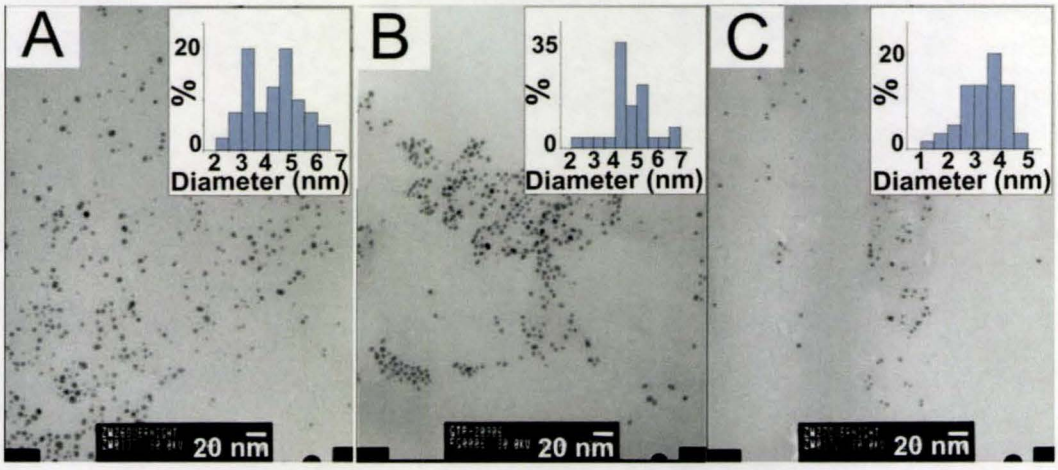

S. Fig. 3.5. *Representative TEM images for AuNPs prepared using TTP (A), GTP (B) and CTP (C) as capping ligands. The average sizes of these AuNPs are 4.9 ± 1.01 nm (A), 4.5 ± 0.96 nm (B) and 4.0 ± 0.77 nm (C), respectively. The molar ratio $HAuCl_4$:ligand:$NaBH_4$ was 1:1:16.7. Scale bar is 20 nm.*

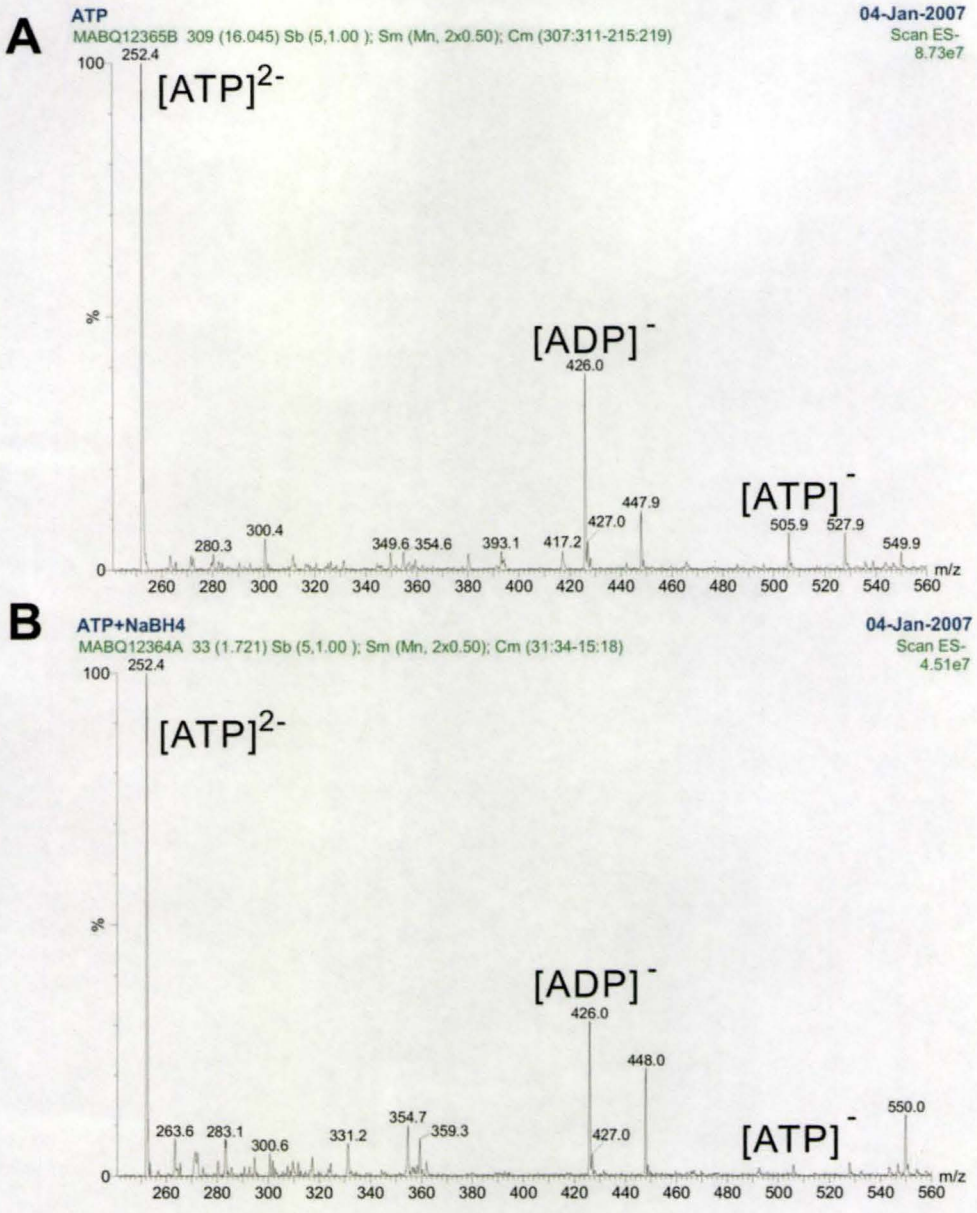

S. Fig. 3.6*. Mass spectroscopy (MS) spectra for (A) ATP (B) ATP after treatment with $NaBH_4$ under the same conditions (e.g. ATP and $NaBH_4$ concentrations, room temperature, reaction time of 2 h) with that for preparation AuNPs. As shown in (A), ATP itself (~ 20-25 %) slowly decomposes to ADP under the investigated conditions (This uncatalyzed hydrolysis of ATP is well known in the literature. For example, Chemistry & Biology, 1995, 2, 729). The $NaBH_4$ treatment did not affect the decomposition process, which indicates that there is no significant damage of ATP by $NaBH_4$ during the reduction process.*

Chapter 4: Enzymatic Cleavage of Nucleic Acids on Gold Nanoparticle: A Generic Platform for Facile Colorimetric Biosensors

The following chapter was published in Small under the citation:

Weian Zhao, Jeffrey C. F. Lam, William Chiuman, Michael A. Brook, Yingfu Li. Enzymatic cleavage of nucleic acid on gold nanoparticle: a generic platform for facile biosensors. *Small*, 2008, in press

Note that Weian Zhao and Jeffrey C. F. Lam contributed equally to this paper. I and Jeffrey C. F. Lam were responsible for all data collection and analysis. William Chiuman provided helpful suggestions on DNA enzyme design and function. I wrote the first draft of the manuscript and Jeffrey C. F. Lam then revised it. Dr. Brook and Dr. Li provided editorial input to generate the final draft of the paper.

4.1 Abstract

The enzymatic cleavage of nucleic acids (DNA or DNA with a single RNA linkage) on well-dispersed gold nanoparticles (AuNPs) was exploited in the design of facile colorimetric biosensors. The assays were performed at salt concentrations such that DNA-modified AuNPs were barely stabilized by the electrostatic and steric stabilization. Enzymatic cleavage of DNA chains on the AuNP surface destabilized the AuNPs, resulting in a rapid aggregation driven by van der Waals attraction, and a red-to-purple color change. Two different systems were chosen, DNase I (a DNA endonuclease) and 8-17 (a Pb^{2+}-depedent RNA-cleaving DNAzyme), to demonstrate the utility of our assay for the detection of metal ions and sensing enzyme activities. Compared with previous studies where AuNP aggregates were converted into dispersed AuNPs by enzymatic cleavage of DNA crosslinkers, the present assay is technically simpler. Moreover, the accessibility of DNA to biomolecular recognition elements (e.g. enzymes) on well-dispersed AuNPs in our assay appeared to be higher than that embedded inside aggregates. This biosensing system should be readily adaptable to other enzymes or substrates for detection of analytes such as small molecules, proteases and their inhibitors.

4.2 Introduction

DNA-modified AuNPs have attracted considerable attention in the last decade due to their utility in biosensors and nanotechnology.[1] AuNPs, with unique physical properties, particularly colors associated with their surface plasmon resonance, are perfectly suitable materials for colorimetric biosensors[1,2] and building blocks for nanostructure assembly.[1,3] The nature of DNA hybridization ensures the specificity and precision required for biosensors and programmable nanoassembly.[1,3,4] Strikingly, DNA molecules on AuNPs can be manipulated in a desirable manner by enzymatic reactions that are routinely used in molecular biology such as cleavage, ligation and polymerisation,.[4] This greatly expands our capacity to assemble and disassemble these building blocks into well-defined nanostructures.[5]

Compared to the efforts made in nanostructure assembly and disassembly, there are only a few studies using enzymatic manipulation of DNA-modified AuNPs for biosensing.[6,7,8] Liu and Lu reported a Pb^{2+} biosensor where they first used a DNAzyme (a man-made, DNA-based enzyme), known as "8-17", and its DNA substrate to assemble AuNPs into three-dimensional aggregates.[6] The enzyme-substrate pairs served as crosslinkers in AuNP aggregates where the substrate strand was cleaved by the DNAzyme strand upon addition of Pb^{2+}, resulting in the dissociation of AuNPs and a purple-to-red color change.[6] More recently, Mirkin and co-workers reported that the cleavage of DNA crosslinkers in AuNP aggregates by protein enzymes such as DNase I (a natural DNA-cleaving protein enzyme) could cause similar dissociation of AuNPs.[7] The purple-to-red color change was therefore used in their study to evaluate enzyme activity and inhibition. The common feature associated with these assays is that AuNP aggregates are first made using inter-particle DNA crosslinking and these aggregates are then broken into dispersed AuNPs upon enzymatic cleavage of DNA crosslinkers. Both studies took advantage of the fact that relevant enzymes can manipulate DNA on AuNPs.

To explore new dimensions of this interesting research area, we provide herein an alternative strategy in which AuNPs are associated into aggregates upon enzymatic cleavage of nucleic acid on well-dispersed AuNPs. In our strategy, the AuNP aggregation is modulated by the colloidal stability changes[9] that is triggered by a specific biomolecular recognition event. We reported previously that the dissociation of DNA strands (colloidal stabilizers) from AuNP surfaces upon binding of a small organic molecule resulted in AuNP aggregation at a desirable salt concentration.[9a] We speculate that we can adopt the similar aggregation mechanism for enzymatic manipulation of DNA-modified AuNPs and the resultant assays should find a number of applications in biosensors, diagnostics and drug discovery. Our concept is illustrated in Figure 4.1. Before enzymatic cleavage, DNA-modified AuNPs are stable even at relatively high salt concentrations (e.g. 40 mM $MgCl_2$) due to the electrostatic and steric stabilization provided by tethered negatively charged DNA polymers.[10] However, the removal of

surface-bound, colloidally stabilized DNA strands by enzymatic cleavage will lead to the rapid aggregation of AuNPs at the same salt concentration. The red-to-purple color

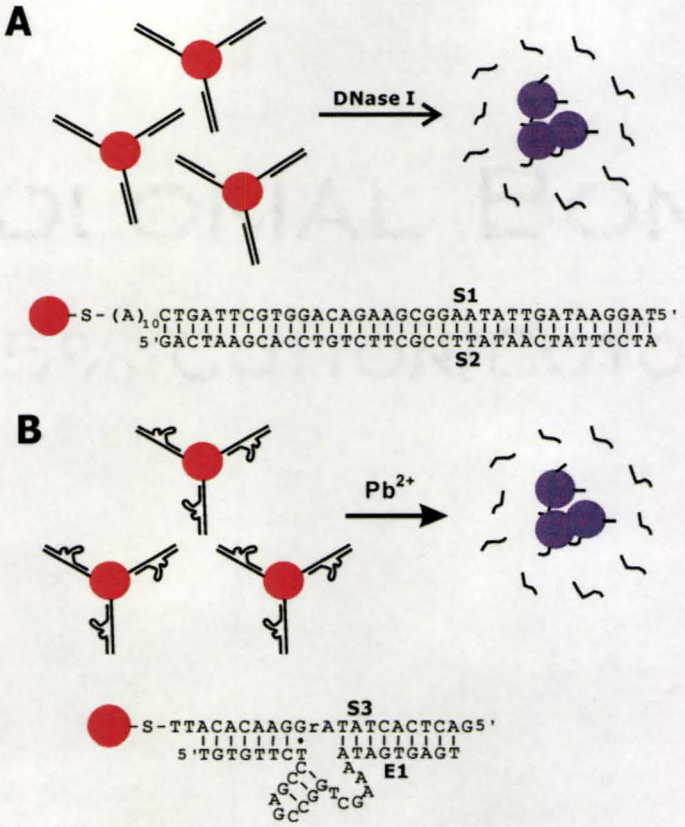

***Figure 4.1**. Schematic illustration of AuNP aggregation and color change triggered by the enzymatic cleavage of DNA on AuNPs. Before enzymatic cleavage, DNA-modified AuNPs are stable at a relatively high salt concentration due to the electrostatic and steric stabilization. The removal of DNA (colloidal stabilizer) on the AuNP surface by enzymatic cleavage destabilizes the AuNP and results in a rapid aggregation. (A) Cleavage of a DNA duplex by DNase I. (B) Pb^{2+}-mediated cleavage of an RNA-containing DNA substrate by the 8-17 DNA enzyme.*

change associated with this event can therefore be used to sense the activity of the cleaving enzyme.

Two different enzymatic systems were used in our proof-of-concept experiments where DNA molecules on AuNPs are cleaved by DNase I or 8-17. These systems were chosen as models for the following reasons. (1) They are of great biological and/or

practical importance. For instance, endonucleases (such as DNase I) play key roles in biological process such as replication, repair and recombination of nucleic acids.[7,11] There is a general need to develop facile biosensors for sensing endonuclease activity and inhibition, which could help the diagnosis of endonuclease-associated diseases or facilitate the discovery of drugs that inhibit these enzymes.[7,11] Meanwhile, Pb^{2+} sensing assays are very useful in fields such as waste treatment and environmental monitoring.[6] (2) As mentioned above, both systems have been used in previous AuNP-based assays where AuNP aggregates were first constructed and then broken into dispersed AuNPs.[6,7] By applying the same enzyme reactions, direct comparison between our strategy and the ones previously reported can be made.

4.3 Results and Discussion

The AuNPs (~13 nm in diameter) used in this study were prepared using the previously reported citrate reduction protocol[12] (see Experimental Section). For DNase I assay, S1-modified AuNPs were prepared via Au-S chemistry according to the reported procedure[12] (the sequence of S1 is shown in Figure 4.1A). S1-modified AuNPs were then briefly treated with 6-mercaptohexan-1-ol (MCH) (~4 μM, 30 min), which initiated a ligand exchange reaction to remove non-specifically adsorbed and some of the chemically bound DNA molecules from nanoparticle surfaces in order to improve the accessibility of DNA on AuNPs by the enzymes used in this study.[9a,13]

To determine the DNA concentration on each AuNP before and after the MCH exchange reaction, radiolabeled S1 (see Figure 4.1A for its sequence) was incorporated in the DNA coupling step (see Experimental Section). After DNA coupling and MCH exchange reaction, the AuNPs were isolated using centrifugation. By comparing the radioactivity on the AuNP pellets and in the supernatant, we found that there were ~100 S1 molecules on each AuNPs after the coupling reaction. The subsequent MCH exchange reaction removed ~30 % of the tethered S1 from each AuNP, and thus, ~71 S1 molecules remained on each AuNP after MCH treatment.

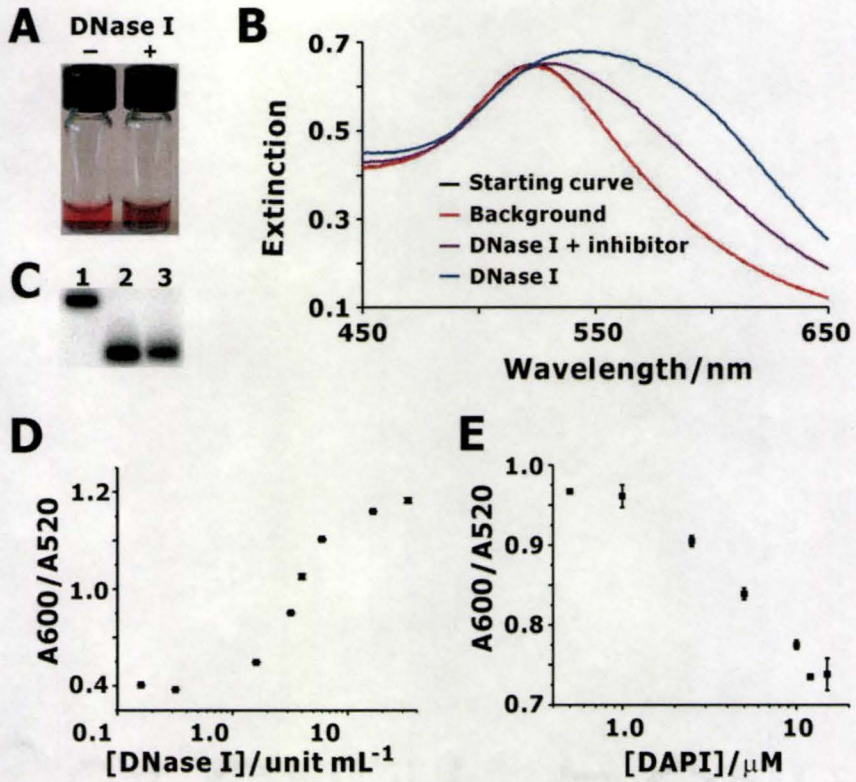

Figure 4.2. *DNase I assay. (**A**) Photographs of Au/S1-2 solution in the absence (left) and presence (right) of DNase I in DNase I buffer (40 mM $MgCl_2$, 0.5 mM $CaCl_2$, 10 mM Tris-HCl, pH 7.5). DNase I reaction was performed at room temperature for 1 min. (**B**) Representative UV/visible spectra of Au/S1-2 in DNase I buffer recorded at 0 min (starting curve, black curve) and 1 min (background, red curve) in the absence of DNase I. Note that these two curves are largely overlapped, suggesting that no significant color change (aggregation) occurred in 1 min at the studied salt concentration in the absence of DNase I. The addition of DNase I (4 units/mL) caused a significant red-shift of surface plasmon band in UV/visible spectra (DNase I, Blue curve). On the other hand, the presence of DNase I inhibitor (DAPI, 7.5 μM), highly inhibited the DNase I activity (DNase I + inhibitor, purple curve). Blue and purple curves were recorded at 1 min after the addition of DNase I. (**C**) 10 % denaturing PAGE analysis of radioactive S1 (lane 1), cleaved product of radioactive S1 in duplex with S2 by DNase I in solution-phase (lane 2) and on AuNPs (lane 3), respectively. Note that the intensity of bands was not used for quantification purpose. Rather, lane 1 and 2 served as markers to assess the size of cleaved product from AuNPs in lane 3. (**D**) A600/A520 calculated from UV/visible spectra recorded at 1 min was plotted as a function of DNase I concentration. (**E**) A600/A520 calculated from UV/visible spectra recorded at 4 min was plotted as a*

function of DAPI concentration. The DNase I concentration used for inhibitor study was 4 units/mL. The effective inhibitor detection range under investigated conditions was from ~1-10 μM. It is interesting to note that, at high concentration (e.g. 100 μM), DAPI itself could cause AuNP aggregation presumably through an inter-particle crosslinking mechanism by its amidine ending groups. Spectra in (B), (D) and (E) were recorded at 37 ° C.

The complementary DNA S2 was then allowed to hybridize with S1 to form DNA duplexes (the substrate for DNase I) on AuNPs (referred to as Au/S1-2). Au/S1-2 were then dispersed in 1× DNase I reaction buffer (10 mM Tris-HCl, pH 7.5, 2.5 mM $MgCl_2$ and 0.5 mM $CaCl_2$). The stability of Au/S1-2 towards salt-induced aggregation was then studied by gradually adding 1 M $MgCl_2$ stock solution to the Au/S1-2 solution. Based on whether a red-to-purple color change or a significant UV/visible spectra shift (see Figure S4.1 in Supporting Information) was observed in 10 min, Au/S1-2 was determined to be stable at ≤40 mM $MgCl_2$ while higher concentrations of $MgCl_2$ (e.g. 50 mM $MgCl_2$) resulted in significant color change or UV/visible spectral shift in 10 min after the addition of $MgCl_2$.

Our hypothesis is that the removal of DNA strands from the surface of nanoparticles, which serve as electrostatic and steric stabilizers at relatively high salt concentrations (e.g. 40 mM $MgCl_2$), results in destabilization and aggregation of AuNPs, a process driven by van der Waals attraction.[10] As anticipated, the addition of DNase I[14] (4 units/mL) to Au/S1-2 solution (250 μL; Au/S1-2: ~2.25 nM; $MgCl_2$: 40 mM; $CaCl_2$: 0.5 mM; Tris-HCl: 10 mM, pH 7.5) generated a rapid red-to-purple color change in 1 min (Figure 4.2A), corresponding to a red shift and broadening of surface plasmon band of AuNP in the UV-visible spectrum (Figure 4.2B).

To verify the hypothesis that AuNP aggregation was induced by the dissociation of DNA from AuNP surfaces upon treatment of DNase I, radiolabeled S1 was again used in the preparation of Au/S1-2. After treatment of DNase I, AuNPs were spun down using centrifugation (22,000 *g*, 16 min). By measuring the radioactivity in the supernatant and on the AuNP pellet, we found that ~82 % of DNA on AuNPs had been cleaved by DNase I. To further confirm the radioactivity in the supernatant was due to cleaved DNA

fragments, instead of the dissociation of intact S1 from AuNP (given that the Au-S bond is kinetically labile[5d]), the supernatant was analyzed by 10 % denaturing polyacrylamide gel electrophoresis (PAGE). As shown in Figure 4.2C, the DNA in the supernatant (lane 3) was comprised of cleaved fragments, as compared with the product obtained from treatment of the free DNA duplex with DNase I (lane 2).

Kinetic studies on the color change in the presence of various amounts of DNase I were studied by UV/visible spectroscopy. It was found that the rate of color change was directly related to the amount of DNase I used in the assay: faster color changes were observed when more DNase I was used. To quantify the concentration of DNase I, the ratios of the absorbance at 600 and 520 nm (A600/A520) at 1 min after the addition of DNase I were plotted as a function of DNase I concentration (Figure 4.2D). The detection range of DNase I in the current assay was shown to range from ~0.5 unit/mL to ~40 unit/mL. One important feature of this assay is that the color change (or response time) is very rapid, particularly when compared with previous assay based on the dissociation of AuNP aggregates into dispersed AuNPs triggered by the same enzymatic reaction.[7] For instance, at the same DNase I concentration (i.e. 10 unit/mL), previous assays required ~30 min whereas our system took merely 1-2 min to reach a maximum color change. We attribute this to the previously established theory[2e,6] that biomolecules on well-dispersed nanoparticles are more accessible to molecular recognition elements than those embedded inside of nanoparticle aggregates.

Importantly, this assay can be used for evaluating the efficiency of enzyme inhibitors, and therefore could be potentially used for drug screening.[7] The addition of 4′,6′-diamidino-2-phenylindole (DAPI) (7.5 μM), a known DNase I inhibitor[7,15] that binds and protects DNA duplex from enzymatic cleavage, to the Au/S1-2 solution significantly inhibited DNase I activity, resulting in reduced changes (Figure 4.2B). Based on the level of change in A600/A520, the degree to which DNase I was inhibited can also be directly related to the amount of inhibitor used in the assay (Figure 4.2E).

In order to show the generality of our system to detect not only the activities of enzymes but other analytes, we employed the Pb^{2+}-dependent 8-17 DNAzyme. This

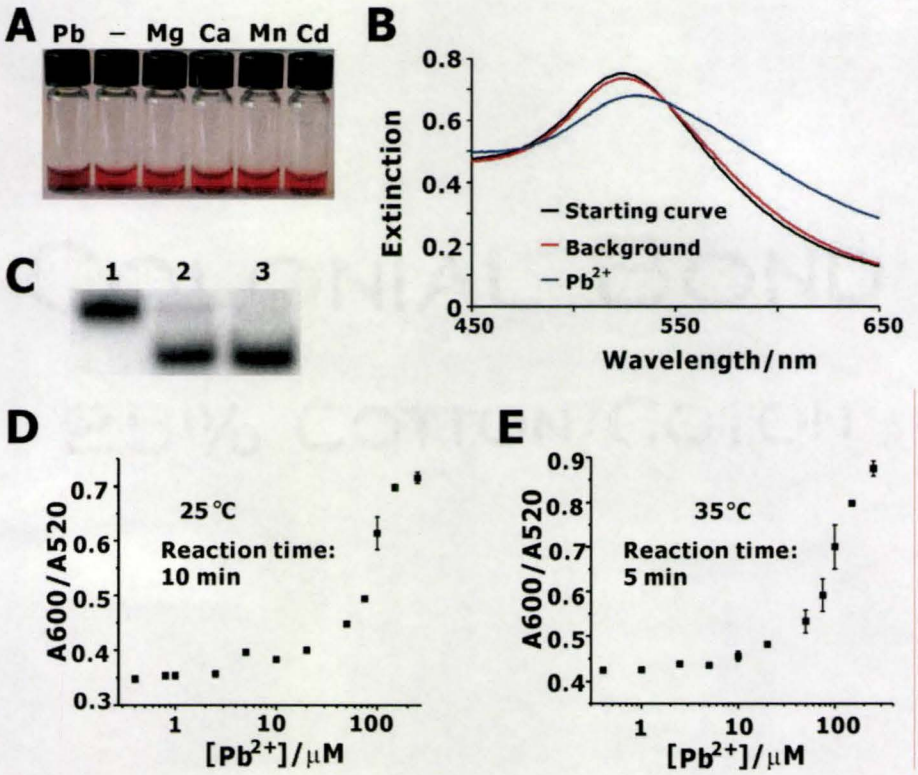

Figure 4.3. *(A) Photographs of Au/S3-E1 solution in the presence of 100 μM Pb^{2+} or other control divalent metal ions. The reaction was performed in "8-17" DNA enzyme buffer (40 mM $BaCl_2$, 300 mM NaCl, 50 mM Tris-HCl, pH = 8.8) at room temperature for 10 min. (B) Representative UV/Visible spectra of Au/S3-E1 in "8-17" DNA enzyme buffer and the spectra were recorded at 0 min (starting curve, black curve) and 10 min (background, red curve). Blue curve (Pb^{2+}) is the UV/visible spectrum of Au/S3-E1 in "8-17" DNA enzyme buffer with 100 μM Pb^{2+}. The spectrum was recorded at 10 min after the addition of Pb^{2+}. (C) 10 % denaturing PAGE analysis of S3 (lane 1), cleaved product of S3 by "8-17" DNA enzyme in solution-phase (lane 2) and AuNPs (lane 3), respectively. (D) A600/A520 calculated from UV/visible spectra recorded at 10 min at room temperature (25 °C) was plotted as a function of Pb^{2+} concentration. (E) A600/A520 calculated from UV/visible spectra recorded at 5 min at 35 °C was plotted as a function of Pb^{2+} concentration.*

DNA enzyme is capable of cleaving a DNA substrate with a single RNA linkage (rA) in the presence of Pb^{2+} (Figure. 4.1B).[16a,17] Originally discovered by Joyce and coworkers as a Mg^{2+}-dependent catalytic DNA,[16b] the 8-17 DNAzyme was found later by the Lu

group to be able to use Pb^{2+} ion as a more efficient divalent metal ion cofactor. It has been extensively used in fluorescence-based assays[16a] as well as AuNP-based colorimetric assays for Pb^{2+} detection.[17] In the present work, an RNA-containing DNA substrate, S3 (see Figure 4.1B for its sequence), was first coupled to AuNP, followed by MCH exchange (see Experimental Section). A similar radioactivity study as described in DNase I section above revealed that there were about 180 and 100 S3 molecules on each AuNP before and after the MCH exchange reaction, respectively. Finally, DNA enzyme strand (E1; see Figure 4.1B) was hybridized with S3 on AuNPs and the product is referred to as Au/S3-E1.

The stability of Au/S3-E1 towards salt-induced aggregation was first examined. Since high concentrations of Mg^{2+} (e.g. 40 mM) can also catalyze the cleavage reaction of the 8-17 DNA enzyme,[16c,18] we chose to use Ba^{2+} to tune the AuNP stability because it has no effect on the activity of this DNAzyme (unpublished work). When Au/S3-E1 was titrated with increasing amounts of Ba^{2+}, it maintained colloidal stability at $\leq$40 mM Ba^{2+} at pH 8.8 (50 mM Tris-HCl, along with 300 mM NaCl) for at least 10 min after the addition of $BaCl_2$. Higher Ba^{2+} concentrations (e.g. 50 mM $BaCl_2$) resulted in significant red-to-purple color change or UV/visible spectral shift. The Pb^{2+} sensing assay was therefore conducted in the presence of 40 mM Ba^{2+}, 300 mM NaCl at pH 8.8.

The addition of Pb^{2+} (100 μM) indeed generated a rapid red-to-purple color change in 10 min at room temperature (Figure 4.3A). The corresponding red shift of the initial surface plasmon band at 520 nm was also observed on UV/visible spectrum (Figure 4.3B). It is important to note that in the presence of 40 mM Ba^{2+}, the effect of small amounts of Pb^{2+} (e.g. 100 μM) on Au/S3-E1 stability in term of screening surface changes is negligible. Indeed, in control tests where 100 μM of Mg^{2+}, Mn^{2+}, Ca^{2+} or Cd^{2+} (all of which had similar charge screening ability with Pb^{2+}) was used, no color change (Figure 4.3A) or significant spectral shift (data not shown) was observed. This demonstrates the specificity of our assay and indicates that the color change observed in the presence of Pb^{2+} was induced by the loss of cleaved DNA fragments from AuNPs. To verify this claim, radiolabeled S3 was conjugated on AuNPs and subsequently cleaved by

8-17. By measuring the radioactivity in the supernatant and on the pellet after centrifugation, it was discovered there was ~55% of S3 was cleaved. PAGE analysis further confirmed the DNA found in the supernatant was the expected cleavage product of the 8-17 DNA enzyme (Figure 4.3C). In previous studies,[6] AuNPs were first crosslinked by 8-17 DNA and its substrate to form AuNP aggregates. These crosslinkers were subsequently cleaved by 8-17 upon addition of Pb^{2+}, resulting in the dispersion of the AuNPs. It was found that the cleaved fragments could not easily dissociate from AuNP aggregates presumably due to steric hindrance of the aggregates.[6] Therefore, these assays had to be performed at lower salt concentrations (30-100 mM NaCl) to facilitate the dissociation of DNA duplex fragments insides AuNP aggregates. Moreover, small pieces of DNA (called invasive DNA)[6a] or asymmetric DNA enzymes[6b] were often required to replace the cleaved DNA fragments from aggregates and accelerate the dissociation process. By contrast, the cleavage and dissociation of chimeric RNA/DNA substrate in the present work was conducted on well-dispersed AuNPs that have much less steric hindrance than AuNP aggregates. As a result, even at high ionic strength (i.e. 40 mM $BaCl_2$, 300 mM NaCl), a large portion of the substrate (~55%) can be cleaved and dissociate from the AuNP surface.

The A600/A520 ratio of Au/S3-E1 at 10-min reaction time was plotted as a function of Pb^{2+} concentration (Figure 4.3D). Under our experimental conditions, the effective Pb^{2+} detection range at room temperature is ~20 μM to 200 μM. Increasing reaction temperature to 35 °C increased the rate of color change and shifted the detection limit to a lower range (~10 μM) (Figure 4.3E). This is presumably because, at a higher temperature, the DNA enzyme cleaves the substrate more effectively[17b] and the dissociation of cleaved fragments from AuNP surface is faster.

With the aim of developing rapid sensing assays, the assaying time used in our work was set to 1 min for DNase I sensing assays and 10 min for Pb^{2+} sensing assays. Within the assaying time allocated for each assay, the untreated AuNPs did not undergo noticeable aggregation or color change at the chosen salt concentration. However, if longer assaying times (e.g. 1 h) were used, the untreated AuNPs could undergo slow

aggregation and the solution gradually changed color from red to purple (see Figure S4.2 for the experimental data). Therefore, if the assays are performed for longer times, the background signal will increase. On the other hand, longer assay times can improve the detection sensitivity. For instance, in the Pb^{2+} assay, 2 μM of Pb^{2+} can be detected within a 1-h assay time (data not shown).

4.4 Conclusions

In summary, we have demonstrated the use of enzymatic cleavage of DNA on well-dispersed AuNPs for designing simple colorimetric biosensors. The method relies on reducing AuNP stability by the removal of colloid stabilizers through enzymatic cleavage at a pre-tuned salt concentration. The basic principle is that once inter-particle repulsion forces from electrostatic and steric stabilization are significantly reduced, van der Waals attraction dominates, which results in rapid AuNP aggregations.[9,10]

Compared with previous studies where AuNP aggregates were converted into dispersed AuNPs by enzymatic cleavage of DNA crosslinkers,[6,7] the present assay is technically simpler. Specifically, it eliminates the extra steps required to prepare AuNP aggregates and avoids the difficulties associated with handling AuNP aggregates due to their instability and sensitivity to experimental conditions such as temperature, pH, ionic strength and gravity.[6,7] Most importantly, since the enzymatic reactions were conducted on well-dispersed AuNPs, the accessibility of DNA by enzymes appeared to be better in comparison to AuNP aggregates where the DNA stranded are embedded inside. It is important to note, though, that the enzymatic cleavage efficiency on well-dispersed AuNPs is still not comparable to solution-phase reaction. For instance, the efficiency of cleavage of DNA duplex on AuNPs by DNase I under the studied conditions was about 82% whereas the cleavage efficiency in solution phase at the same conditions was nearly 100% (data not shown). Similarly, the cleavage efficiency using the Pb^{2+}-mediated DNA enzyme on AuNPs and in solution phase was about 55% and 95%, respectively (data not shown). This may partially explain why previous Pb^{2+} sensing assays,[17] where cleavage reactions were conducted in solution phase first and the cleaved fragments were then

used for AuNP assemblies, could achieve better sensitivity (~0.4 μM) than the present assay. Finally, a conceivable disadvantage of the present assay is that enzyme reaction may not be performed at its optimized conditions (e.g. optimal salt concentration) since a specific salt concentration is required to modulate the AuNP stability and aggregation. Therefore, one may need to either choose a salt that has no effect on the enzymatic activity (such as Ba^{2+} in the 8-17 DNAzyme assay) or seek a compromise between enzyme performance and AuNP stability at a specific salt concentration.

The proof-of-concept experiments in the current study exploited DNA or chimeric RNA/DNA substrates of relevant enzymes to assess endonuclease activity or detect Pb^{2+} ion. We reason that similar strategies can be adopted for the detection of other analytes such as small molecules, particularly when allosteric DNA enzymes (or aptazymes)[19] are incorporated. Meanwhile, the use of other substrates such as peptides, amino acids, nucleotides can further expand the detection scope of this assay to other targets such as proteases and their inhibitors.[20]

4.5 Experimental Section

Materials: Trisodium citrate, $HAuCl_4$, 6-mercaptohexan-1-ol (MCH), $Pb(OAc)_2$, 4′,6′-diamidino-2-phenylindole (DAPI) and ethyl acetate were purchased from Sigma and used as received. [γ-^{32}P] ATP was obtained from Amersham Biosciences. Thiol-modified and unmodified DNA were obtained from Integrated DNA Technologies (IDT) and purified by standard 10% denaturing (8M urea) polyacrylamide gel electrophoresis (PAGE). DNase I and T4 polynucleotide kinase (PNK) were purchased from MBI Fermentas.

Preparation of 13 nm AuNPs[12]: Trisodium citrate (25 mL, 38.8 mM) was added to a boiling solution of $HAuCl_4$ (250 mL, 1 mM). Within several minutes, the color of the solution changed from pale yellow to deep red. The mixture was allowed to heat under reflux for 30 min to ensure complete reduction and was slowly cooled to room temperature. The nanoparticles were filtered through a 450-nm filter and its concentration

was estimated by UV/visible spectroscopy to be about 13 nM, based on an extinction coefficient of 2.7×10^8 M^{-1} cm^{-1} at $\lambda = 520$ nm for 13 nm particles.[12a]

DNA radiolabeling and radioactivity measurements: Radiolabeled DNA molecules were prepared via a phosphorylation reaction using the manufacturer-supplied protocol. Briefly, a typical phosphorylation reaction (50 μL) contained DNA (5 μL, 100 μM), 1× reaction buffer (50 mM Tris-HCl (pH 7.6), 10 mM $MgCl_2$, 5 mM DTT, 0.1 mM spermidine and 0.1 mM EDTA), [γ-^{32}P] ATP (1 μL) (10 μCi), and PNK (1 μL, 10 units). The radiolabeled DNA was purified using standard 10% denaturing PAGE and quantified by standard spectrophotometer using absorbance at 260 nm. Radioactivity was measured using a Geiger counter (GSM 500, Wm. B. Johnson & Associates Inc.) for estimating DNA concentrations before and after MCH treatment on each AuNP or using PhosphoImager and ImageQuant software (Molecular Dynamics) for quantifying DNA cleavage efficiency on AuNPs.

Conjugation of thiol-modified DNA on AuNPs[12]: DNA modified AuNPs were prepared by mixing the AuNP solution (600 μL, ~13 nM) with thiol-modified oligonucleotides (280 μL, 6.6 μM; S1 for DNase I: 5′-TAG GAA TAG TTA TAA GGC GAA GAC AGG TGC TTA GTC AAA AAA AAA A-thiol-3′; or S3 for "8-17" DNA enzyme: 5′-GAC TCA CTA Tribo-AG GAA CAC ATT-thiol-3′. To quantify the DNA concentration on each AuNPs after coupling, radiolabeled DNA was incorporated according to reported procedures[12]. The solution was initially incubated at room temperature for 12 h. Subsequently, Tris-HCl (10 μL, 1 M, pH 7.4) and aqueous NaCl (90 μL, 1M) were added to the mixture and incubated for another 28 h. Additional Tris-HCl (5 μL, 1M, pH 7.4) and aqueous NaCl (50 μL, 5 M) were added and the mixture was further incubated for 18 h at room temperature. The final solution was separated in a centrifuge at 22,000 *g* for 16 min. The precipitated DNA-modified AuNPs (Au/S1 or Au/S3) were washed with 600 μL of the DNase I buffer (10 mM Tris-HCl, pH = 7.5, 2.5 mM $MgCl_2$ and 0.5 mM $CaCl_2$) or the DNA enzyme buffer (50 mM Tris-HCl, pH = 8.8, 300 mM NaCl) through centrifugation. Finally, the DNA-modified AuNPs were redispersed in the same buffer (1.2 mL).

MCH treatment: The DNA-modified AuNPs (Au/S1 or Au/S2) solution (radiolabeled DNA-modified AuNPs were used to access the DNA concentration on each AuNPs after MCH exchange reaction) prepared above was first diluted with an equal volume of the DNase I buffer or the DNA enzyme buffer. MCH was then added to the mixture to reach a final concentration of ~4 μM. The MCH treatment was performed at room temperature for 30 min and the reaction was quenched by adding an equal volume of ethyl acetate in order to remove excess MCH from the aqueous solution. Finally, the AuNPs were spun down using centrifugation and redispersed in 600 μL of same buffer.

Preparation of Au/S1-2 and Au/S3-E1: The hybridization of S2 (5′-GAC TAA GCA CCT GTC TTC GCC TTA TAA CTA TTC CTA-3′) or E1 (5′-TGT GTT CTC CGA GCC GGT CGA AAT AGT GAG T-3′) to Au/S1 or Au/S3, respectively, was conducted as follows: S2 (or E1) (4.5 μL, 200 μM) was added to Au/S1 (or Au/S3) solution (600 μL, ~3 nM). The solution was heated at 90 °C for 15 s and slowly cooled at room temperature for 30 min.

DNase I sensing assay: The stability of Au/S1-2 towards salt-induced aggregation was first examined. $MgCl_2$ (1 M) stock solution was gradually added (to increase $MgCl_2$ concentration by 10 mM each time) to the Au/S1-2 solution (10 mM Tris-HCl, pH = 7.5, 2.5 mM $MgCl_2$ and 0.5 mM $CaCl_2$) until a red-to-purple color change or a significant UV/visible spectra shift (see Supporting Information, Figure S4.1) was observed in ~10 min. Consequently, Au/S1-2 was determined to be stable at ≤40 mM $MgCl_2$ and higher $MgCl_2$ concentrations (e.g. 50 mM $MgCl_2$) resulted in significant color change or UV/visible spectra shift in 10 min (see Supporting Information, Figure S4.1). A typical DNase I assay solution contained Au/S1-2 (~2.25 nM), $MgCl_2$ (40 mM), $CaCl_2$ (0.5 mM), Tris-HCl (10 mM, pH = 7.5) and various amounts of DNase I. Immediately after the addition of DNase I, the mixtures were incubated at 37 °C for 1 min and absorption spectra were recorded using a Cary 300 UV/visible spectrophotometer. For DNase I inhibitor studies, the same assay was repeated using a fixed concentration of DNase I (4 units/mL) against various amounts of DAPI.

Pb^{2+} sensing assay: The stability of Au/S3-E1 towards salt-induced aggregation was first examined similar to the procedure described above but $BaCl_2$ (1 M) instead of $MgCl_2$ was used to tune the AuNP stability. As a result, Au/S3-E1 was determined to be stable at ≤40 mM $BaCl_2$ for at least 10 min after the addition of $BaCl_2$. Note that a second MCH exchange reaction could be performed to further decrease the AuNP stability. A typical Pb^{2+} sensing assay solution contained Au/S3-E1 (~2.25 nM), $BaCl_2$ (40 mM), NaCl (300 mM), Tris-HCl (50 mM, pH = 8.8) and various amounts of Pb^{2+}. After the addition of Pb^{2+} to the mixture, absorption spectra were recorded continuously for 10 min at room temperature or 35 °C using a Cary 300 UV/visible spectrophotometer.

Determination of cleavage efficiencies: To determine the cleavage efficiency and the size of cleaved DNA fragments, S1 and S3 were radiolabeled. The radiolabeled oligonucleotides were then conjugated onto AuNPs as described above to generate Au/S1-2 (or Au/S3-E1). The DNA-modified nanoparticles were cleaved in their respective assays (mediated by DNase I or Pb^{2+}) and were spun down using centrifugation. The supernatant was analyzed by 10% denaturing PAGE and quantified using Molecular Dynamics PhosphoImager and ImageQuant software.

4.6 Acknowledgments

We thank Kenny Schlosser for helpful discussions. This work was supported by Natural Sciences and Engineering Research Council of Canada (NSERC), Sentinel Bioactive Paper Network, Canada Foundation for Innovation and Ontario Innovation Trust. Y.L. holds a Canada Research Chair. J.C.F.L. is an Ontario Graduate Scholarship recipient.

4.7 References

[1] a) N. L. Rosi, C. A. Mirkin, *Chem. Rev.* 2005, *105*, 1547; b) E. Katz, I. Willner, *Angew. Chem.* 2004, *116*, 6166; *Angew. Chem. Int. Ed.* 2004, *43*, 6042; c) Y. Lu, J. Liu,

Curr. Opin. Biotechnol. 2006, *17*, 580; d) R. Baron, B. Willner, I. Willner, *Chem. Commun.* 2007, *28*, 323.

[2] a) R. Elghanian, J. J. Storhoff, R. C. Mucic, R. L. Letsinger, C. A. Mirkin, *Science* 1997, *277*, 1078; b) M. K. Beissenhirtz, R. Elnathan, Y. Weizmann, I. Willner, *Small* 2007, *3*, 375; c) M. Zayats, R. Baron, I. Popov, I. Willner, *Nano Lett.* 2005, *5*, 21; d) C. Sonnichsen, B. M. Reinhard, J. Liphardt, A. P. Alivisatos, *Nat. Biotechnol.* 2005, *23*, 741; e) J. Liu, Y. Lu, *Angew. Chem.* 2005, *118*, 96; *Angew. Chem. Int. Ed.* 2005, *16*, 90; f) W. J. Parak, T. Pellegrino, C. M. Micheel, D. Gerion, S. C. Williams, A. P. Alivisatos, *Nano Lett.* 2003, *3*, 33; g) K. Akamatsu, M. Kimura, Y. Shibata, S. Nakano, D. Miyoshi, H. Nawafune, N. Sugimoto, *Nano Lett.* 2006, *6*, 491.

[3] a) J. Zheng, P. E. Constantinou, C. Micheel, A. P. Alivisatos, R. A. Kiehl, N. C. Seeman, *Nano Lett.* 2006, *6*, 1502; b) F. A. Aldaye, H. F. Sleiman, *J. Am. Chem. Soc.* 2007, *129*, 4130; c) F. A. Aldaye, H. F. Sleiman, *Angew. Chem.* 2006, *118*, 2262; *Angew. Chem. Int. Ed.* 2006, *45*, 2204; d) Z. Deng, Y. Tian, S. H. Lee, A. E. Ribbe, C. Mao, *Angew. Chem.* 2005, *117*, 3648; *Angew. Chem. Int. Ed.* 2005, *44*, 3582; e) C. Lin, Y. Liu, H. Yan, *Nano. Lett.* 2007, *7*, 507; f) S. Beyer, P. Nickels, F. C. Simmel, *Nano. Lett.* 2005, *5*, 719; g) B. Kannan, R. P. Kulkarni, A. Majumdar, *Nano Lett.* 2004, *4*, 1521.

[4] N. C. Seeman, N. C. *Trends. Biotechnol.* 1999, *17*, 437.

[5] a) A. G. Kanaras, Z. Wang, A. D. Bates, R. Cosstick, M. Brust, *Angew. Chem.* 2003, *115*, 201; *Angew. Chem. Int. Ed.* 2003, *42*, 191; b) A. G. Kanaras, Z. Wang, M. Brust, R. Cosstick, A. D. Bates, *Small* 2007, *3*, 590; c) A. G. Kanaras, Z. Wang, I. Hussain, M. Brust, R. Cosstick, A. D. Bates, *Small* 2007, *3*, 67; d) S. R. Nicewarner Pena, S. Raina, G. P. Goodrich, N. V. Fedoroff, C. D. Keating, *J. Am. Chem. Soc.* 2002, *124*, 7314; e) W. Zhao, Y. Gao, S. A. Kandadai, M. A. Brook, Y. Li, *Angew. Chem.* 2006, *118*, 2469; *Angew. Chem. Int. Ed.* 2006, *45*, 2409. f) C. S. Yun, G. A. Khitrov, D. E. Vergona, N. O. Reich, G. F. Strouse, *J. Am. Chem. Soc.* 2002, *124*, 7644; g) W. J. Qin, L. Y. L. Yung, *Langmuir* 2005, *21*, 11330.

[6] a) J. Liu, Y. Lu, *J. Am. Chem. Soc.* 2005, *127*, 12677; b) J. Liu, Y. Lu, *Org. Biomol. Chem.* 2006, *4*, 3435.

[7] X. Xu, M. S. Han, C. A. Mirkin, *Angew. Chem.* 2007, *119*, 3538; *Angew. Chem. Int. Ed.* 2007, *46*, 3468.

[8] a) B. M. Reinhard, S. Sheikholeslami, A. Mastroianni, A. P. Alivisatos, J. Liphardt, *Proc. Natl. Acad. Sci. USA* 2007, *104*, 2667; b) Y. Weizmann, R. Elnathan, O. Lioubashevski, I. Willner, *J. Am. Chem. Soc.* 2005, *127*, 12666; c) Z. Wang, R. Lévy, D. G. Fernig, M. Brust, *J. Am. Chem. Soc.* 2006, *128*, 2214.

[9] a) W. Zhao, W. Chiuman, M. A. Brook, Y. Li, *ChemBioChem* 2007, *8*, 727; b) W. Zhao, W. Chiuman, J. C. F. Lam, M. A. Brook, Y. Li, *Chem. Commun.* 2007, 3729; c) H. Li, L. Rothberg, *Proc. Natl. Acad. Sci. USA* 2004, *101*, 14036; (d) K. Sato, K. Hosokawa, M. Maeda, *J. Am. Chem. Soc.* 2003, *125*, 8102; (e) L. Wang, X. Liu, X. Hu, S. Song, *Chem. Commun.* 2006, *2*, 3780.

[10] D. H. Napper, in Polymeric Stabilization of Colloidal Dispersions, Academic Press New York, 1983.

[11] a) E. S. Rangarajan, V. Shankar, *FEMS Microbiol. Rev.* 2001, *25*, 583; b) L. A. Mitscher, *Chem. Rev.* 2005, *105*, 559; c) P. A. Johnston, *Drug Discovery Today* 2002, *7*, 353.

[12] a) H. D. Hill, C. A. Mirkin, *Nat. Protoc.* 2006, *1*, 324; b) J. Liu, Y. Lu, *Nat. Protoc.* 2006, *1*, 246.

[13] S. Park, K. A. Brown, K. Hamad-Schifferli, *Nano Lett.* 2004, *4*, 1925.

[14] Control experiment showed DNase I itself, under investigated conditions, has no effect (stabilization or destabilization) on AuNPs.

[15] R. A. Ikeda, P. B. Dervan, *J. Am. Chem. Soc.* 1982, *104*, 296.

[16] a) J. Li, Y. Lu, *J. Am. Chem. Soc.* 2000, *122*, 10466. b) S. W. Santoro, G. F. Joyce, *Proc. Natl. Acad. Sci. U.S.A.* 1997, 94, 4262.

[17] a) J. Liu, Y. Lu, *J. Am. Chem. Soc.* 2003, *125*, 6642; b) J. Liu, Y. Lu, *Chem. Mater.* 2004, *16*, 3231; c) J. Liu, Y. Lu, *J. Am. Chem. Soc.* 2004, *126*, 12298.

[18] a) J. Liu, Y. Lu, *J. Am. Chem. Soc.* 2002, *124*, 15208; b) A. K. Brown, J. Li, C. M. B. Pavot, Y. Lu, *Biochemistry* 2003, *42*, 7152.

[19] L. Liu, Y. Lu, *Anal. Chem.* 2004, *76*, 1627.

[20] a) C. Guarise, L. Pasquato, V. D. Filippis, P. Scrimin, *Proc. Natl. Acad. Sci. USA* 2006, *103*, 3978; b) Y. Choi, N. Ho, C. Tung, *Angew. Chem.* 2007, *119*, 721; *Angew. Chem. Int. Ed.* 2007, *46*, 707; c) R. Lévy, N. T. Thanh, R. C. Doty, I. Hussain, R. J. Nichols, D. J. Schiffrin, M. Brust, D. J. Fernig, *J. Am. Chem. Soc.* 2004, *126*, 10076.

4.8 Supplementary Information

Determination of salt concentration used in the assays

Determination of a salt concentration at which untreated AuNPs are barely stabilized at the investigated assaying time (~10 min) is crucial to achieve the optimal sensing performance. The salt concentration was determined based on the red-to-purple color change (observed by naked eye) or significant UV/visible spectral shift upon adding salt solutions to the AuNP solution. In the DNase I sensing assay, for example, $MgCl_2$ (1 M) stock solution was gradually added to the Au/S1-2 solution (such that $MgCl_2$ concentration in the final solution increased by 10 mM each time) until a red-to-purple color change or a significant UV/visible spectral shift (Figure S4.1) was observed in a short period of time (~10 min). Consequently, Au/S1-2 was determined to be stable at ≤40 mM $MgCl_2$ and higher $MgCl_2$ concentrations (e.g., 50 mM $MgCl_2$) resulted in significant color change or UV/visible spectral shift in 10 min (Fig. S4.1). Similarly, in the Pb^{2+} sensing assay, 40 mM $BaCl_2$ was determined to be optimal in order to achieve the best sensor performance.

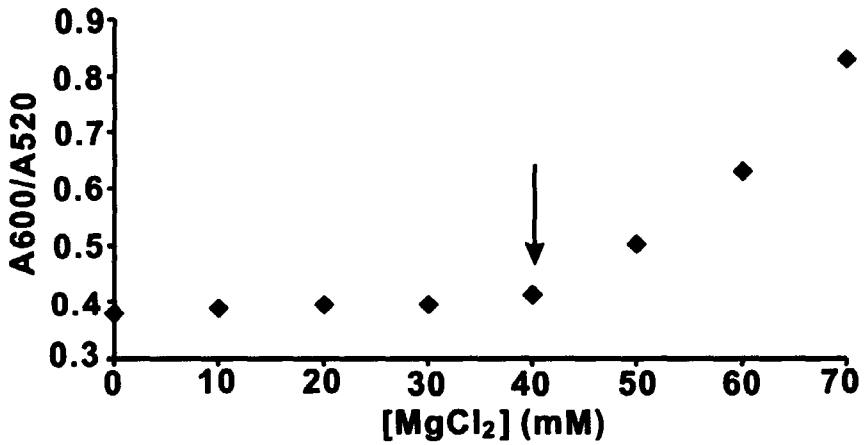

Figure S4.1. The amount of Au/S1-2 solution color change (A600/A520, calculated from UV/visible spectra) at 10 min after the addition of various amounts of $MgCl_2$.

Aggregation profile of untreated AuNPs for longer assay time

The AuNP aggregation at certain salt concentrations is a dynamic process. With the aim of developing rapid sensing assays, the assaying time used in the present paper was set to 1 min for DNase I sensing assay (or 10 min for Pb^{2+} sensing assay) during which the untreated AuNPs did not undergo significant aggregation or color change at the chosen salt concentration (e.g. 40 mM $MgCl_2$). However, if a longer time (e.g. 1 h) was applied, even the untreated AuNPs (for example, Au/S1-2) underwent a slow aggregation process and the solution gradually changed color from red to purple (Figure S4.2). Moreover, the aggregation rate is dependent on the salt concentration: a higher salt concentration (e.g., 50 mM $MgCl_2$) results in a faster aggregation process. The AuNPs may eventually precipitate out from the solution at higher salt concentrations (e.g., 50 mM $MgCl_2$) if left for a long enough time (e.g., overnight).

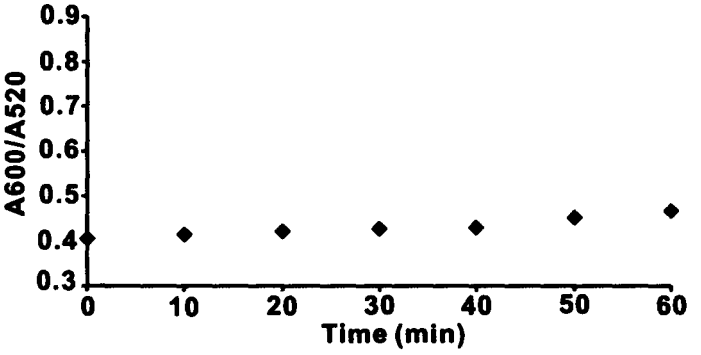

Figure S4.2. Aggregation behavior of Au/S1-2 (judged from the A600/A520 ratio) at 40 mM $MgCl_2$ as a function of time, which shows the aggregation is a dynamic and continuous process.

Chapter 5: Simple and rapid colorimetric biosensors based on DNA aptamer and non-crosslinking gold nanoparticle aggregation

The following chapter was published in ChemBioChem under the citation:

Weian Zhao, William Chiuman, Michael A. Brook, Yingfu Li. Simple and rapid colorimetric biosensors based on DNA aptamer and non-crosslinking gold nanoparticle aggregation. *ChemBioChem*, **2007**, 8, 727-731.

I was responsible for all data collection and analysis. William Chiuman provided helpful suggestions on aptamer design and function. I wrote the first draft of the manuscript and Dr. Brook and Dr. Li provided editorial input to generate the final draft of the paper.

5.1 Introduction

Recently, gold nanoparticles (AuNPs) have emerged as novel colorimetric reporters for the detection of various substances including DNA,[1] metal ions,[2] and proteins.[3] The advantages of using AuNPs include: 1) their simplicity, 2) the fact that no complicated and expensive analytical instruments are needed, and 3) the extremely high extinction coefficients ($\geq$ 1000 times larger than those of organic dyes) and the strongly distance-, shape-, and size-dependent optical properties of AuNPs, which allow AuNP-based colorimetric detection to have comparable sensitivity and selectivity to conventional fluorescent detection.[2, 3]

AuNP's use as a colorimetric reporter relies on its unique surface plasmon resonance (SPR): the dispersed AuNP solution is red whereas the aggregated AuNP solution appears purple (or blue), a phenomenon that can be well explained by the Mie theory.[4] Based on this principle, two general types of colorimetric assays (referred to as type I and type II in this report) have been developed.[1–3] In type I assays, the color of the AuNP solution changes from red (dispersed particles) to purple (aggregates), in type II assays, the color changes from purple (aggregates) to red (dispersed particles). Mirkin and co-workers pioneered the type I assay in which AuNP was used for the detection of DNA.[1a] In their study, AuNPs that were modified with two different oligonucleotides aggregated upon the addition of the complementary DNA target, which acted as a crosslinker to result in a color change from red to purple.[1a] Liu and Lu reported a type II assay for the detection of lead ions in which the aggregated AuNPs, crosslinked by cleavable DNA enzymes, were dissociated into dispersed AuNPs in the presence of Pb^{2+}.[2] More recently, Liu and Lu have extended this concept for the detection of small organic compounds (such as ATP) by using AuNPs crosslinked by DNA aptamers.[5] Aptamers are single-stranded (ss) DNA or RNA molecules created by in vitro selection for binding to a chosen target with high affinity and specificity.[6] In the aptamer-based assay designed by Liu and Lu, oligonucleotide-modified AuNPs were first crosslinked by a DNA aptamer sequence to form aggregates. Upon the addition of a desirable target, the aptamer underwent a structural switch[7] that caused the dissociation of the AuNP

aggregates; this was accompanied by the purple-to-red color change.[5] The marriage of AuNP and aptamers in these studies allows the AuNP-based assay to be generic, in principle, for any analyte for which an appropriate aptamer is available.[5]

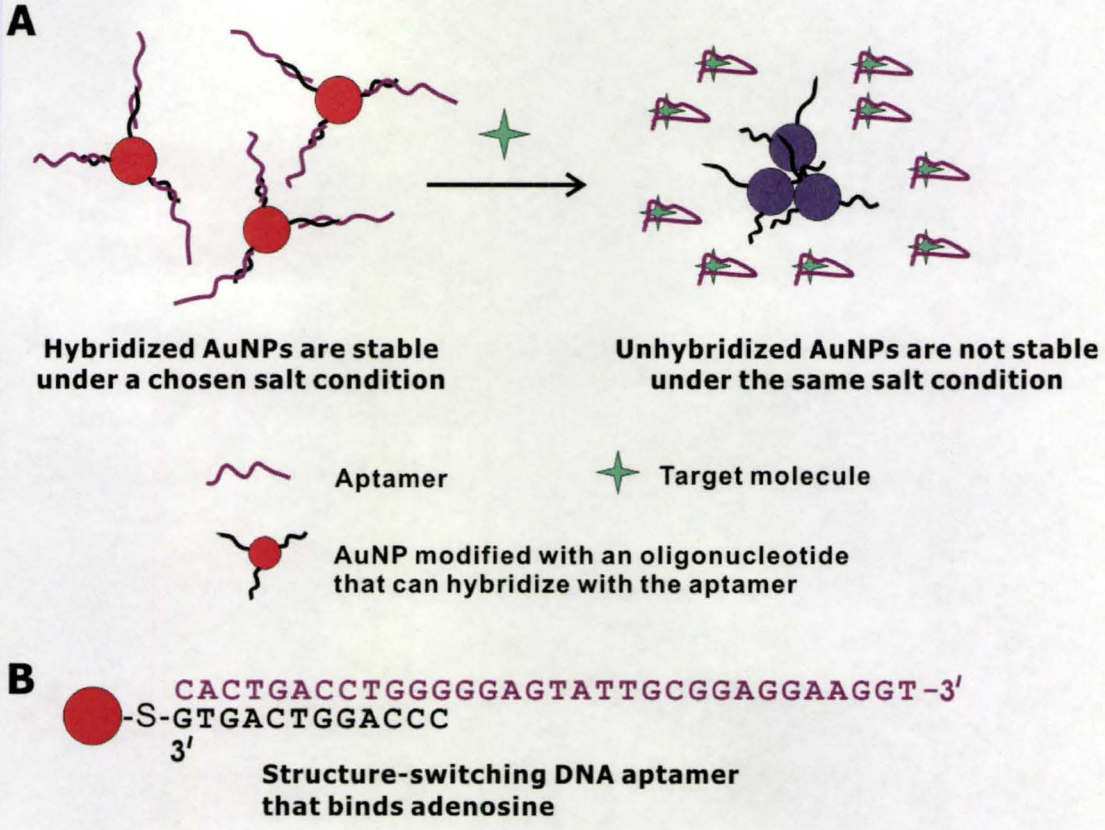

Figure 5.1*. (A) The working principle of the structure-switching aptamer based, salt-induced AuNP sensor. See the main text for the explanation. (B) The sequences of the DNA molecules used for the construction of the structure-switching aptamer sensor for adenosine detection.*

We present here a simple and rapid colorimetric assay that exploits structure-switching DNA aptamers[7] and the phenomenon of salt-induced, noncrosslinking AuNP aggregation. Conceptually, as shown in Figure 5.1A, a structure-switching DNA aptamer is first hybridized with a short complementary oligonucleotide attached to AuNPs at a chosen salt concentration in which hybridized AuNPs are stable and well dispersed in solution, which is red. Upon binding of the target, the aptamer strands undergo the structure-switching event that leads to their dissociation from AuNPs. The unhybridized

AuNPs are unstable at the same salt concentration and aggregate immediately; this causes a rapid, red-to-purple color change. It is important to note that our sensor design was inspired by previous work exploring salt-induced aggregation of AuNPs modified or adsorbed with DNA. In one study, Maeda and co-workers demonstrated that ssDNA-modified AuNPs have different stability against salt-induced aggregation in the presence of complementary DNA.[8] In another study, Rothberg and coworkers found that ssDNA and double-stranded (ds) DNA have different binding affinities for AuNP surfaces. Based on the different AuNP stabilities in the presence of ssDNA or dsDNA, they developed a type I assay in which the AuNP aggregation was induced by a high salt concentration.[9a] More recently, Wang et al. showed that unmodified AuNPs adsorbed with DNA oligonucleotides that have the tendency to form guanine-quartet structures (a unique higher-order DNA structure that is known to be stabilized by potassium ions) could function as a colorimetric sensor for K^+.[9b] They found that AuNPs adsorbed with such DNA oligonucleotides were stable in the absence of K^+. It was assumed that, under these conditions, the DNA oligonucleotide was unstructured and strongly adsorbed onto the surface of AuNPs, thereby preventing AuNP aggregation. The addition of K^+ caused the red-to-purple color change indicative of AuNP aggregation, which was attributed to the formation of guanine-quartet structure and reduced adsorption of the structured DNA molecule. Although the authors suggested that their approach could be extended to other non-metal-ion targets by using aptamers isolated by in vitro selection, no such examples have been provided. Therefore, the generality of their approach remains to be demonstrated.

To illustrate our approach, outlined in Figure 5.1A, we adopted a previously isolated, well-studied adenosine-binding DNA aptamer[10] as the model sensor. This aptamer has recently been utilized by our group in the design of fluorescent sensors based on a structure-switching strategy: the DNA aptamer is configured into a duplex with a short complementary oligonucleotide, the presence of adenosine (the target) then causes the aptamer to switch its structure from the DNA duplex to the aptamer/target complex,

because the aptamer preferentially binds to its target molecule.[7] The same design and sequences (Figure 5.1B) were used for this work.

5.2 Results and discussion

The first step in our design required conjugation of a short oligonucleotide to AuNPs so that the DNA aptamer could be subsequently attached to the AuNP surface through hybridization (Figure 5.1 B). The oligonucleotide-modified AuNPs (referred as AuNP-OD) were prepared by Au–S chemistry[1,11] (the details are provided in the Experimental Section). To determine the number of oligonucleotides on each AuNP (13 nm in diameter), a radiolabeled oligonucleotide was used. By measuring the radioactivity

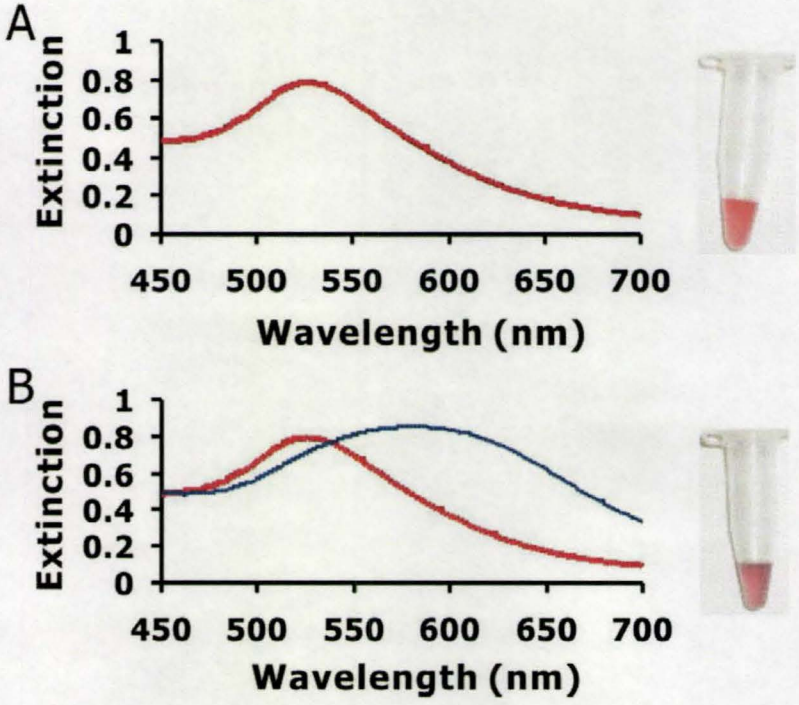

***Figure 5.2**. UV-Vis spectra of (A) AuNP-OD-APT and (B) AuNP-OD solutions before (red line) and after (blue line) adding $MgCl_2$ (a final concentration of 35 mM) to the solution that contained 300 mM NaCl, 20 mM Tris-HCl, pH 7.4. The tubes on the right are photographs of AuNP-OD-APT (A) and AuNP-OD (B) at 30 mM $MgCl_2$, 300 mM*

NaCl and 20 mM Tris-HCl, pH 7.4. The spectra and photos were taken 1 min after the addition of $MgCl_2$.

in the supernatant and on the AuNP pellet after centrifugation, the average number of attached oligonucleotides on each AuNP was estimated to be ~150. The stability of these AuNP-ODs was then examined. Throughout the study, the buffer concentration, pH (Tris-HCl, 20 mm, pH 7.4), and NaCl concentration (300 mM) were kept constant, while the $MgCl_2$ concentration was varied in order to assess its effect on the stability of DNA-modified AuNPs. We found that the AuNP-ODs were highly stable, even at >500 mM $MgCl_2$. This is consistent with the previous study[1b] and is due to the fact that the highly negatively charged phosphate groups in DNA molecules can stabilize the AuNP against aggregation by electrostatic repulsion.[1b] However, such a highly stabilized AuNP-OD is not desirable for our sensor design, because the structure-switching aptamers cannot function well under such a high divalent metal concentration.[10]

To tune the stability of AuNP-ODs, we briefly treated them (room temperature, 2 h) with 6-mercaptohexan-1-ol (MCH; 5 μM). This ligand-exchange process can remove both the nonspecifically adsorbed DNA and some of the thiol-tethered DNA so that the concentration of DNA on each AuNP can be reduced.[1b, 12] Indeed, radioactivity studies showed that after MCH treatment the average number of oligonucleotides on each AuNP was reduced to ~100. One would expect, therefore, that after MCH exchange the AuNP-OD should have a lower stability against salt-induced aggregation. Indeed, we found that after MCH treatment AuNP-ODs can only be stabilized at salt concentrations less than 3 mM $MgCl_2$, 300 mM NaCl, and 20 mM Tris-HCl (pH 7.4). Higher $MgCl_2$ concentrations quickly (1 min) led to a solution color change from red to purple.

It is noteworthy that MCH treatment of AuNP-ODs can significantly increase the hybridization efficiency between attached oligonucleotides on AuNPs and aptamers.[1b, 12] This is because the dilution of oligonucleotide concentration on the AuNP surface and their conformational change after MCH treatment make them more accessible for hybridization.[1b, 12] Indeed, through the use of a radiolabeled aptamer, we found that the hybridization efficiency between attached oligonucleotide and aptamer for the MCH-

treated AuNPs was as high as about 90%, whereas the hybridization efficiency for untreated AuNPs was only about 40 %.

More importantly, AuNP-OD hybridized with the aptamer (AuNP-OD-APT) was found to be significantly more stable than AuNP-OD. AuNP-OD-APT solution was stable at $MgCl_2$ concentrations as high as 35 mM; that is, there is no color change or peak shift in the UV-visible spectra (Figure 5.2A) for 1 min, a time period designated for subsequent sensing experiments. These results indicate that AuNP-OD and AuNP-OD-APT solutions have vastly different stabilities at 35 mM $MgCl_2$, 300 mM NaCl, and 20 mM Tris-HCl (pH 7.4) and set the stage for us to examine the ligand induction of this sensing solution.

It should be noted, however, that the color of AuNP-OD-APT gradually changed from red to purple after a few hours' incubation under the above salt conditions, and that AuNP-OD-APT precipitated in a few days.

As expected, upon addition of the aptamer target (adenosine, 1 mM), the AuNP-OD-APT solution immediately changed from red to purple (Figure 5.3A, tube 2); correspondingly, a red shift of the SPR band in the UV-visible spectrum was observed (Figure 5.3B). In contrast, the control experiments, in which inosine, guanosine, and cytosine (all at 1 mM) were used, did not show any color change, as expected (Figure 5.3A, tubes 3–5).

In order to confirm the dissociation of the aptamer from the AuNP surface in the presence of adenosine, an AuNP-OD-APT was prepared with radiolabeled aptamer. After 10 min of incubation with 1 mM adenosine at room temperature, the AuNP solution was separated in a centrifuge at 22 000g for 15 min. By measuring the radioactivity in the supernatant and on the AuNP pellet, we found that about 75% of the aptamer was released from the AuNP surface. This experiment showed that the aptamer on nanoparticle surfaces retained the structure switching capability.

The aggregation of AuNPs in the presence of adenosine was further confirmed by transmission electron microscopy (TEM). As shown in Figure 5.3D, irregular AuNP

aggregates of a few hundred nanometers to microns in diameter were observed after incubation with 1 mM adenosine for 10 min. This serves as complementary evidence,

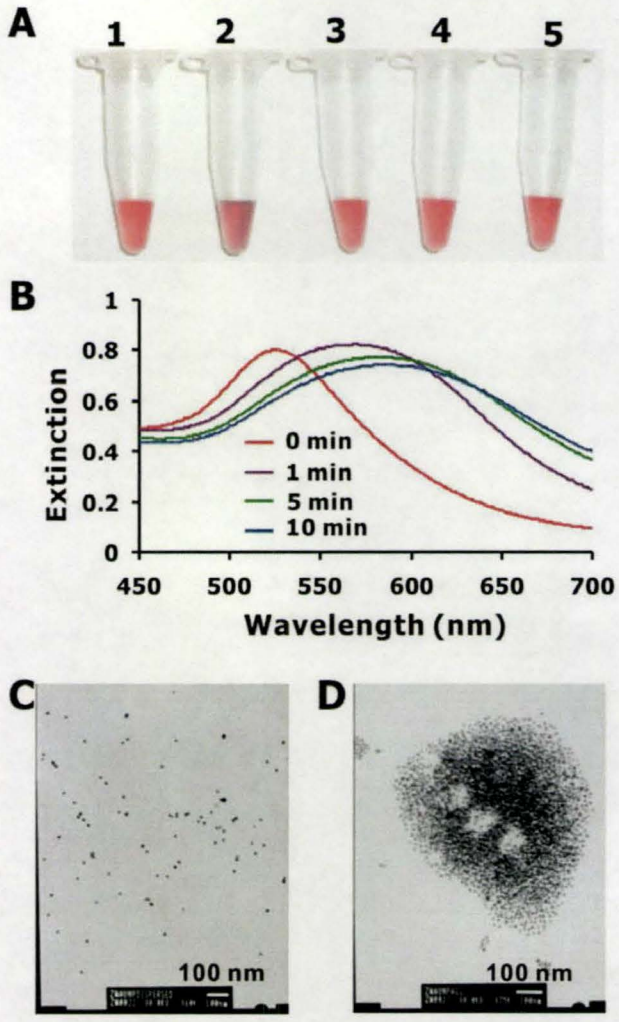

Figure 5.3. *(A) Photographs of AuNP-OD-APT solution in the absence of target (tube 1) and in the presence of 1 mM adenosine (tube 2), inosine (tube 3), guanosine (tube 4) and cytosine (tube 5). Photos were taken 1 min after the addition of concerned nucleosides. (B) Representative UV-Vis spectra of AuNP-OD-APT in the present 1 mM adenosine at different detection time. (C) and (D) are the representative TEM images of AuNP-OD-APT solution before and after adding adenosine, respectively.*

together with UV-visible spectroscopy, that the color change is indeed due to the aggregation of AuNPs.

Kinetic studies on the color change in the presence of various amounts of adenosine were recorded by UV-visible spectroscopy. To quantify the color change, the ratios of the absorbance at 700 and 525 nm (A700/A525) were plotted as a function of detection time, as shown in Figure 5.4A. Clearly, faster increases were obtained at higher adenosine concentrations. To further quantify the adenosine concentration, A700/A525 at 1 min after the addition of adenosine was plotted as a function of adenosine concentration (Figure 5.4B). The detection limit of the assay under our conditions was about 10 μM, which is ~20 times better than that of the type II assay in which purple AuNP aggregates dissociated to red, dispersed AuNPs when using the same aptamer construction.[5a] Interestingly, there are two response regimes in Figure 5.4B, which might reflect the fact that this aptamer is known to bind two adenosine molecules with different affinities.[10b,c] It should be noted that while further optimization (e.g., changing the AuNP concentration and the number of aptamer molecules on each AuNP) could be conducted to improve the sensitivity, the inherent affinity of the aptamer and the switching capability of the structure switching aptamer construct[7a] are the key factors that determine the detection limit of our assay.

It is well known that high salt concentrations can screen the charge on colloids, counter-acting the electrostatic stabilization, and leading to aggregates.[13] Elegant assays for the detection of DNA by using AuNP have been developed based on this principle.[8, 9] For instance, Maeda and co-workers developed a colorimetric assay to detect DNA by taking advantage of the different stability of ssDNA-attached AuNPs before and after the hybridization of the complementary DNA.[8] Surprisingly, they found that fully matched dsDNA-attached AuNPs had a lower stability than ssDNA-attached AuNPs. It was proposed that the conformational change from ssDNA to rigid duplex contributed to this effect.[8] By contrast, we found that AuNP-OD-APT, which contains a short duplex domain (12 base pairs) and single-stranded domain (20 nucleotides; Figure 5.1 B), was

much more stable than AuNP-OD, which has a 12-nucleotide ssDNA. We attributed this to the extra DNA aptamer strand's carrying more negative charges, so that the AuNP was

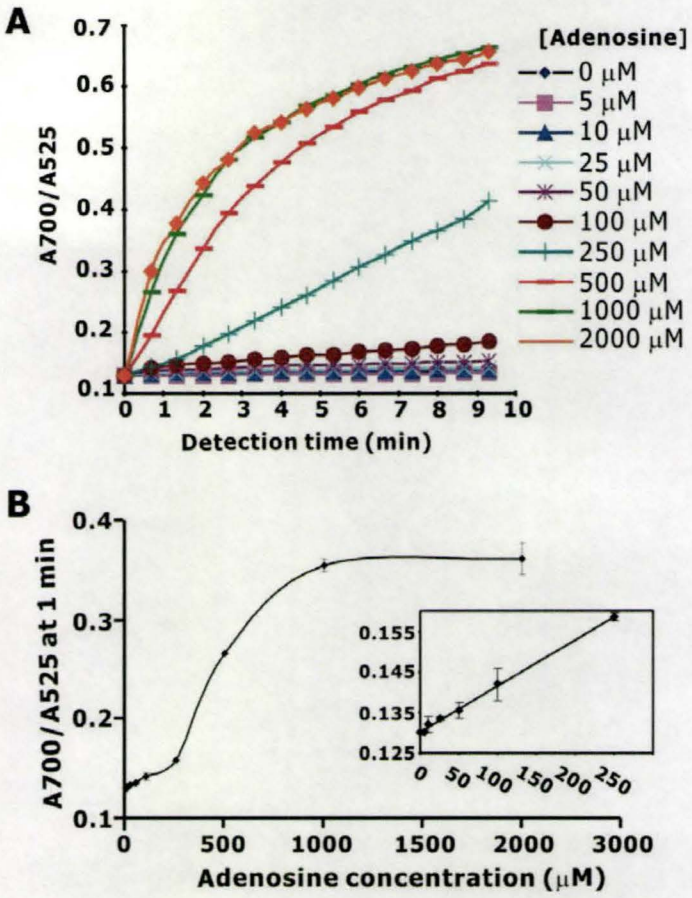

Figure 5.4. *(A) Kinetics of AuNP aggregation in the presence of various amounts of adenosine. (B) A_{700}/A_{525} at 1 min was plotted as a function of adenosine concentration in order to quantify adenosine. The Inset shows the responses at low analyte concentration region.*

more stabilized by electrostatic repulsion. This hypothesis was supported by the electrophoretic mobility study: the zeta potential of AuNP-OD-APT was -5.12 mV, whereas that of AuNP-OD was only -1.21 mV at the same ionic strength (300 mM NaCl, 20 mM Tris-HCl, pH 7.4). The steric effect might also play a role: the steric stabilization effect,[13] caused by DNA polymers on AuNPs, could be reduced when the DNA aptamer

dissociated from the AuNP surface in the presence of adenosine, leading to AuNP aggregation.

5.3 Conclusion

In summary, we have demonstrated a simple and rapid colorimetric assay that involves the principle of salt-induced, noncrosslinking AuNP aggregation and the use of structure-switching DNA aptamers. Besides the inherent advantages of AuNP-based assays (e.g. simplicity, no need for special detection instruments, etc.) and DNA aptamers (target generality[5]), this method offers two extra benefits. 1) Salt-induced noncrosslinking aggregation is generally faster than the aggregation process induced by crosslinking (type I).[8] This is presumably due to the different aggregation mechanisms: in a noncrosslinking system, the aggregation is driven by London–van der Waals attractive force between the nanoparticles.[8] At relatively high salt concentrations, at which the negative charges on nanoparticle surfaces are highly screened and thus the electrostatic repulsion is significantly reduced, the attractive forces dominate to result in rapid aggregation. By contrast, in a crosslinking system, the aggregation is mainly driven by random collisions between nanoparticles with relatively slow Brownian motion.[8] Indeed, the assay in the present study could be completed in 1 min. 2) The sensitivity of this assay is comparable to that of the previous fluorescence-based assays[7, 14] and higher than that of the type II assay in which the same aptamer construction was used.[5] It was found that the resuspension of aggregates to dispersed particles was rather difficult, presumably due to steric hindrance or the poor accessibilities of the biomolecules inside the aggregates.[2b, 5] To achieve the best detection performance, the assay sometimes needs to be conducted at a relatively high temperature that was only ~2–3 °C below the melting temperature of aptamer-crosslinked aggregates.[5a,b] By contrast, aptamers attached to well-dispersed AuNPs are more accessible to the binding of target molecules; this might explain the improved sensitivity of our assay.

5.4 Experimental Section

Materials: Trisodium citrate, $HAuCl_4$, MCH, adenosine, guanosine, cytosine, inosine, and ethyl acetate were purchased from Sigma and used as received. γ-^{32}P ATP was obtained from Amersham Biosciences. Thiol-modified DNA was obtained from Keck Biotechnology Resource Laboratory at Yale University. Unmodified DNA was purchased from the Central Facility at McMaster University.

Preparation of AuNP-OD: AuNPs 13 nm in diameter were prepared according to a previously described protocol,[11] and their concentration was estimated by UV/Vis spectroscopy to be about 13 nM, based on an extinction coefficient of $2.7\times10^8\ M^{-1}cm^{-1}$ at λ=520 nm for 13 nm particles.[1b] AuNP-ODs were then prepared by mixing the AuNP solution (600 μL, ~13 nM) with thiol-modified oligonucleotide (5'-CCCAGGTCAGTG-thiol-3'; 280 μL, 6.6 μM). The solution was incubated at room temperature for 45 h. Tris-HCl buffer (10 μL, 1M, pH 7.4) and aqueous NaCl (90 μL, 1M) were added, and the mixture was incubated for another 28 h. After that, Tris-HCl buffer (5 μL, 1M, pH 7.4) and aqueous NaCl (50 μL, 5M) were added, and the mixture was further incubated for 18 h at room temperature. The solution was then separated in a centrifuge at 22000g for 15 min. The precipitated AuNP-ODs were washed with wash buffer (2 × 1 mL; 20 mM Tris-HCl, pH 7.4, 300 mM NaCl) through centrifugation. Finally, the AuNP-ODs were redispersed in wash buffer (600 μL). For the synthesis of radioactive oligonucleotide, γ-^{32}P ATP (20 μCi) was incorporated through a previously described phosphorylation reaction.[11]

MCH treatment: The AuNP-OD solution prepared above was diluted with an equal volume of wash buffer before the addition of MCH to a final MCH concentration of 5 μM. The MCH treatment was performed at room temperature for 2 h. The reaction was quenched by three washes with equal volume of ethyl acetate, which removed excess MCH from the aqueous solution.

Preparation of AuNP-OD-APT: The adenosine-binding aptamer (5'-CACTGACCTGGGGGAGTATTGCGGAGGAAGGT-3'; 19.8 μL, 55.5 μM) was added to AuNP-OD solution (1 mL, ~6 nM). The hybridization solution was slowly cooled from

70 °C to room temperature over 1 h. The solution was then centrifuged and washed once with an equal volume of wash buffer and finally resuspended in wash buffer (1 mL).

Sample measurements: The absorption spectra of AuNP-OD-APT solution (250 μL, ~3 nM) with various amounts of adenosine were recorded on a Cary300 UV/Vis spectrophotometer at room temperature. TEM samples were prepared by dropping AuNP solution (4 μL) onto a carbon-coated copper grid. The solution was wicked from the edge of the grid with a piece of filter paper after 1 min. TEM images were taken with a JEOL 1200 EX. The electrophoretic mobilities of the nanoparticles were measured at room temperature by using a ZetaPlus (Brookhaven Instruments Corporation, Holtsville, NY). The reported values were based on 10 measurements with 15 cycles for each sample.

5.5 Acknowledgements

This work was supported by Natural Sciences and Engineering Research Council of Canada (NSERC), Sentinel: Canadian Network for the Development and Use of Bioactive Paper, and the Canadian Institutes for Health Research (CIHR). Y.L. holds a Canada research Chair.

5.6 References

[1] a) R. Elghanian, J. J. Storhoff, R. C. Mucic, R. L. Letsinger, C. A. Mirkin, *Science*, **1997**, 277, 1078; b) L. M. Demers, C. A. Mirkin, R. C. Mucic, R. A. Reynolds, R. L. Letsinger, R. Elghanian, G. Viswanadham, *Anal. Chem.* **2000**, 72, 5535.

[2] a) J. Liu, Y. Lu, *J. Am. Chem. Soc.* **2003**, 125, 6642; b) J. Liu, Y. Lu, *J. Am. Chem. Soc.* **2004**, 126, 12298.

[3] a) Y. Chen, S. Chen, Y. Chien, Y. Chang, H. Liao, C. Chang, M. Jan, K. Wang, C. Liu, *Chembiochem.* **2005**, 6, 1169. b) C. Huang, Y. Huang, Z. Cao, W. Tan, H. Chang, *Anal. Chem.* **2005**, 77, 5735.

[4] G. Mie, *Ann. Phys.* **1908**, 25, 377.

[5] a) J. Liu, Y. Lu, *Angew. Chem.* **2006**, 118, 8123; *Angew. Chem. Int. Ed.* **2006**, 45, 90; b) J. Liu, Y. Lu, *Nat. Protocol.* **2006**, 1, 246; c) J. Liu, Y. Lu, *Adv. Mater.* **2006**, 18, 1667.

[6] a) A. D. Ellington, J. W. Szostak, *Nature*, **1990**, 346, 818; b) C. Tuerk, L. Gold, *Science*, **1990**, 249, 505.

[7] a) R. Nutiu, Y. Li, *J. Am. Chem. Soc.* **2003**, 125, 4771; b) R. Nutiu, Y. Li, *Angew. Chem.* **2005**, 117, 1085; *Angew. Chem. Int. Ed.* **2005**, 44, 1061; c) R. Nutiu, Y. Li, *Angew. Chem.* **2005**, 117, 5600; *Angew. Chem. Int. Ed.* **2005**, 44, 5464; d) R. Nutiu, J. M. Yu, Y. Li, *Chembiochem.* **2004**, 5, 1139.

[8] K. Sato, K. Hosokawa, M. Maeda, *J. Am. Chem. Soc.* **2003**, 125, 8102.

[9] a) H. Li, L. Rothberg, *Proc. Nat. Acad. Sci. USA.* **2004**, 101, 14036; b) L. Wang, X. Liu, X. Hu, S. Song, C. Fan. *Chem. Commun.*, **2006**, 3780.

[10] a) D. E. Huizenga, J. W. Szostak. *Biochemistry*, **1995**, 34, 656. b) C. H. Lin, D. J. Patel, *Chem. Biol.* **1997**, 4, 817; c) S. Jhaveri, R. Kirby, R. Conrad, E. Maglott, M. Bowser, R. T. Kennedy, G. Glick, A. D. Ellington, *J. Am. Chem. Soc.* **2000**, 122, 2469.

[11] W. Zhao, Y. Gao, S. A. Kandadai, M. A. Brook, Y. Li, *Angew. Chem.* **2006**, 118, 2469*; Angew. Chem. Int. Ed.* **2006**, 45, 2409.

[12] a) S. Park, K. A. Brown, K. Hamad-Schifferli, *Nano Lett.* **2004**, 4, 1925; b) E. Huang, M. Satjapipat, S. Han, F. Zhou, *Langmuir*, **2001**, 17, 1215.

[13] E. A. Hauser, *Colloidal phenomena: an introduction to the science of colloids.* New York; London: McGraw-Hill, **1939**.

[14] M. Levy, S. F. Cater, A. D. Ellington, *Chembiochem*, **2005**, 6, 2163.

Chapter 6: DNA aptamer folding on gold nanoparticles: from colloid chemistry to biosensors

The following chapter was published in Journal of American Chemical Society under the citation:

Weian Zhao, William Chiuman, Jeffrey C. F. Lam, Simon A. McManus, Wei Chen, Yuguo Cui, Robert Pelton, Michael A. Brook,* Yingfu Li.* DNA aptamer folding on gold nanoparticle: from colloid chemistry to biosensors. *J. Am. Chem. Soc.*, **2008**, 130, 3610-3618.

I was responsible for all data collection and analysis with exception that DLS data were collected by Wei Chen and Yuguo Cui. William Chiuman provided helpful discussions on the design of DNA aptamer systems. Jeffrey C. F. Lam helped in purifying DNA oligonucleotides. Simon A. McManus provided helpful suggestion in K^+ aptamer design and its structure analysis. Dr. Robert Pelton provided helpful discussions on the mechanism of colloidal stability and aggregation. I wrote the first draft of the manuscript and Dr. Brook and Dr. Li provided editorial input to generate the final draft of the paper.

6.1 Abstract

We have investigated the effect of the folding of DNA aptamers on the colloidal stability of gold nanoparticles (AuNPs) to which an aptamer is tethered. Based on the studies of two different aptamers (adenosine aptamer and K^+ aptamer), we discovered a unique colloidal stabilization effect associated with aptamer folding: AuNPs to which folded aptamer structures are attached are more stable towards salt induced aggregation than those tethered to unfolded aptamers. This colloidal stabilization effect is more significant when a DNA spacer was incorporated between AuNP and the aptamer or when lower aptamer surface graft densities were used. The conformation that aptamers adopt on the surface appears to be a key factor that determines the relative stability of different AuNPs. Dynamic light scattering (DLS) experiments revealed that the sizes of AuNPs modified with folded aptamers were larger than those of AuNPs modified with unfolded (but largely collapsed) aptamers in salt solution. From both the electrostatic and steric stabilization points of view, the folded aptamers that are more extended from the surface have a higher stabilization effect on AuNP than the unfolded aptamers. Based on this unique phenomenon, colorimetric biosensors have been developed for the detection of adenosine, K^+, adenosine deaminase and its inhibitors. Moreover, distinct AuNP aggregation and redispersion stages can be readily operated by controlling aptamer folding and unfolding states with the addition of adenosine and adenosine deaminase.

6.2 Introduction

The effect of polymers, particularly charged polymers (or polyelectrolytes), on colloidal stabilization/aggregation has been a subject of extensive study over the last century due to their applications in a large variety of areas such as biological fluids, the paper-making industry, water treatment, pharmaceuticals, paints and coatings, among others.[1] The study of biopolymers such as negatively charged nucleic acids (DNA or RNA) on colloidal systems has recently gained considerable attention, owing to their biological importance and applications.[2]

The nanobiotechnology revolution over the last decade has made nucleic acid/colloid systems one of the most exciting research fields, owing to their potential applications for biosensors, nanomedicine and nanoelectronics.[2] DNA/gold nanoparticle (AuNP) systems are good examples of such systems. Owing to its unique Watson-Crick hydrogen-bonding nature, DNA ensures the specificity and precision required by biosensors and programmable nanoassemblies.[3] AuNPs, with desirable nano-scaled sizes and unique physical properties (particularly the colors associated with their surface plasmon resonance), are highly suitable signal-transducers for biosensors[4] and building blocks in nanoassemblies.[5] Mirkin and co-workers pioneered the study of DNA-modulated AuNP assembly and biosensors.[3d,4a] In their studies, DNA-modified AuNPs are associated into aggregates in the presence of complementary DNA strands that are used as crosslinkers; the aggregation of AuNPs is accompanied by a red-to-purple (or blue) color change. More recently, the redispersion of DNA-crosslinked AuNP aggregates, associated with the inverse purple-to-red color transition, has also been developed by Lu and co-workers for the detection of metal ions and small molecules.[6]

In addition to inter-particle crosslinking (or bridging) mechanisms, colloid stabilization/aggregation can be adjusted by a number of other factors such as surface charge and the use of non-crosslinked surface-grafted polymers.[7] These phenomena, although extensively studied in colloid chemistry, are largely unexplored for biosensing and nanoassembly applications. We[8] and others[9,10] have recently developed biosensing assays that take advantage of AuNP aggregation induced by the loss (or screening) of surface charges.

The colloidal stabilization/aggregation phenomena of DNA-modified AuNPs are rather complicated. Like other polyelectrolytes, both the charge and polymeric nature of DNA molecules must be considered when discussing the stabilization/aggregation of DNA-modified colloids. The unique nature of DNA can complicate normal considerations because of the potential for inter-particle forces such as hydrogen-bonding and hydrophobic forces. More strikingly, molecular recognitions between colloidal particle bound ssDNA molecules and their complementary DNA strands (or non-nucleic

acid targets such as small molecules) makes it more difficult to predict the colloidal stability of these particles. For instance, Maeda and co-workers found the hybridization of complementary DNA strands with colloid-tethered DNA molecules resulted in a decrease of colloidal stability toward salt-induced aggregation.[9] This is somewhat surprising because, with respect to electrostatic stabilization, the addition of extra negative charges associated with the complementary DNA molecules should lead to more highly stabilized colloids. While the precise mechanism was not fully explained, the authors attributed this to the entropic loss associated with the formation of a rigid DNA duplex. This work clearly suggests that the conformations DNA molecules adopt on a colloid surface may have a significant influence on colloidal stability.

In addition to hybridization with its complementary nucleic acid strand via Watson-Crick hydrogen-bonding and base-stacking, some DNA (or RNA) molecules known as aptamers[11] can also specifically recognize non-nucleic acid targets such as small molecules, metal ions and proteins. These aptamers are of great biological importance and find increasing success in applications as biosensors, controlling nanostructure assemblies, drug delivery and diagnostics.[12] For instance, recent work revealed that RNA aptamers, modulated by the binding of a specific metabolite, played an important role in gene regulation *in vivo*.[13] Moreover, DNA aptamers, isolated from random ssDNA pools *in vitro*, have been widely applied as recognition motifs in biosensors.[12a] A key feature associated with the recognition of an aptamer with its target is a conformational transition (or folding) from loose random coil to a compact tertiary structure. This conformational change is not only essential for aptamer function, but can be exploited as a very useful tool in the design of optical and electronic biosensors.[14] An improved understanding of aptamer conformational transitions upon binding of its target on surfaces will greatly facilitate the understanding of bio-recognition mechanisms on surfaces, particularly for the development of surface-based biosensing devices (e.g., microarray and nanoparticles)[12b,c] that can then serve as a guide for improving device performance. While its importance is acknowledged, little experimental and theoretical

work has been conducted on understanding aptamer conformational behaviors on surfaces.

We are interested in understanding the relationship between aptamer conformational transitions on colloid surfaces and colloidal stability. Unlike traditional polyelectrolytes, DNA aptamers can fold into compact tertiary structures in the presence of their cognate targets.[11] Little is known about how these rigid structures behave on surfaces and how they affect the colloidal properties (e.g., stability). We speculate that the improved understanding of the behavior of these entities will facilitate the development of applications in biosensors and nanotechnology.

AuNP was chosen as a model colloid system mainly because its aggregation/redispersion is directly observed by a solution color change owing to surface plasmon coupling.[15] The color change can be used as a convenient tool to test the colloidal stability and monitor the aggregation process.[16] If aptamer conformational transitions on AuNP surface, upon binding of its target, lead to changes in AuNP colloidal stability, the system can be directly transformed into a colorimetric biosensor for this target.

In the present study, two different systems (i.e., adenosine and potassium aptamers) were used to study how aptamer folding on AuNP surface affects colloidal stability. A surprising colloidal stabilizing effect associated with the aptamer folding on AuNPs was discovered: AuNPs bearing folded aptamer-target complexes were surprisingly shown to be more stable toward salt-induced aggregation than aptamer-modified AuNPs without targets. In this paper, we will first discuss this phenomenon and propose mechanisms for the observed stability, and then demonstrate its utilities for the design of colorimetric biosensors.

6.3 Results and Discussion

6.3.1 The colloidal stability upon DNA aptamer folding on AuNPs

We first investigated the effect on colloidal stability of adenosine aptamer folding on AuNP surfaces. Adenosine aptamers were chemically coupled onto AuNPs using Au-

S chemistry[17] (see Supporting Information, Experimental Section). Radiolabeled aptamers were used to determine the concentration of aptamers on each AuNP.[3e,8a] By measuring the radioactivity in the supernatant and on the pellets after the coupling and washing steps, it was found that there were ~180 DNA aptamers on each gold nanoparticle. Adenosine aptamer-modified AuNPs (Au-Ado) were briefly treated with 6-

Table 6.1. *Oligonucleotides used in the study. Ado and T10Ado refer to adenosine aptamers without and with T10 linker, respectively. AdoM is the adenosine aptamer mutant. K and KM represent K^+ aptamer and its mutant, respectively.*

Names	Sequences
Ado	5'-HS-ACCTGGGGGAGTATTGCGGAGGAAGGT-3'
T10Ado	5'-HS-TTTTTTTTTTACCTGGGGGAGTATTGCGGAGGAAGGT-3'
AdoM	5'-HS-ACCTGTGGGAGTATTGCGTAGGAAGGT-3'
K	5'-GGTTGGTGTGGTTGG-SH-3'
KM	5'-GGTTGGTGTTTTTGG-SH-3'

mercaptohexan-1-ol (MCH) solution (4 μM) for 30 min at room temperature. This ligand exchange reaction can remove nonspecifically adsorbed and some of the chemically attached DNA from the AuNP surface, which helps to improve subsequent biomolecular recognition (e.g., hybridization) efficiency.[18a-b,8a] Based on a similar radioactivity measurement, it was found that ~96 aptamers were attached on each AuNPs after MCH treatment.

Before the addition of adenosine, the ssDNA aptamer on AuNPs adopts a loose random coil structure, since there is no strong intra-molecular base-pairing, based on an analysis using *mfold* software.[19a] By contrast, the aptamer folds into a well-characterized tertiary structure (see Supporting Information, Figure S6.1)[19b,c] in the presence of adenosine (1 mM) in a buffer containing 4 mM $MgCl_2$, 100 mM NaCl, 20 mM Tris-HCl (pH = 7.5). We will refer to the AuNPs with folded aptamer/target complex as Au-Ado-Target. At a salt concentration of 4 mM $MgCl_2$ and 100 mM NaCl, both Au-Ado and Au-Ado-Target are colloidally stable and the solutions appeared red in color. The stability of Au-Ado and Au-Ado-Target towards salt-induced aggregation was then determined by gradually adding $MgCl_2$ (1 M) solution (with the NaCl concentration fixed at 100 mM)

until a rapid red-to-purple color change was observed over a short period of time (e.g., 1 min). It was determined that Au-Ado was stable only up to $MgCl_2$ concentrations of approximately ≤ 5 mM: at or above this concentration a rapid red-to-purple color change resulted. By contrast, Au-Ado-Target is much more stable: the particles were colloidally stable up to 30 mM $MgCl_2$. These differences are illustrated in Fig. 6.1. To provide a direct contrast between the colloidal stability of aptamer-modified AuNPs in the presence and absence of adenosine, 30 mM $MgCl_2$ was added to both solutions. As shown in Fig.

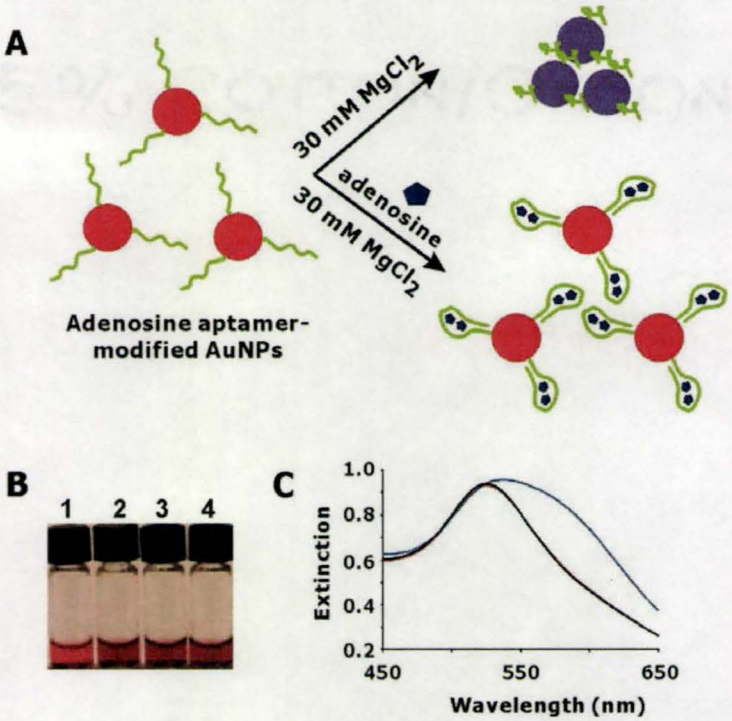

Figure 6.1. *(A) Schematic illustration of the different stability of AuNPs with folded and unfolded adenosine binding DNA aptamer. (B) Photographs for (1) Au-Ado + adenosine, (2) Au-Ado, (3) Au-Ado + inosine, and (4) Au-AdoM + adenosine. 30 mM $MgCl_2$ was used in these solutions and the photographs were taken 10 minutes after the addition of $MgCl_2$ to AuNP solutions. (C) UV-visible spectra of Au-Ado before (black curve) and after (blue curve) the addition of 30 mM $MgCl_2$. Red curve is the UV-visible spectrum for Au-Ado-Target with 30 mM $MgCl_2$. Spectra were taken 10 minutes after the addition of $MgCl_2$.*

6.1B, Au-Ado-Target did not show any significant color change (vial 1) within 10 min. By contrast, Au-Ado turned purple at the same conditions (vial 2): the characteristic red-shift was accompanied by broadening of the surface plasmon band in UV-visible

spectrum (Fig. 6.1C, blue curve). TEM experiments have further confirmed the color change was indeed induced by the aggregation of AuNPs (data not shown).

Although we could not provide the direct evidence for aptamer folding on AuNP surfaces at this stage, it is implicated: when control experiments using AuNPs modified with mutant aptamer (AdoM in Table 6.1) or using inosine as target, there was no colloidal stabilization effect (Fig. 6.1B, vial 3, 4). This confirmed that the colloidal stabilization effect was indeed due to specific aptamer folding upon binding its target (i.e., adenosine).

6.3.2 The effect of DNA spacer and aptamer graft density

To fully understand this phenomenon, we examined how the incorporation of a DNA spacer between AuNP and aptamer affects the additional colloidal stabilization provided by the aptamer folding on AuNPs. An adenosine aptamer with a T10 spacer (T10Ado, Table 6.1) was grafted onto AuNPs using the same Au-S chemistry to give a product referred to as Au-T10Ado. A similar MCH exchange reaction was then conducted and the radioactivity study showed that there were ~160 and ~ 94 aptamers on each AuNP before and after MCH treatment, respectively. Similar to Au-Ado, Au-T10Ado complexed with adenosine (referred to as Au-T10Ado-Target) was more stable than Au-T10Ado towards salt-induced aggregation. Specifically, the stability of Au-T10Ado and Au-T10Ado-Target are $\leq$ 10 mM $MgCl_2$ and $\leq$ 60 mM $MgCl_2$, respectively.

In order to determine how the T10 spacer affects the colloidal stabilization effect resulted from aptamer folding, the aggregation kinetics of Au-Ado and Au-T10Ado with and without adenosine were investigated. As shown in Fig. 6.2, the AuNP aggregation process was interpreted using the increase of the ratio of extinction at 600 nm and 520 nm (A600/A520) as a function of time. These experiments were conducted at salt concentrations such that Au-Ado-Target or Au-T10Ado-Target was barely stabilized. Thus, the $MgCl_2$ concentrations used for Au-Ado/Au-Ado-Target and Au-T10Ado/Au-T10Ado-Target were 30 mM and 60 mM, respectively. At their respective salt concentrations, both Au-Ado-Target and Au-T10Ado-Target showed little aggregation as indicated by insignificant A600/A520 increases (Fig. 6.2A, B). By contrast, Au-Ado and

Au-T10Ado both underwent rapid aggregation, and Au-T10Ado had a faster aggregation rate than Au-Ado (Fig. 6.2A, B). This indicates that the stability difference between Au-T10Ado-Target and Au-T10Ado is larger than that of Au-Ado-Target and Au-Ado, which suggests the T10 spacer enhances the colloidal stabilization effect resulted from aptamer folding on AuNPs.

We reasoned the efficacy of the effect of aptamer folding on colloidal stability could be affected by the available space on the AuNP surface and therefore examined

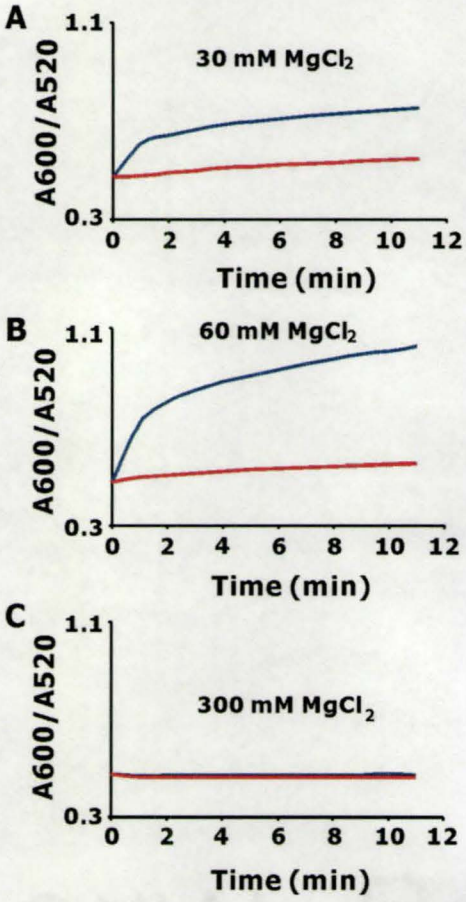

Figure 6.2. *Effects of DNA spacer and aptamer graft density on the colloidal stabilization of AuNP attached with folded aptamers. The samples in (A), (B) and (C) are MCH-treated Au-Ado, MCH-treated Au-T10Ado and non-MCH-treated Au-T10Ado, respectively. Red and blue curves are in the presence and absence of adenosine (1 mM), respectively. In (A) and (B), a rapid aggregation over the first two minutes was observed, followed by a slower aggregation phase. This may be due to the fact that the aggregation is characterized by the color change. Once the AuNPs start to aggregate, the surface plasmon peak shifts from 520 nm to the longer wavelength (e.g., 600 nm), which leads to*

the decrease of A520 and increase of A600 nm. Therefore, A600/A520 showed a sharp increase at the initial aggregation stage. However, as aggregation continues, the surface plasmon peak may further shift to even longer wavelength (e.g., 700 nm). As a result, the increase of A600 (and therefore A600/A520) may not be as aggressive as that at the initial aggregation stage.[16]

how aptamer graft density influences colloidal stabilization. To tune aptamer graft density, aptamer-modified AuNPs were treated with MCH, a ligand exchange reaction where some thiol-modified aptamer strands are displaced by MCH molecules.[18a,b] Negatively charged DNA polymers are mainly responsible for the colloidal stability of DNA-modified AuNPs via both electrostatic and steric effects (see Section 6.3.3 for details). Thus, MCH treatment affects AuNP colloidal stability by reducing the number of DNA molecules on each AuNP: these uncharged small molecules themselves have little (if any) effect on colloidal stability, however, the loss of stabilizing DNA molecules from the surface can facilitate aggregation of DNA-modified AuNPs.[8a, 18c-f]

The highest aptamer graft densities were observed with AuNPs before the MCH exchange reaction. Stability studies showed that these non-MCH-treated AuNPs were much more stabilized towards salt-induced aggregation than the MCH treated AuNPs. For instance, the stability of AuNP-T10Ado before MCH treatment is larger than 300 mM $MgCl_2$, evidenced by the fact that no color change or A600/A520 increase (Fig. 6.2C) was observed at salt concentrations up to 300 mM $MgCl_2$. Non-MCH-treated Au-T10Ado showed similar aggregation kinetics with and without adenosine (1 mM) in all investigated salt concentrations (300 mM $MgCl_2$ in Fig. 6.2C as an example), suggesting that the addition of adenosine did not significantly increase the colloidal stability of Au-T10Ado with high aptamer graft density (~160 aptamers/AuNP). By contrast, as demonstrated in Fig. 6.2B, Au-T10Ado with lower graft density (~94 aptamers/AuNP) obtained by MCH treatment showed significant colloidal stability difference before and after the addition of adenosine.

In summary, AuNPs modified with aptamers with a DNA spacer or with a lower surface graft density showed higher stability contrast in the presence and absence of adenosine. This may be because the incorporation of spacers[20] or the decrease of aptamer

graft density[8a,18a,b] provides more available space for bio-recognition and therefore improve the aptamer folding or binding efficiency to adenosine. As demonstrated in Section 6.3.1, AuNPs with folded aptamer-target complex appeared to be more stable than AuNPs with unfolded aptamers. Therefore, parameters (e.g., spacers and aptamer graft density) that can help the aptamer folding will enhance the AuNP colloidal stabilization.

6.3.3 Proposed mechanisms

The effect of polyelectrolytes on colloidal stabilization/aggregation is, although extensively studied, highly complicated.[1] Colloids with charged biopolymers such as proteins and nucleic acids are more complex systems than most due to the unique inter- and intra-biomolecular interactions such as hydrogen-bonding and hydrophobic interaction.

It was initially a surprise that AuNPs with folded aptamer structures were more stable than those with unfolded structures towards salt-induced aggregation. Maeda and co-workers found AuNPs with rigid double-stranded (ds) DNA duplexes were less stable than AuNPs with flexible single-stranded (ss) DNA, presumably due to the entropic loss upon formation of the rigid DNA duplexes.[9] Guided by this finding, we expected to observe a similar phenomenon with AuNPs bearing rigid folded aptamer structures. As noted, this expectation was completely opposite to our experimental results.

Whether colloids are stabilized or undergo aggregation depends on the net potential of inter-particle attraction and repulsion forces.[7] In the present work, the inter-particle attraction force is van der Waals force, which is responsible for the AuNP aggregation.[7,21] The two major repulsion forces that contribute to AuNP stabilization are electrostatic and steric repulsion forces.[1,7,21]

Electrostatic repulsion results from the negatively charged phosphate groups along DNA backbone. These negative charges, together with the counterions in the medium, form a repulsive electric double layer that stabilizes colloids against van der Waals attraction.[7] The thickness of the electric double layer is a measure of how far the repulsive potential extends from the colloid surface. A characteristic feature of the

electrostatic repulsion force is that it is highly sensitive to the bulk ionic strength: the electrostatic repulsion force diminishes significantly at high salt concentration where electric double layer is highly suppressed.[7] This explains why AuNPs modified with aptamers (folded or unfolded) are stable at low salt concentrations but undergo aggregation at high salt concentrations. With respect to the AuNPs with folded and unfolded aptamers, one conceivable difference between these two systems might be the charge distribution. Like other polyelectrolyte-grafted colloids, the surface charges in the current system are extended along the DNA backbone from the surface.[1,21] Therefore, the conformation of DNA (such as folded and unfolded structures) on AuNP surface, which directly contributes to the surface charge distribution, could be a key factor determining their relative colloidal stability.

Steric stabilization (or polymeric stabilization)[1,21] is another key contribution to the repulsion forces in the current system. Macromolecules grafted on colloid surfaces impart a polymeric barrier that prevents colloids from coming close enough such that van der Waals attractive forces can dominate.[1,21] Steric stabilization is highly dependent on the thickness of polymer layer and surface graft density.[1,21] In general, thicker polymer layers and higher graft densities lead to more effective steric stabilization effect. This is exactly the case for the non-MCH-treated aptamer-modified AuNPs: they are stabilized in solutions up to 300 mM $MgCl_2$. Although it would be expected that electrostatic repulsion is significantly reduced under these conditions,[7] their stability appeared not to be sensitive to salt concentration. The stability of the MCH-treated aptamer-modified AuNPs are much lower, whether with folded or unfolded aptamers ($\leq$ 60 mM $MgCl_2$), presumably due to the decreased surface density of DNA on AuNPs produced by MCH exchange reactions.[18a,b] In principle, AuNPs bearing folded and unfolded aptamers share the same aptamer chain length and graft density. Nevertheless, they may adopt different conformations: the folded aptamer has a well-defined compact structure whereas the unfolded aptamer chain may be more randomly configured. These conformational factors, which highly impact on the stabilization/aggregation of steric-stabilized colloids,[1,21] may

also contribute to the different stability observed for AuNPs with folded and unfolded aptamers.

To examine the effect of AuNP surface-bound aptamer conformations on colloidal stability, dynamic light scattering (DLS) studies, a technique commonly used for characterizing colloidal properties such as size, shape, polydispersity and thickness of

Table 6.2. *Particle sizes obtained from DLS measurement. The concentrations of $MgCl_2$ and adenosine are 4 mM and 1 mM, respectively.*

Particles	Bare AuNP	Non-MCH-treated Au-T10Ado		MCH-treated Au-T10Ado			MCH-treated Au-Ado		
		H_2O	$MgCl_2$	H_2O	$MgCl_2$	$MgCl_2$+ adenosine	H_2O	$MgCl_2$	$MgCl_2$+ adenosine
Diameter (nm)	19.6±0.1	29.4±1.1	28.5±0.3	29.3±0.6	24.9±0.8	27.3±0.9	27.3±1.1	24.2±0.3	25.6±0.5

surface coatings,[22] were conducted. The results are summarized in Table 6.2. Bare AuNP (before the modification of aptamer) have a diameter of 19.6 nm. The size of bare AuNP measured by DLS is larger than that obtained from TEM study (13.5 nm), which is mainly due to the fact that DLS measures the hydrodynamic radius while TEM provides a more precise measurement of the hard AuNP core.[23] After modification with aptamer-T10Ado (aptamer-Ado behaved similarly with T10Ado in DLS studies and therefore will not be discussed herein in detail) and MCH treatment, Au-T10Ado is 29.3 nm in diameter in ddH_2O, which corresponds to a thickness of DNA layer of 4.8 nm. By contrast, Au-T10Ado has a diameter of 24.9 nm in salt solution (4 mM $MgCl_2$, 20 mM Tris-HCl, pH 7.5), with a DNA coating thickness of 2.6 nm. The reduced thickness of the DNA layer of Au-T10Ado in the salt solution can be explained as follows: in ddH_2O, negative charges distributed along DNA backbones create a significant electrostatic repulsive force between DNA chains.[21] This repulsion facilitates DNA chain extension, which results in thicker DNA layer.[21] In contrast, the addition of salt largely suppresses the electric double layer and reduces the electrostatic repulsion between DNA chains.[21] DNA molecules therefore tend to collapse back towards AuNP surface, leading to smaller

particle size and DNA layer thickness.[21] This size shrinkage appears to be significant only for the MCH-treated Au-T10Ado. For non-MCH-treated ones, the particle diameters are 29.4 nm and 28.5 nm in ddH_2O and salt solution, respectively. This is presumably due to that there is not sufficient room for the DNA layer to collapse in the case of non-MCH-treated Au-T10Ado with high surface graft density. Importantly, the AuNP with folded

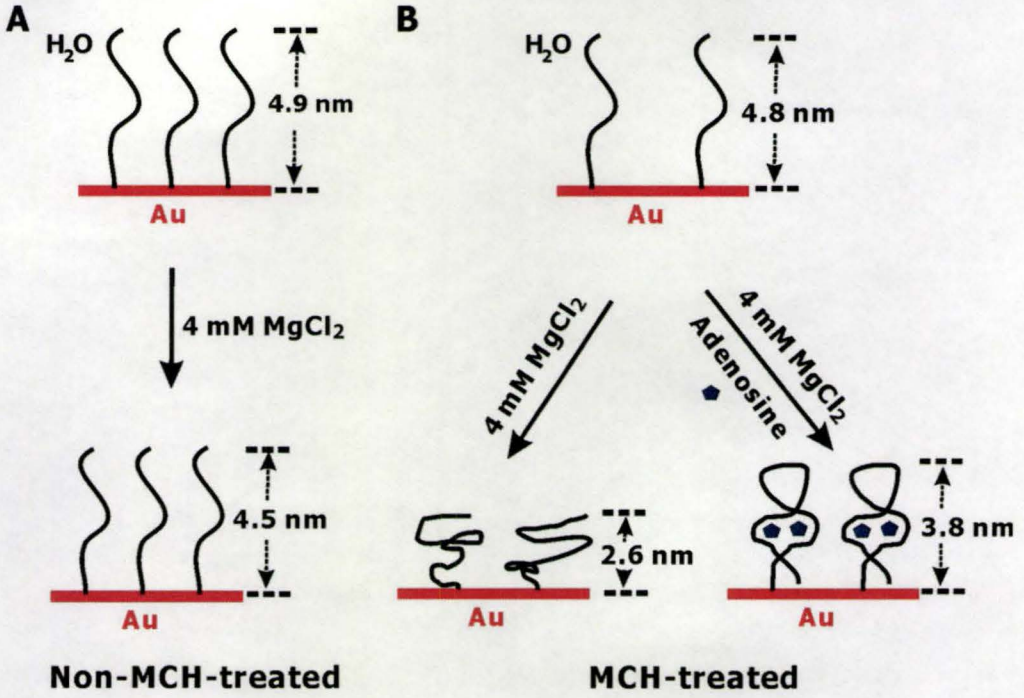

Figure 6.3. *Schematic illustration of aptamer conformational behaviours on (A) non-MCH-treated Au-T10Ado in H_2O and 4 mM $MgCl_2$, (B) MCH-treated Au-T10Ado in H_2O and 4 mM $MgCl_2$ (with and without adenosine).*

aptamers, obtained by mixing MCH-treated Au-T10Ado and adenosine (1 mM) in 4 mM $MgCl_2$, 20 mM Tris-HCl, pH 7.5, has a diameter of 27.3 nm. The height of folded aptamer structure was therefore determined to be 3.8 nm, which is in good agreement with the theoretical value obtained from the previous NMR study.[19b] These results indicate that the height (or thickness) of folded aptamer structure is larger than that of unfolded (but largely collapsed) aptamers in a given salt solution. To assess the size of individual particles, the salt concentration (4 mM $MgCl_2$, 20 mM Tris-HCl) used for DLS experiments was relatively low (but sufficient for the aptamer folding) and AuNPs with folded and unfolded aptamers are both stabilized. Higher salt concentration may initiate

the aggregation process for AuNP attached with unfolded aptamers, which makes the DLS measurement of individual particle size difficult. However, due to the nature of unfolded aptamer structures, it is reasonable to predict that the size of AuNPs with unfolded aptamers (no target bound) may undergo further shrinkage at higher salt concentrations. By contrast, the size of AuNP with folded aptamer structures would not be significantly affected by higher salt concentrations (e.g., 30 mM $MgCl_2$) due to their rigid and compact structures. DLS experiments support this theory: the size of Au-Ado (or Au-AdoT10) with folded aptamer in the presence of adenosine at 30 mM $MgCl_2$ (or 60 mM $MgCl_2$) is 25.3 ± 0.3 nm (or 27.6 ± 0.6 nm), which is comparable to their sizes at lower $MgCl_2$ concentrations (i.e., 4 mM) (Table 6.2).

The heights (or thickness) of aptamer structures in different AuNP samples are illustrated in Fig. 6.3. From the electrostatic stabilization point of view, the repulsive force is dependent on the thickness of electric double layer.[7] For AuNP with folded aptamers, the negative charges (and thus formed electric double layer) may be more extended from the surface than those of AuNP with unfolded aptamers at higher salt concentrations owing to their different heights on surface (Fig. 6.3B). This could be a reason why AuNPs with folded aptamer structures are more stable towards salt-induced aggregation.

With respect to the steric stabilization, it is known that thicker coated polymer layers and higher surface graft densities yield more effective repulsive forces.[1,21] This is certainly the case for non-MCH-treated Au-T10Ado that can be stabilized even in solutions up to 300 mM $MgCl_2$, where electrostatic repulsion is significantly diminished. The size measurements obtained from DLS support this theory. Only a small decrease in thickness was found for non-MCH-treated Au-T10Ado in the salt solution (Fig. 6.3A), which is presumably due to the limited space available for aptamer to collapse. Therefore, AuNPs are always coated by a relatively thick, dense DNA layer regardless of bulk salt concentration. This DNA layer serves as an effective polymeric stabilizer to prevent AuNP aggregation. This steric stabilization should play a dominating role at high salt concentration where electrostatic repulsion is negligible. For MCH-treated AuNPs (with

folded or unfolded aptamers), their stability dropped significantly, as a result of the decrease of aptamer graft density and thickness (Fig. 6.3B). MCH-treated AuNPs with unfolded aptamers showed a lower graft thickness in salt solution than AuNPs with folded aptamers (Fig. 6.3B). Therefore, compared to the AuNPs with folded aptamers, the AuNPs with unfolded (but largely collapsed) aptamers can more readily come close to an interparticle distance such that van der Waals forces will give a net attractive potential. This might be another reason why AuNP with folded aptamer is more stable than that with unfolded aptamers.

In summary, the conformations that adopted by aptamers on the AuNP surface seem to be a key factor in determining their relative colloidal stability. Although the suggested mechanisms can explain the obtained experimental results, we acknowledge that we are still far from having a precise understanding for this unique phenomenon because of its complex nature.

We have only considered so far the effect of Mg^{2+} on aptamer conformational change through screening the charges associated with phosphate groups on DNA backbone. Meanwhile, the Mg^{2+} may target other binding sites associated with nucleobases, which may or may not affect the secondary (or tertiary) structures of unbound and bound aptamers. For unbound aptamers in the absence of adenosine, the prediction of aptamer structure at different Mg^{2+} concentration (0 – 60 mM) using *mfold* software[19a] did not show any specific secondary structures. This suggests that, without a target, the aptamer adopts a rather randomly distributed form, and the addition of $MgCl_2$ does not contribute to any specific aptamer secondary structure formation other than collapsing the aptamer by screening charges associated with aptamer. A certain amount of Mg^{2+} (e.g., 4 mM) is required for the folding of the aptamer in the presence of adenosine. Once folded into a rigid, compact structure, the further addition of Mg^{2+}, under studied conditions (Mg^{2+} concentration: 4 – 60 mM), seems to have little (if any) effect on the secondary (or tertiary) structure of folded aptamer/target complex. This assessment is supported by the present work where we showed above that Mg^{2+} concentration has little effect on the size of AuNPs with folded aptamers, as well as by a

previous study[12j] in which the adenosine aptamer functions similarly at Mg^{2+} concentrations ranging from 4 – 60 mM. Nevertheless, there is no quantitative data or precise model available on how Mg^{2+} interacts with the adenosine aptamer before and after folding with adenosine, or how that affects aptamer secondary (or tertiary) structures. These questions represent our future research interests.

Since the amount of counterions (e.g., Mg^{2+}) and H_2O molecules associated with aptamers before and after folding with adenosine might be different,[24] the electrophoretic properties of aptamers in folded and unfolded states could be another factor that affects the colloidal stability. Unfortunately, our preliminary results obtained from Zeta potential measurements and agarose gel electrophoresis[25] could not differentiate the AuNPs with folded and unfolded aptamers (data not shown). Quantitative calculations[24] of the amount of charges associated with aptamers before and after folding will be conducted in the future work. Furthermore, we could not provide the quantitative data for the entropic factors associated with target-induced specific aptamer folding and salt-induced nonspecific aptamer collapse. In general, the formation of rigid polymer structures or the loss of polymer flexibility on colloid surface results in an entropic penalty that can destabilize the colloids.[9] In the present work, it seems likely that even if there is more entropic loss in the aptamer folding process than that associated with aptamer collapse induced by salt, this entropic penalty can be overcome by the electrostatic and steric contributions mentioned above.

The interparticle attraction forces that cause AuNP aggregation have so far been attributed to van der Waals attraction. However, due to the particular nature of DNA, one may argue that other interparticle bridging forces (e.g., hydrogen-bonding, hydrophobic force) may also exist. We think these forces are less likely the key factors that dominate the AuNP aggregation in this study for the following reasons. First, for the AuNP aggregation induced by the complementary DNA bridging, at least 12 base pairs are required to provide a sufficient hybridization.[4a] There is no such designed base-pairing in the present study. More importantly, the AuNP aggregation induced by interparticle DNA bridging is known as a relatively slow process:[4a] it generally requires hours to observe a

red-to-purple color change and an annealing process controlled by temperature is normally applied. In the present work, an instant color change associated with AuNP aggregation was observed at room temperature right after the addition of salt. This rapid aggregation is a characteristic feature of van der Waals attraction induced colloidal aggregation.[7] Furthermore, we studied the aggregation process at an elevated temperature

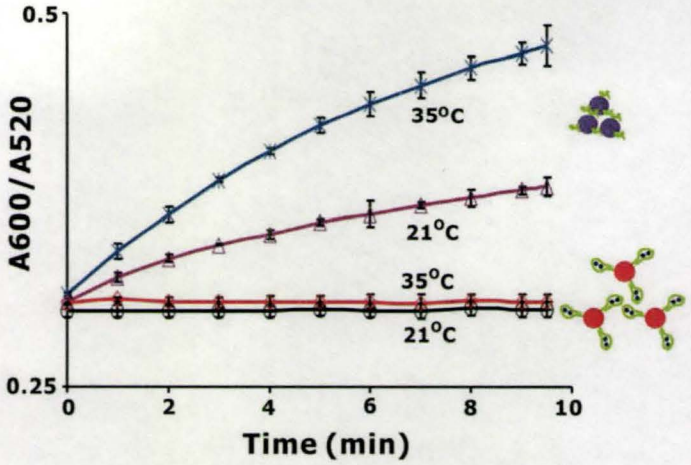

Figure 6.4. *Temperature effect on aggregation kinetics of Au-T10Ado with and without adenosine.*

(Fig. 6.4). If the aggregation was indeed induced by interparticle DNA base-pairing, it would be expected that the aggregation process would be diminished as the interparticle bonds (e.g., hydrogen-bonds) are broken at higher temperatures. In contrast, we found that the AuNP aggregation is more rapid at elevated temperatures, a typical phenomenon found in van der Waals force controlled aggregation: higher temperature causes a faster colloid collision rate and therefore more rapid aggregation.[7] This suggests the AuNP aggregation in the present study is less likely due to interparticle bridging forces.

6.3.4 Biosensors for adenosine, adenosine deaminase (ADA) and ADA inhibitor

One of the advantages of using AuNP as a model colloid is that aggregation (or redispersion) processes are associated with a visible red-to-purple (or purple-to-red) color change, which allows the system to be directly transformed into colorimetric biosensors. As shown in Fig. 6.5, A600/A520 at 10 minutes after the addition of adenosine was

plotted as a function of adenosine concentration. Since aptamer folding in the presence of adenosine stabilizes AuNPs (decreases the aggregation rate), the addition of adenosine inhibited the color change (or red shift in the UV-vis spectra). Importantly, the degree of the inhibition of color change is directly related to the amount of adenosine used, and a standard target concentration titration curve was established (Fig. 6.5). The detection

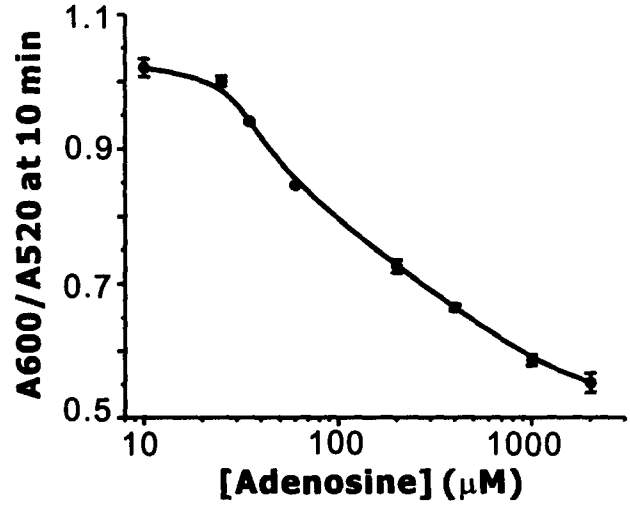

Figure 6.5. *The inhibition of red-to-purple color change (A600/A520) as a function of the concentration of adenosine.*

range of adenosine in the current assay is ~20 μM-2000 μM. Furthermore, the dissociation constant (K_d), which is 263 μM, was obtained based on the binding curves in Fig. 6.5 (see Figure S6.2 in Supporting Information for the K_d calculation). This K_d value, which reflects the aptamer affinity on AuNP surface, is larger than that (~6 μM[19c]) obtained from free aptamers in solution. This is presumably because aptamers on surfaces are less accessible to their targets than those in solution.

As demonstrated previously, the stabilization effect associated with aptamer folding is specific to adenosine, but not to other control molecules such as inosine. This provided a simple colorimetric assay for the detection of adenosine deaminase (ADA), an enzyme that converts adenosine to inosine (Fig. 6.6A) and is of great biological and clinical importance.[26] In the ADA detection assay, AuNPs with folded aptamer/adenosine complex were used as starting materials. They are stabilized at a relatively high salt

concentration and these well-dispersed AuNPs exhibit a red color. The addition of ADA (1 unit/ml) that converts adenosine into inosine destabilized AuNPs and resulted in a red-to-purple color change and a red shift on UV-vis spectra (Fig. 6.6B, C). The degree of color change is directly related to the ADA concentration used in the assay (Fig. 6.6D). The detection range of ADA under investigated conditions ranges from 0.4 to 4 units/ml.

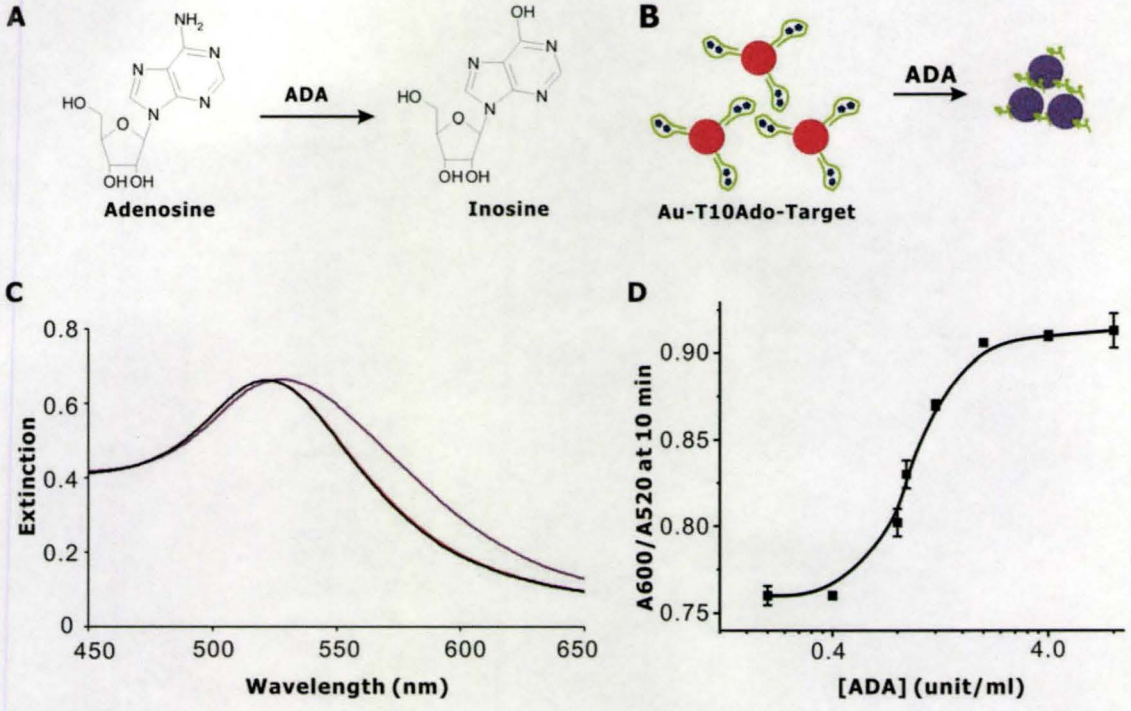

Figure 6.6. *(A) Adenosine can be converted into inosine by ADA. (B) The aggregation of Au-T10Ado-Target can be induced by ADA that converts adenosine to inosine. (C) UV-visible spectra of Au-T10Ado-Target (black curve), Au-T10Ado-Target + ADA (purple curve) and Au-T10Ado-Target + ADA + inhibitor (red curve). The spectra were taken 10 min after mixing all the ingredients in each sample. (D) A600/A520 at 10 min after the addition of ADA is plotted as a function of the ADA concentration.*

Meanwhile, the addition of *erythro*-9-(2-hydroxy-3-nonyl)adenine (EHNA) (400 μM), a known inhibitor of ADA,[26a] significantly inhibited the color change (Fig. 6.6C, red curve). This colorimetric assay can therefore find potential applications in the diagnostic of ADA related diseases and drug discovery.

6.3.5 Aggregation reversibility

One fascinating feature of the current system is that the aggregation process of aptamer-modified AuNPs at high salt can be halted by the addition of adenosine, and

aggregation can even be partially reversed using adenosine. This process, depicted in Fig. 6.7A, was monitored by A600 in UV-visible spectrum (Fig. 6.7B). The addition of $MgCl_2$ (60 mM) to aptamer-modified AuNPs (3 nM) led to aggregation and a gradual increase of A600. Adenosine (1 mM) was added during the aggregation process, and it resulted in a partial (60-70 %) redispersion of aggregated AuNPs as indicated by the drop in A600.

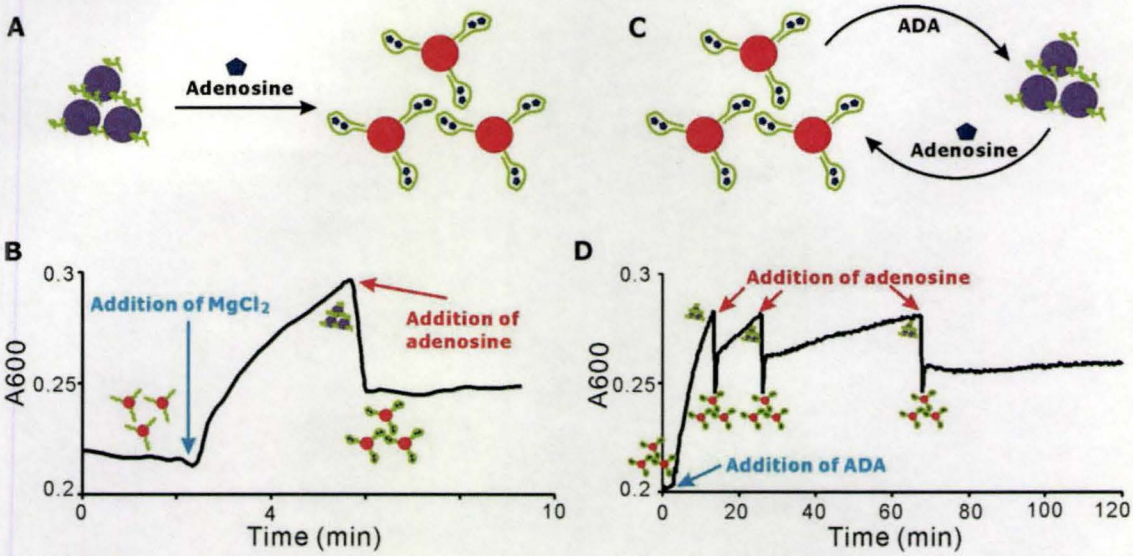

Figure 6.7. *(A) The addition of adenosine during the aggregation process of aptamer-modified AuNPs can halt the aggregation and partially redisperse some of the aggregates. This process was monitored by the change of A600 in UV-Visible spectroscopy in (B). (C) Schematic illustration of the operation of multiple aggregation/redispersion cycles: ADA converts adenosine to inosine, which causes the aggregation of Au-T10Ado-Target at high salt concentration (60 mM $MgCl_2$). The addition of adenosine redisperses the formed aggregates. Because ADA is always present in the system, the newly added adenosine will be gradually converted into inosine again, resulting in AuNP aggregation. This aggregation/redispersion process is monitored by A600 in UV-visible spectra (D).*

The reversibility was further illustrated by introducing multiple aggregation/redispersion cycles that were achieved by incorporating ADA in the system. As illustrated in Fig. 6.7C, AuNPs with folded aptamer/adenosine complex (Au-T10Ado-Target; 3 nM) were initially stabilized at 60 mM $MgCl_2$. The addition of ADA (4 units/ml) that converted adenosine to inosine led to AuNP aggregation. The addition of adenosine (1 mM) to the system partially redispersed the aggregates to stabilized AuNPs again. Since ADA was always present in the system, adenosine was being continuously

consumed, which eventually resulted in AuNP aggregation. This process was monitored at A600 (Fig 6.7D). Note that, under the current investigated conditions, this aggregation/redispersion process can only operate for a few cycles and it took longer time for ADA to consume adenosine to reach the same aggregation level than it required in the previous cycle. There are probably two reasons for this: the denaturation of ADA by AuNPs during the process or the inhibition effect from accumulated inosine product. We think the former one is the major reason in this case because our previous work[26a] where the same enzyme reaction was conducted in the absence of AuNPs showed that the aptamer/adenosine association/disassociation process can be operated by ADA many more cycles.

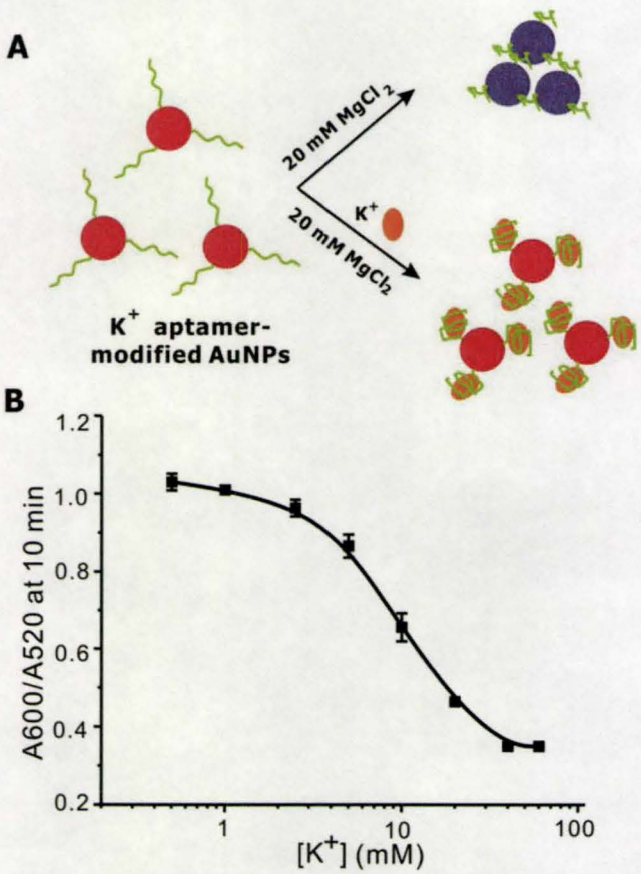

Figure 6.8. *(A) Schematic illustration of the different stability for AuNPs with folded and unfolded K^+ binding aptamer. (B) To quantify K^+, A600/A520 at 10 min after the addition of K^+ is plotted as a function of the K^+ concentration. 20 mM $MgCl_2$ was used in these assays.*

6.3.6 Generality

To test the generality of the colloidal stabilization effect observed for AuNP with folded aptamers, we investigated another DNA aptamer that specifically binds to K^+ and folds into a well-characterized tertiary structure known as G-quartet.[27] Similarly with the adenosine aptamer/AuNP system described above, AuNPs with the K^+ folded aptamer were more stable than those with its unfolded structure at high salt concentration (Fig. 6.8). Using a similar strategy as described in the adenosine sensing assay, a quantification curve where A600/A520 at 10 minutes after the addition of K^+ is plotted as a function of K^+ concentration was obtained (Fig. 6.8B). The K_d for K^+ aptamer on AuNP was then estimated to be ~15 mM (see Figure S6.3 in Supporting Information). Note that the control experiments where Na^+, Li^+, or aptamer mutant sequence (KM, Table 6.1) was used did not show significant stabilization effect (data not shown), indicating that the stabilization effect is indeed due to the specific K^+ aptamer folding.

6.4 Conclusion

This work serves as a first step towards understanding the nature of DNA aptamer folding on AuNP surfaces and its influence on colloid properties. The discoveries in this exploration would not only complement traditional polymer/colloid theories, but could also directly lead to a number of applications in nanobiotechnology including biosensors and nanoassemblies. In addition to the two different aptamer investigated in the present work, DNA and RNA can have other functions (e.g., catalytic capability) and can adopt a number of other structures such as hairpin and i-motif.[12a] The study of the behaviors of these functions and structures on surfaces should provide more insight to the complex nature of nucleic acid/colloid systems, which could lead to broader applications. Meanwhile, given the difficulties associated with the prediction of nucleic acid secondary and tertiary structures, the facile colorimetric AuNP-based assays may be applied for the study of nucleic acid folding and interpretation of their structural information.[28]

6.5 Acknowledgements

We thank Dr. An-Chang Shi for the helpful discussions. This work was supported by Natural Sciences and Engineering Research Council of Canada (NSERC), Sentinel: Canadian Network for the Development and Use of Bioactive Paper, and the Canadian Institutes for Health Research (CIHR). Y.L. holds a Canada Research Chair.

6.6 References

(1) (a) Napper, D. H. *Polymeric stabilization of collodial dispersions*; Academic Press: London, **1983**. (b) Vasconcelos, C. L. De.; Pereira, M. R.; Fonseca, J. L. C. *J. Disp. Sci. Technol.* **2005**, *26*, 59-70.

(2) (a) Rosi, N. L.; Mirkin, C. A. *Chem. Rev.* **2005**, *105*, 1547-1562. (b) Katz, E.; Willner, I. *Angew. Chem. Int. Ed.* **2004**, *43*, 6042-6108. (c) Lu, Y.; Liu, J. *Acc. Chem. Res.* **2007**, *40*, 315-323.

(3) (a) Lin. C.; Liu, Y.; Rinker, S.; Yan, H. *Chem. Phys. Chem.* **2006**, *7*, 1641-1647. (b) Deng, Z.; Lee, S. H.; Mao, C. *J. Nanosci. Nanotechnol.* **2005**, *5*, 1954-1963. (c) Seeman, N. C. *Nature* **2003**, *421*, 427. (d) Mirkin, C. A.; Letsinger, R. L.; Mucic, R. C.; Storhoff, J. J. *Nature* **1996**, *382*, 607-609 (e) Zhao, W.; Gao, Y.; Kandadai, S. A.; Brook, M. A.; Li, Y. *Angew. Chem. Int. Ed.* **2006**, *45*, 2409-2413. (f) Zhao, W.; Gao, Y.; Brook, M. A.; Li, Y. *Chem. Commun.* **2006**, 3582-3584.

(4) (a) Elghanian, R.; Storhoff, J. J.; Mucic, R. C.; Letsinger, R. L.; Mirkin, C. A. *Science* **1997**, *277*, 1078-1081. (b) Storhoff, J. J.; Elghanian, R.; Mucic, R. C.; Mirkin, C. A.; Letsinger, R. L. *J. Am. Chem. Soc.* **1998**, *120*, 1959-1964. (c) Liu, J.; Lu, Y. *J. Am. Chem. Soc.* **2003**, *125*, 6642-6643. (d) Pavlov, V.; Xiao, Y.; Shlyahovsky, B.; Willner, I. *J. Am. Chem. Soc.* **2004**, *126*, 11768-11769. (e) Wang, Z.; Lévy, R.; Fernig, D. G.; Brust, M. *J. Am. Chem. Soc.* **2006**, 128, 2214-2215. (f) Reinhard, B. M.; Sheikholeslami, S.; Mastroianni, A.; Alivisatos, A. P.; Liphardt, J. *Proc. Natl. Acad. Sci. USA.* **2007**, *104*, 2667-2672.

(5) (a) Pinto, Y. Y.; Le, J. D.; Seeman, N. C.; Musier-Forsyth, K.; Taton, T. A.; Kiehl, R. A. *Nano Lett.* **2005**, *5*, 2399-2402. (b) Aldaye, F. A.; Sleiman, H. F. *J. Am. Chem. Soc.* **2007**, *129*, 4130-4131.

(6) (a) Liu, J.; Lu, Y. *J. Am. Chem. Soc.* **2005**, *127*, 12677-12683. (b) Liu, J.; Lu, Y. *Angew. Chem. Int. Ed,* **2006**, *45*, 90-94.

(7) (a) Hunter, R. J. *Foundations of colloid science*; Oxford University Press: New York, **2004**. (b) Evans, D. F.; Wennerström, H. *The colloidal domain where physics, chemistry, biology and technology meet*; VCH: New York, **1994**.

(8) (a) Zhao, W.; Chiuman, W.; Brook, M. A.; Li, Y. *ChemBioChem.* **2007**, *8*, 727-731. (b) Zhao, W.; Chiuman, W.; Lam, J.; Brook, M. A.; Li, Y. *Chem. Commun.*, **2007**, 3729-3732.

(9) (a) Sato, K.; Hosokawa, K.; Maeda, M. *J. Am. Chem. Soc.* **2003**, *125*, 8102-8103. (b) Sato, K.; Hosokawa, K.; Maeda, M. *Nucleic Acids. Res.* **2005**, *33*, e4. c) Miyamoto, D.; Tang, Z.; Takarada, T.; Maeda, M. *Chem. Commun.*, **2007**, 4743-4745.

(10) (a) Li, H.; Rothberg, L. *Proc. Natl. Acad. Sci. USA*, **2004**, *101*, 14036-14039. (b) Wang, L.; Liu, X.; Hu, X.; Song, S. *Chem. Commun.* **2006**, *2*, 3780-3782.

(11) Sven Klussmann, *The Aptamer Handbook: Functional Oligonucleotides and Their Applications*; Wiley-VCH: Weinheim, **2006**.

(12) (a) Navani, N. K.; Li, Y. *Curr. Opin. Chem. Biol.* **2006**, *10*, 272-281. (b) Willner, I.; Zayats, M. *Angew. Chem. Int. Ed.* **2007**, *46*, 6408-6418. (c) Lin, C.; Katilius, E.; Liu, Y.; Zhang, J.; Yan, H. *Angew. Chem. Int. Ed.* **2006**, *45*, 5296-5301. (d) Eckstein, F. *Expert. Opin. Biol. Ther.* **2007**, *7*, 1021-1034. (e) Farokhzad, O. C.; Karp, J. M.; Langer, R. *Expert. Opin. Drug. Deliv.* **2006**, *3*, 311-324. (f) Nutiu, R.; Li, Y. *Methods* **2005**, *37*, 16-25. (g) Nutiu, R.; Yu, J. M.; Li, Y. *ChemBioChem.* **2004**, *5*, 1139-1144. (h) Nutiu, R.; Li, Y. *Chem. Eur. J.* **2004**, *10*, 1868-1876. (i) Nutiu, R.; Li, Y. *J. Am. Chem. Soc.* **2003**, *125*, 4771-4778. (j) Rupcich, N.; Chiuman, W.; Nutiu, R.; Mei, S.; Flora, K. K.; Li, Y.; Brennan, J. D. *J. Am. Chem. Soc.* **2006**, *128*, 780-790.

(13) Winkler, W. C.; Breaker, R. R. *Ann. Rev. Microbiol.* **2005**, *59*, 487-517.

(14) (a) Sharma, J.; Chhabra, R.; Yan, H.; Liu, Y. *Chem. Commun.* **2007**, 477-479. (b) Ueyama, H.; Takagi, M.; Takenaka, S. *J. Am. Chem. Soc.* **2002**, *124*, 14286-14287. (c) Liu, D.; Bruckbauer, A.; Abell, C.; Balasubramanian, S.; Kang, D. J.; Klenerman, D.; Zhou, D. *J. Am. Chem. Soc.* **2006**, *128*, 2067-2071. (d) Zayats, M.; Huang, Y.; Gill, R.;

Ma, C. A.; Willner, I. *J. Am. Chem. Soc.* **2006**, *128*, 13666-13667. (e) Xiao, Y.; Piorek, B. D.; Plaxco, K. W.; Heeger, A. J. *J. Am. Chem. Soc.* **2005**, *127*, 17990-17991. (f) Radi, A. E.; Acero Sanchez, J. L.; Baldrich, E.; O'Sullivan, C. K. *J. Am. Chem. Soc.* **2006**, *128*, 117-124.

(15) Mie, G. *Ann. Phys.* **1908**, *25*, 377-452.

(16) Storhoff, J. J.; Elghanian, R.; Mirkin, C. A.; Letsinger, R. L. *Langmuir* **2002**, *18*, 6666-6670.

(17) (a) Hill, H. D.; Mirkin, C. A. *Nat. Protocols.* **2006**, *1*, 324-336. (b) Liu, J.; Lu, Y. *Nat. Protocols* **2006**, *1*, 246-252.

(18) (a) Park, S.; Brown, K. A.; Hamad-Schifferli, K. *Nano Lett.* **2004**, *4*, 1925-1929. (b) Huang, E.; Satjapipat, M.; Han, S.; Zhou, F. *Langmuir* **2001**, *17*, 1215-1224. (c) Li, Z.; Jin, R.; Mirkin, C. A. ; Letsinger, R. L. *Nucleic Acids Res.* **2002**, 30, 1558-1562. (d) Storhoff, J. J. ; Elghanian, R. ; Mirkin, C. A. ; Letsinger, R. L. *Langmuir*, **2002**, 18, 6666-6670. (e) Weitz, D. A.; Lin, M. Y.; Sandroff, C. J. *Surf. Sci.* **1985**, 158, 147-164. (f) Blatchford, C. G.; Campbell, J. R.; Creighton, J. A. *Surf. Sci.* **1982**, 120, 435-455.

(19) (a) Zuker, M. *Nucleic Acids Res.* **2003**, 31, 3406-3415. (b) Lin, C. H.; Patel, D. J. *Chem. Biol.* **1997**, *4*, 817-832. (c) Huizenga, D. E.; Szostak, J. W. *Biochemistry*, **1995**, *34*, 656-665.

(20) Demers, L. M.; Mirkin, C. A.; Mucic, R. C.; Reynolds, R. A., III; Letsinger, R. L.; Elghanian, R.; Viswanadham, G. *Anal. Chem.* **2000**, *72*, 5535-5541.

(21) (a) Glomm. W. R. *J. Dispersion Sci. Technol*, **2005**, *26*, 389-414. (b) Walker, H. W.; Grant, S. B. *Langmuir*, **1996**, *12*, 3151-3156.

(22) Rodríguez-Fernández, J.; Pérez-Juste, J.; Liz-Marzán, L. M.; Lang, P. R. *J. Phys. Chem. C* **2007**, *111*, 5020-5025.

(23) Sikkema, F. D.; Comellas-Aragonès, M.; Fokkink, R. G.; Verduin, B. J. M.; Cornelissen, J. J. L. M.; Noltea, R. J. M. *Org. Biomol. Chem.* **2007**, *5*, 54-57.

(24) Shen, G.; Tercero, N.; Gaspar, M. A.; Varughese, B.; Shepard, K.; Levicky, R. *J. Am. Chem. Soc.* **2006**, *128*, 8427-8433.

(25) (a) Zanchet, D.; Micheel, C. M.; Parak, W. J.; Gerion, D.; Alivisatos, A. P. *Nano Lett.*, **2001**, *1*, 32-35. (b) Parak, W. J.; Pellegrino, T.; Micheel, C. M.; Gerion, D.; Williams, S. C.; Alivisatos, A. P. *Nano Lett.* **2003**, *3*, 33-36.

(26) (a) Nutiu, R.; Li, Y. *Angew. Chem. Int. Ed.* **2005**, *44*, 5464-5467. (b) Rupcich, N.; Nutiu, R.; Li, Y.; Brennan, J. D. *Angew. Chem. Int. Ed.* **2006**, *45*, 3295-3299.

(27) Radi, A.; O'Sullivan, C. K. *Chem. Commun.*, **2006**, 3432-3434.

(28) (a) Jennings, T. L.; Schlatterer, J. C.; Singh, M. P.; Greenbaum, N. L.; Strouse, G. F. *Nano Lett.* **2006**, *6*, 1318-1324. (b) Chah, S.; Hammond, M. R.; Zare, R. N. *Chem. Biol*, **2005**, *12*, 323-328.

6.7 Supporting Information

Experimental Section

Materials. Trisodium citrate, hydrogen tetrachloroaurate(III) ($HAuCl_4$), 6-mercaptohexan-1-ol (MCH), adenosine, adenosine 5'-triphosphate (ATP), potassium chloride (KCl), sodium chloride (NaCl), lithium chloride (LiCl), inosine, *erythro*-9-(2-hydroxy-3-nonyl)adenine (EHNA), ethyl acetate and adenosine deaminase (ADA) were purchased from Sigma and used as received. [γ-^{32}P]-ATP was obtained from Amersham Biosciences. DNA molecules were obtained from Integrated DNA Technologies (IDT).

Preparation of aptamer-modified AuNPs. AuNPs (~13.5 nm in diameter based on transmission electron microscopy (TEM) measurement) were prepared according to previously described protocols.[1] The concentration was estimated using UV/vis spectroscopy to be ~13 nM, based on an extinction coefficient of 2.7×10^8 M^{-1} cm^{-1} at λ=520 nm.[1a] Aptamer-modified AuNPs were then prepared using the standard surface modification protocol based on Au-S chemistry.[1] Briefly, an AuNP solution (600 μL, ~13 nM) was mixed with thiol-modified oligonucleotides (280 μL, 6.6 μM) (see Table 6.1 for the sequences of adenosine, K^+ aptamers and their mutants). The solution was incubated at room temperature for 12 h. Tris-HCl buffer (10 μL, 1 M, pH 7.5) and aqueous NaCl (90 μL, 1M) were added, and the mixture was incubated for another 12 h. After that, Tris-HCl buffer (5 μL, 1 M, pH 7.5) and aqueous NaCl (50 μL, 5M) were added, and the

mixture was further incubated for 18 h at room temperature. The solution was then separated by a centrifuge at 22000 *g* for 15 min. The precipitated aptamer-modified AuNPs were washed with double-deionized (dd) H_2O (600 μL) and isolated using centrifugation. Finally, adenosine aptamer-modified AuNPs (referred to as Au-Ado and Au-T10Ado for the aptamer without and with T10 linker, respectively) and K^+ aptamer-modified AuNPs (referred to as Au-K) were redispersed in 600 μL adenosine buffer (Tris-HCl (20 mM), pH = 7.5, NaCl (100 mM)) and ddH_2O, respectively. For the synthesis of radioactive oligonucleotide, [γ-^{32}P] ATP (20 μCi) was incorporated using the manufacturer-supplied protocol.

MCH treatment. The aptamer-modified AuNPs were treated with MCH as described elsewhere.[2] Briefly, Au-Ado (or Au-T10Ado) solution prepared above was diluted with an equal volume of adenosine buffer, MCH was then added to give a final MCH concentration of ~ 4 μM. The MCH treatment was performed at room temperature for 30 min. The reaction was quenched by three washes with equal volumes of ethyl acetate, which removed excess MCH from the aqueous solution. A similar procedure was used for Au-K with an exception that ddH_2O was used instead of adenosine buffer. The aptamer-modified AuNPs were spun down using centrifugation at 22 000 *g* for 15 min. The final Au-Ado (or Au-T10Ado) and Au-K were redispersed in 600 μL adenosine buffer and ddH_2O, respectively.

Au-Ado (or Au-T10Ado) stability with and without adenosine. Adenosine aptamer folding on Au-Ado (or Au-T10Ado) was conducted in a solution that contained Au-Ado (or Au-T10Ado) (~ 3 nM), adenosine (1 mM), Tris-HCl (20 mM), pH = 7.5, 4 mM $MgCl_2$ and NaCl (100 mM). At this salt concentration (4 mM $MgCl_2$ and100 mM NaCl), both Au-Ado (or Au-T10Ado) and Au-Ado with folded aptamer/adenosine complex (referred to as Au-Ado-Target) (or Au-T10Ado-Target) were stable and the solutions appeared red. To determine their stability, $MgCl_2$ (1 M) solution was gradually added into AuNP solutions until a red-to-purple color change was observed over a short period of time (~ 1 min).

Au-K stability with and without K^+. K^+ aptamer folding on Au-K was performed in an aqueous solution containing Au-K (~ 3 nM) and KCl (10 mM). Using a strategy that is similar to the adenosine system, the stability of Au-K and Au-K with the folded aptamer/K^+ complex (referred to as Au-K-Target) was studied by gradually adding $MgCl_2$ (1 M) until a red-to-purple color change was observed over a short period of time (~ 1 min).

Adenosine and K^+ sensing assays. In the case of adenosine, assay solutions (250 μL) contained various amounts of adenosine, Au-T10Ado (~ 3 nM), Tris-HCl (20 mM), pH = 7.5, NaCl (100 mM) and $MgCl_2$ (60 mM). Specifically, a mixture (180 μL) of Au-T10Ado (~ 4.14 nM), Tris-HCl (28 mM) and NaCl (138 mM) was first prepared. A solution (70 μL) of $MgCl_2$ (214 mM) and various amounts of adenosine were then added, after which UV-visible spectra were recorded continuously on a Cary300 UV/vis spectrophotometer for 10 min at room temperature (21 °C) or 35 °C.

A similar assay was performed for the detection of K^+. Briefly, assay solutions (250 μL) contained various amounts of K^+, Au-K (~ 3 nM), and $MgCl_2$ (20 mM). UV-visible spectra were recorded continuously on a Cary300 UV/vis spectrophotometer for 10 min at room temperature immediately after the addition of KCl and $MgCl_2$.

Adenosine deaminase (ADA) sensing assay. Au-T10Ado (~ 3 nM) was mixed with adenosine (1 mM) solution in a buffer containing Tris-HCl (20 mM), pH = 7.5, $MgCl_2$ (60 mM) and NaCl (100 mM). Various amounts of ADA were then added, after which UV-visible spectra were recorded on Cary300 UV/vis spectrophotometer at room temperature. To study the inhibition, the ADA inhibitor, EHNA (400 μM), was incorporated in above Au-T10Ado solution before the addition of ADA.

Characterizations. TEM samples were prepared by dropping AuNP solutions (4 μL) onto a carbon-coated copper grid. The solution was wicked from the edge of the grid with a piece of filter paper after 1 min. TEM images were taken with a JEOL 1200 EX. UV-visible spectra were recorded on a Cary300 UV/vis spectrophotometer. Dynamic light scattering (DLS) measurements were performed at 25 °C and a scattering angle of 90° using a Brookhaven (Holtsville, NY) 256 channel BI-APD 8590 correlator and a 35

mW 632.8 nm laser. The particle size (diameter) was calculated by cumulative intensity distribution using the program CONTIN. Each reported particle size was the average of 10 measurements.

Supporting Figures

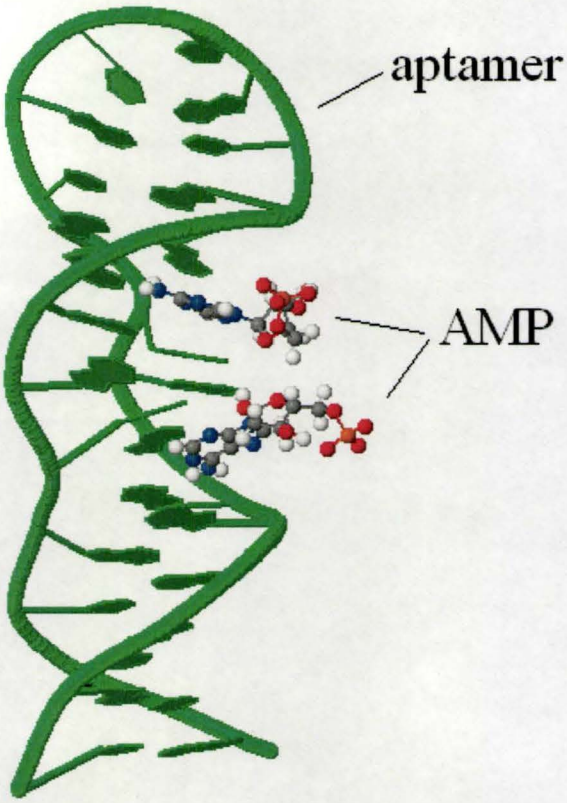

Figure S6.1. *Three-dimensional model for folded DNA aptamer/adenosine monophosphate (AMP) complex. This structure, obtained based on a previous NMR study,[3] is adopted from the RCSB protein data bank. Aptamer backbone together with nucleobases are shown in green. In AMP model structure, C, N, O, P and H are shown in grey, blue, red, orange and white, respectively. One aptamer/AMP complex contains two adjacently bound AMP molecules. Detailed structural information can be found in reference 3.*

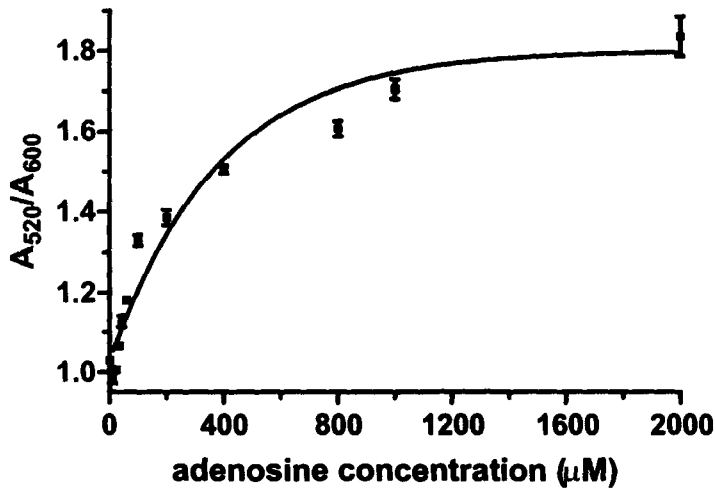

Figure S6.2. *Determination of the dissociation constant (K_d) for adenosine-binding DNA aptamer. The A_{520}/A_{600} (abbreviated as A) vs. adenosine concentration data were fit into a modified one phase exponential association equation, $A = A_{min} + (A_{max} - A_{min}) \times (1-e^{-k[adenosine]})$, where the best-fit A_{min} = 1.026 with the A_{max} constraint of ≥1.8, with R^2 = 0.95. K_d was approximated from the mid-point of the equation, –ln(0.5/k), where k (an arbitrary constant) has a value of 0.002632. By this method, a K_d of 263 μM was obtained.*

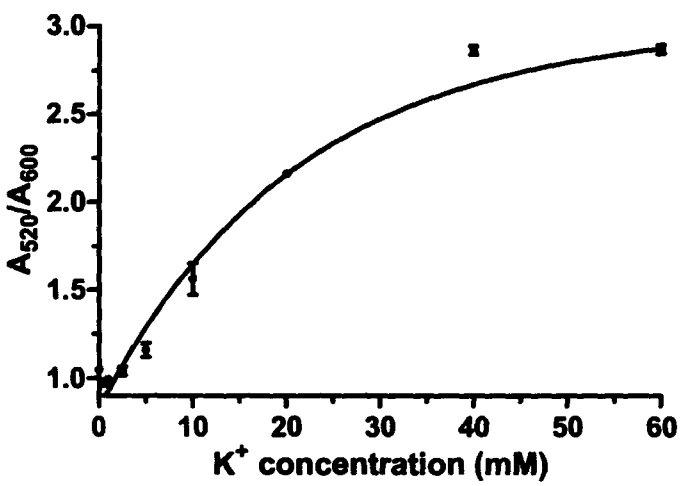

Figure 6.3. *Determination of K_d for potassium ion-binding DNA aptamer. The A_{520}/A_{600} vs. potassium concentration data were fit into a modified one phase exponential association equation, $A = A_{min} + (A_{max} - A_{min}) \times (1-e^{-k[potassium]})$, where the best-fit A_{min} = 0.83 with the A_{max} constraint = 3, with R^2 = 0.98. K_d was approximated from the mid-*

point of the equation, –ln(0.5/k), where k has a value of 0.047. By this method, a K_d of 15 mM was obtained.

References

(1) (a) Hill, H. D.; Mirkin, C. A. *Nat. Protocols*. **2006**, *1*, 324-336. (b) Liu, J.; Lu, Y. *Nat. Protocols* **2006**, *1*, 246-252.

(2) (a) Park, S.; Brown, K. A.; Hamad-Schifferli, K. *Nano Lett.* **2004**, *4*, 1925-1929. (b) Huang, E.; Satjapipat, M.; Han, S.; Zhou, F. *Langmuir* **2001**, *17*, 1215-1224. (c) Zhao, W.; Chiuman, W.; Brook, M. A.; Li, Y. *ChemBioChem*. **2007**, *8*, 727-731.

(3) Lin, C. H.; Patel, D. J. *Chem. Biol*. **1997**, *4*, 817-832.

Chapter 7: DNA polymerization on gold nanoparticles through rolling circle amplification: towards novel scaffolds for three-dimensional periodic nanoassemblies

The following chapter was published in Angewandte Chemie International Edition under the citation:

Weian Zhao, Yan Gao, Srinivas A. Kandadai, Michael A. Brook, Yingfu Li. DNA polymerization on gold nanoparticles through rolling circle amplification: towards novel scaffolds for three-dimensional periodic nanoassemblies. *Angew. Chem. Int. Ed.*, 2006, 45, 2409-2413.

I was responsible for all data collection and analysis with the exception that Dr. Yan Gao conducted the AFM experiments. Dr. Srinivas A. Kandadai trained me with DNA-based techniques and also helped in the collection of PAGE data. I wrote the first draft of the manuscript and Dr. Brook and Dr. Li provided editorial input to generate the final draft of the paper.

7.1 Introduction

Recent years have witnessed an explosion of interest in the use of DNA-nanoparticle bioconjugates for programmed nanostructures, 1D or 2D nanoparticle arrays, nanoelectronics, and biosensing and biodiagnostics.[1-9] DNA was chosen as a polymeric material in these studies owing mainly to the specificity of DNA base-pairing, the predictability of inter- or intramolecular interactions, its physicochemical stability, and mechanical rigidity. In addition, DNA can be manipulated and modified by a wide range of enzymes, including DNA polymerase, ligase, and restriction endonucleases. The powerful, convenient, and specific enzymatic manipulations make DNA a highly desirable building block for the construction of various nanostructures. In the current study, we set out to investigate whether we can perform rolling circle amplification (RCA) between a DNA oligonucleotide tethered to gold nanoparticles (AuNPs) as the primer and a single-stranded circular DNA as a template, catalyzed by a special DNA polymerase known as ϕ29 DNA polymerase (ϕ29DNAP).

RCA is a powerful but simple biochemical method that can be used to generate long single-stranded DNA (ssDNA) with a repeating sequence unit.[10-11] In a typical RCA process, a DNA polymerase, such as ϕ29DNAP, which has a strong ability to displace newly synthesized DNA strands, makes continuous nucleotide additions to a growing DNA chain over a short circular single-stranded DNA as the template under isothermal conditions. As a result, long, linear tandemly repetitive single strands of DNA are produced. As the synthesized long DNA molecules contain many repeating sequence motifs, RCA coupled with ensuing hybridization with fluorescent DNA probes has been used as an on-chip signal-amplification tool for sensitive biosensing.[12-16] Recently, it has been shown that long DNA molecules from RCA can be used as scaffolds for assembling nanoparticles to form 1D nanoparticle arrays.[17-18] However, to our knowledge, performing the RCA reaction on gold nanoparticles and using the resultant special DNA-AuNP assemblies to form 3D nanoparticle array have not been demonstrated.

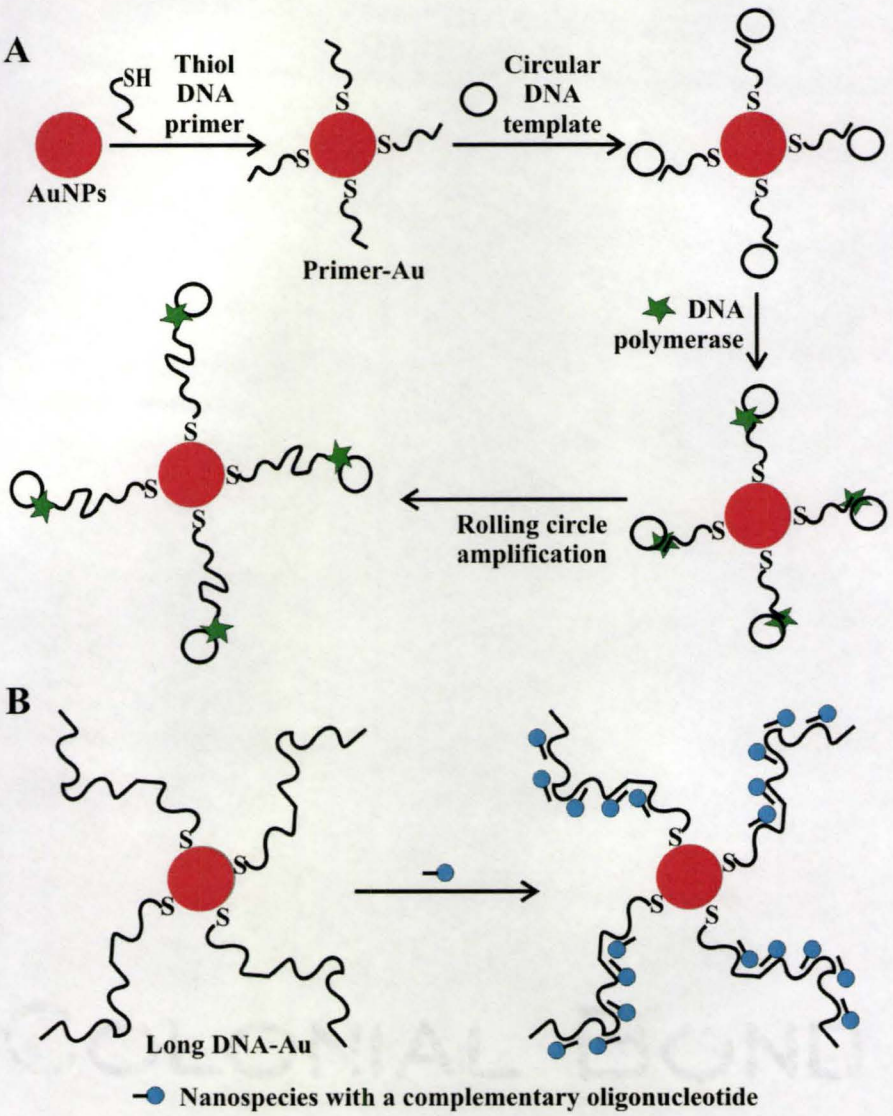

Figure 7.1. *A) Schematic illustration of RCA on gold nanoparticles (AuNPs). B) DNA-Au conjugates produced by RCA as a scaffold for the formation of 3D nanostructures.*

7.2 Results and discussion

Figure 7.1 schematically illustrates the RCA process on gold nanoparticles and its scaffolding for 3D periodical nanoassemblies. Gold nanoparticles of 15 nm diameter were first prepared by the classical citrate reduction route. Thiol modified DNA primers (41 nucleotides) were then functionalized onto the nanoparticles following Mirkin's approach.[5] The concentration of DNA primers on the gold nanoparticles, referred to

hereafter as primer-Au, was determined using UV/Vis spectroscopy by measuring the amount of DNA in solution before and after coupling; each primer-Au contained approximately 230 DNA primer strands. A 63-nucleotide-long circular DNA template was then annealed with the DNA-functionalized gold nanoparticles. The hybridization efficiency, as examined by measuring the radioactivity on the gold nanoparticles and in solution after annealing with a radiolabeled circular DNA template, was estimated to be approximately 30 %, which is consistent with a previous study.[19] A control experiment in which a non-complementary radiolabeled circular DNA template was annealed with primer-Au showed negligible non-specific binding.

To achieve the best RCA performance, we optimized the experimental conditions. Our foremost concern was the stability of primer-Au in the presence of dithiothreitol (DTT). Primer-Au nanoparticles underwent irreversible aggregation in the presence of 4 mM DTT (a condition recommended by the manufacturer of ϕ29DNAP) at 30 °C in 30 min. As ϕ29DNAP was supplied in a stock solution containing 1 mM DTT that was critical to the storage of the enzyme, we next performed the RCA reaction using diluted conditions (50 μM DTT and 5 units of ϕ29DNAP in 10 μL reaction solution). At this concentration of DTT, primer-Au was found to be stable (no detectable color change and no aggregation). Note that further dilution of the ϕ29DNAP stock solution produced an ineffective enzyme concentration for RCA. The second point of concern was the effect of the concentration of primer-Au conjugates on the performance of ϕ29DNAP. To investigate this issue, we conducted the RCA reaction in solution in the presence of T20-Au (gold nanoparticles functionalized with DNA oligonucleotides containing 20 thymine bases) and found that these nanoparticles, particularly at high concentration (typically over 3 nM), significantly inhibited the activity of ϕ29DNAP (data not shown) presumably because some enzymes were nonspecifically adsorbed and denatured by the gold nanoparticles. On the basis of these results, we subsequently carried out the RCA reaction at relatively low concentrations of primer-Au (*ca.* 0.67 nM) and over a relatively short period (30 min), considering the high efficiency of DNA polymerase. The reaction temperature was fixed at 30 °C, as recommended by the manufacturer.

The resultant DNA was displaced from the surface of the gold nanoparticles by incubation with 250 mM mercaptoethanol at 37 °C overnight. The band obtained at the top of a 10% PAGE gel (Figure 7.2, lane 1) indicated that a large amount of high-molecular-weight DNA product was formed by RCA on the gold nanoparticles. As a critical test of the rolling circle amplification, a restriction endonuclease digestion experiment was performed. Each repetitive DNA unit contained a TCGA site that can be digested by the endonuclease Taq I. In the presence of Taq I, the long DNA molecules were indeed converted into much shorter DNA fragments (monomer, dimer, trimer, etc.) after 2 h digestion (lane 2 of Figure 7.2). It was difficult to determine precisely the length of the DNA produced by RCA; however, we estimated (based on the counting of DNA fragments as the marker in lane 2 of Figure 7.2) that the DNA molecules produced on the gold nanoparticles were significantly larger than 1000 nt (nt = nucleotide).

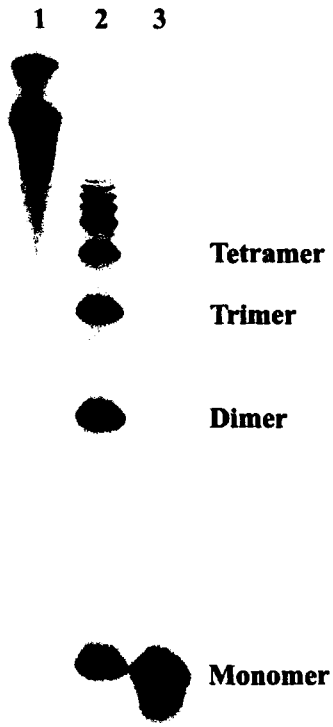

Figure 7.2. *10% denaturing polyacrylamide gel electrophoresis (PAGE) for the product obtained by RCA and synthesized from radiolabeled dNTPs (lane 1), the product obtained after digestion by Taq I (lane 2), and a 63-nt-long linear DNA oligonucleotide (lane 3).*

The long-DNA-Au conjugates were also directly investigated by atomic force microscopy (AFM). A DNA brush conformation, in which long DNA (typically hundreds of nanometers to microns in length) grafted from gold nanoparticles by RCA, was clearly observed (Figure 7.3, A and B). The long ssDNA, unlike rigid double-stranded DNA (dsDNA), cannot be fully stretched; that is, some of the ssDNA may stick together and condense into globular structures. Indeed, in some cases, two ssDNA (Figure 7.3B, blue

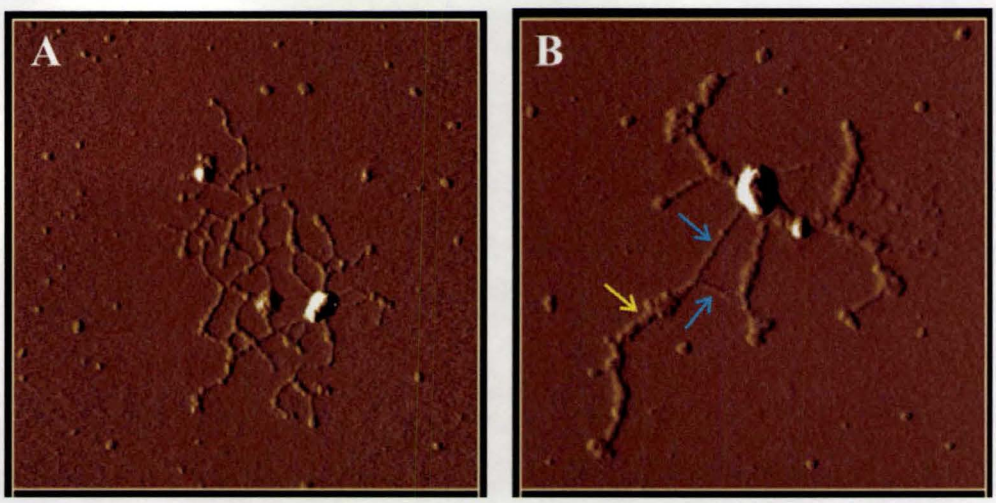

Figure 7.3. *Tapping mode AFM images (amplitude mode) for long-DNA-Au conjugates obtained through RCA with gold nanoparticles. Scale: A) 1000 × 1000 nm^2; B) 800 × 800 nm^2. In (B), the blue arrows indicate ssDNA strands, and the yellow arrow indicates dsDNA-like structures.*

arrow) appeared to merge into dsDNA-like structures (Figure 7.3B, yellow arrow). It was a surprise that there were only tens or less of ssDNA grafted from each gold nanoparticle, considering that there were about 230 primers on each nanoparticle. Such a low graft density may be attributed to the fact that 1) the hybridization efficiency of the circular DNA template and primer-Au was poor (*ca.* 30%), 2) the DTT present (even at a low concentration) could displace the primer from the surface by thiol exchange, or 3) the DNA polymerase could be inhibited by the Au surface due to enzyme denaturation and steric effects. Note also that the size of these gold nanoparticles as measured by AFM was larger than those of both unfunctionalized "bare" gold nanoparticles and primer-Au (AFM data not shown), which is a typical phenomenon when one uses AFM to characterize a rigid nanoparticle core with polymer brushes collapsed on the surface.[20]

We next tested the capabilities of the DNA-Au nanoparticle conjugates, referred to as long-DNA-Au, to act as 3D scaffolds for further nanoassemblies by incubating long-DNA-Au with 5-nm gold nanoparticles that were modified with a 25-nt antisense oligonucleotide overnight. The resultant long-DNA-Au/5-nm-AuNP complexes were isolated by centrifugation at a relatively low speed (5000 rpm for 10 min) and analyzed by transmission electron microscopy (TEM).

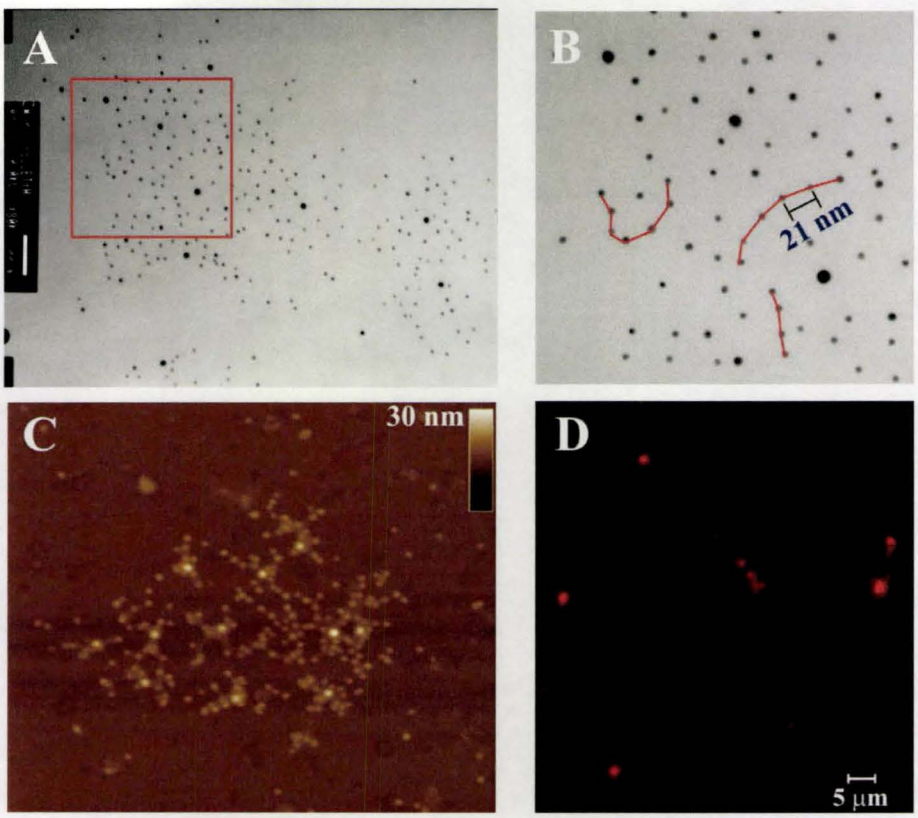

Figure 7.4. *A) TEM images of nanoassembled superstructures prepared from 5-nm gold nanoparticles modified with antisense DNA and long-DNA-Au scaffolds. Scale bar: 100 nm. The red box was zoomed in to obtain the image shown in part (B). C) Height-mode AFM image of nanoassembled superstructures constructed from long-DNA-Au and 5-nm gold nanoparticles. The brighter and bigger dots correspond to the 15-nm gold nanoparticles. Scale: 2000 × 2000 nm^2. D) Confocal microscopy images of long-DNA-Au decorated with complementary DNA-capped Alexa 647. Scale bar: 5 μm.*

A typical nanoassembled superstructure (Figure 7.4 A) showed that 5-nm gold nanoparticles appeared only in the area (typically a few hundred nanometers in diameter) surrounding the 15-nm gold nanoparticles, indicating that these complexes were formed specifically by Watson-Crick base pairing. The average number of assembled 5-nm gold nanoparticles on each long-DNA-Au conjugate was approximately 26, as obtained statistically from 157 individual nanoassembled architectures. Remarkably, the distance between 5-nm gold nanoparticles along the long DNA (to clarify, attempts were made to trace DNA; see Figure 7.4B, red line) in most cases was in good agreement with the theoretical distance (ca. 21 nm), given that the distance between 5-nm gold nanoparticles is identical to the length of the 63-nucleotide-long DNA template and the separation between base pairs in a typical B-form dsDNA helix is 0.34 nm. These data strongly suggest that the nanoassembly events occurred in a well-defined, periodic manner along these long DNA. This conclusion was further confirmed by AFM studies in which the successful periodical assembly of 5-nm gold nanoparticles along these long DNA surrounding the 15-nm gold nanoparticles was clearly observed (Figure 7.4C). Control experiments in which 5-nm gold nanoparticles that were not functionalized with antisense DNA were incubated with long-DNA-Au, did not show any well-defined superstructures (data not shown). Indeed, neither long-DNA-Au nanoparticles nor 5-nm gold nanoparticles could be spun down by using the same centrifugation speed (5000 rpm for 10 min).

The long-DNA-Au conjugates were also investigated as scaffolds that could be decorated with dyes (Alexa 647) modified with antisense DNA. After incubation, the complex was isolated, purified by centrifugation, and analyzed by confocal microscopy. Bright fluorescent dots, with diameters of hundreds of nanometers to microns, were clearly observed (Figure 7.4D). In contrast, the control experiment in which Alexa 647 modified with non-complementary DNA was used did not show any fluorescence (data not shown). Given that the RCA process itself is a signal-amplification tool and is widely used for microarray-based biodetections,[12-16] the adaptation of RCA on nanoparticles can potentially open a new avenue for ultrasensitive nanoparticle-based biosensing. This

application may be particularly useful when the unique properties of nanoscaled materials are incorporated.

7.3 Conclusion

In conclusion, we have demonstrated that long single-stranded DNA can be grafted directly from gold nanoparticles and the resultant DNA-AuNP assemblies can be further used as a unique scaffold that may find a number of applications in nanotechnology and biodiagnostics. The envisioned applications include the design of well-ordered 3D nanoparticle arrays, nanocomputing devices, nanophotonics and electronics, bioimaging tools, and ultrasensitive biosensors. While there are still some drawbacks (e.g. high polydispersity of DNA polymers synthesized by RCA, thiol exchange by DTT, interparticle crosslinking during nanoassembly when AuNPs are attached with multiple DNA strands, etc.) associated with this strategy that need to be overcome, the scaffolding on the basis of this long-DNA-Au scaffold has several significant advantages: 1) The assembly events are performed in a three-dimensional and periodic manner, given that these DNA polymer brushes containing repetitive sequences are grafted from a gold nanoparticle core. 2) This assembly is fully controllable, that is, the distance between assembled nanospecies can be readily varied by adjusting the length of the circular DNA template. 3) The assembly is entirely reversible owing to the nature of DNA base pairing. 4) Multiple assemblies, wherein two or more nanospecies are constructed simultaneously, can be readily achieved simply by assembling different species functionalized with different antisense DNA or by performing different RCA process on each single nanoparticle.

7.4 Experimental Section

15-nm gold nanoparticles were prepared following the reported approach with minor modifications.[5] Trisodium citrate (Sigma; 25 mL, 38.8 mM) was added to a boiling solution of $HAuCl_4$ (Sigma; 250 mL, 1 mM). Within several minutes, the color of the solution changed from pale yellow to deep red. The mixture was allowed to heat

under reflux for another 30 min to ensure complete reduction, before it was slowly cooled to room temperature, and the nanoparticles were filtered through a 200-nm filter.

Primer-Au conjugates were prepared according to a published method.[5] Briefly, 5'-thiol-modified DNA primers (5'-thiol-TTTTTTTTTTTTTTTTTTTTGGCGAAGACAGGTGCTTAGTC, Keck Biotechnology Resource Laboratory, Yale University; 5.6 μL, 70 μM) were mixed with H_2O (25 μL) and then added to the gold nanoparticles (50 μL, 13.4 nM). The solution was aged overnight and then added to phosphate buffer (10 mM, pH 7, NaCl, 0.1M) and aged for another 12 h. NaCl (0.3M) and phosphate (10 mM, pH 7) were then added to the mixture and the solution was allowed to stand for another 12 h. The resultant solution was centrifuged, and the particles were washed once with sodium phosphate buffer (200 μL, 0.3M, pH 7). The primer-Au conjugates were then redispersed in water (50 μL).

The circular DNA template was prepared according to a procedure adapted from a published protocol.[21] First, linear DNA (5'-TGTCTTCGCCTTCTTGTTTCCTTTCCTTGAAACTTCTTCCTTTCTTTCTTTCGAC TAAGCACC, Central Facility, McMaster University; 16.3 μL, 30.6 μM) was phosphorylated by T4 polynucleotide kinase (MBI Fermentas) using the manufacturer-supplied protocol. The enzyme was denatured by heating at 90 °C for 5 min. This solution was used directly for DNA ligation in the presence of ligation templates (5'-GGCGAAGACAGGTGCTTAGTC, Central Facility, McMaster University; 7.6 μL, 78.5 μM and T4 DNA ligase (MBI Fermentas) at room temperature overnight. The circular DNA was purified by 10% PAGE and redispersed in water.

RCA on the gold nanoparticles was performed as follows: First, the circular DNA template was annealed with primer-Au. In a typical experiment, a solution of the primer-Au (4 μL, *ca.* 13.4 nM) and an excess of the circular template were mixed in RCA buffer solution (50 mM Tris-HCl, 10 mM $MgCl_2$, 10mM $(NH_4)_2SO_4$, pH 7.5, 20 μL). This mixture was heated at 60 °C for 5 min and then annealed at room temperature for 30 min. Two centrifugation/redispersion cycles were applied to get rid of the non-specifically bound circular template by RCA buffer solution (50 μL), and the final product was

redispersed in RCA buffer solution (20 μL). ϕ29 DNA polymerase (NEB, 4 μL, 40 units) and dNTPs (dATP, dTTP, dCTP, dGTP; MBI Fermentas, 4 μL, 1 mM) were added to the above solution, and the final volume was brought to 80 μL with RCA buffer solution. For the synthesis of radioactive RCA product, [α-^{32}P]-dGTP (Amersham Biosciences; 2 μL, specific activity: 20 μCi) was incorporated. The reaction was performed at 30 °C for 30 min. The product (long-DNA-Au) was washed twice with RCA buffer (50 μL) and H_2O (50 μL) using centrifugation and redispersed in water (20 μL). For AFM experiments, the solution of long-DNA-Au was diluted 10-fold and 30 μL of the resultant solution was spin-coated (3500 rpm) onto a freshly cleaved mica surface and investigated by AFM (Digital Instruments Nanoscope II). For gel electrophoresis experiments, the resultant DNA was displaced from the surface of the gold nanoparticles by treating with a solution of mercaptoethanol (Sigma, 250 mM) at 37 °C overnight. Endonuclease digestion was performed by Taq I (MBI Fermentas) using conditions recommended by the manufacturer, and the resultant DNA fragments were analyzed by 10% denaturing PAGE.

To form the assembly with 5-nm gold nanoparticles, 5'-biotinylated oligonucleotide (5'-biotin-CCTTGAAACTTCTTCCTTTCTTTCT, Keck Biotechnology Resource Laboratory, Yale University; 2.5 μL, 91.8 μM) was incubated with streptavidin-capped 5-nm gold nanoparticles (Canemco Inc & Marivac Inc; 50 μL) in a buffer solution (20 mM Tris-HCl, 20 mM EDTA, 300 mM NaCl, pH 7.5, 300 μL) at room temperature for 30 min. The resultant antisense-DNA-AuNP complex was washed twice with RCA buffer (200 μL) using centrifugation and redispersed in RCA buffer solution (20 μL). Long-DNA-Au in RCA buffer solution (20 μL) was then added. The mixture was frozen in a bath of dry ice and propan-2-ol and then thawed at room temperature overnight, an approach known to facilitate the hybridization of DNA-attached gold nanoparticles.[5] The nanoassembled complex was isolated by centrifugation at 5000 rpm for 10 min and redispersed in RCA buffer. The TEM sample was prepared by dropping this solution (5 μL) onto a copper coated grid. After 5 min, the solution was wicked from the edge of the grid with a piece of filter paper. TEM images were measured with a JEOL 1200EX transmission electron microscope.

To prepare the fluorophore-functionalized nanoparticles, oligonucleotide modified at the 5' position with Alexa 647 (5'-Alexa 647-TGAAACTTCTTCCTTTCTTTCTTTC, Invitrogen; 0.5 μL, 90 μM) and long-DNA-Au (10 μL) were added to RCA buffer (10 μL). The mixture was heated at 65 °C for 5 min and then annealed at room temperature for 15 min. The resultant complex was washed twice with RCA buffer (50 μL), isolated by centrifugation, and analyzed by confocal microscopy (SLM 8100 spectrofluorimeter, Spectronic Instruments, Rochester, NY).

7.5 Acknowledgement

The authors wish to thank Andy M. Duft for help with AFM measurements. Financial support was provided by the Natural Sciences and Engineering Research Council of Canada (NSERC) and the Canadian Institutes for Health Research (CIHR). Y.L. holds a Canada Research Chair.

7.6 References

[1] a) B. Samorì, G. Zuccheri, *Angew. Chem. Int. Ed.* **2005**, 44, 1166-1181; b) E. Katz, I. Willner, *Angew. Chem. Int. Ed.* **2004**, 43, 6042-6108.

[2] N. L.Rosi, C. A. Mirkin, *Chem. Rev.* **2005**, 105, 1547-1562.

[3] S. Brakmann, *Angew. Chem. Int. Ed.* **2005**, 44, 1166-1181.

[4] C. A. Mirkin, R. L Letsinger, R. C. Mucic, J. J. Storhoff, *Nature* **1996**, 382, 607-609.

[5] R. Elghanian, J. J. Storhoff, R. C. Mucic, R. L. Letsinger, C. A. Mirkin, *Science* **1997**, 277, 1078-1080.

[6] D. Zanchet, C. M. Micheel, W. J. Parak, D. Gerion, A. P. Alivisatos, *Nano Lett.* **2001**, 1, 32-35.

[7] C. Sönnichsen, B. M. Reinhard, J. Liphardt, A. P. Alivisatos, *Nat. Biotechnol.* **2005**, 23, 741-745.

[8] J. Liu, Y. Lu, *J.Am. Chem. Soc.* **2004**, 126, 12298-12305.

[9] T. Niazov, V. Pavlov, Y. Xiao, R. Gill, I. Willner, Nano Lett. 2004, 4, 1683-1687.

[10] A. Fire, S. Xu, Proc. *Natl. Acad. Sci. USA* **1995**, 92, 4641-4645.

[11] D. Liu, S. L. Daubendiek, M. A. Zillman, K. Ryan, E. T. Kool, *J. Am. Chem. Soc.* **1996**, 118, 1587-1594.

[12] P. M. Lizardi, X. Huang, Z. Zhu, P. Bray-Ward, D. C. Thomas, D. C. Ward, *Nat. Genet.* **1998**, 19, 225-232.

[13] B. Schweitzer, S. Wiltshire, J. Lambert, S. O'Malley, K. Kukanskis, Z. Zhu, S. F. Kingsmore, P. M. Lizardi, D. C. Ward, *Proc. Natl. Acad. Sci. USA* **2000**, 97, 10113-10119.

[14] B. Schweitzer, S. Roberts, B. Grimwade, W. Shao, M. Wang, Q. Fu, Q. Shu, I. Laroche, Z. Zhou, V. T. Tchernev, J. Christiansen, M. Velleca, S. F. Kingsmore, *Nat. Biotechnol.* **2002**, 20, 359-365.

[15] Y. Chen, M. R. Shortreed, D. Peelen, M. Lu, L. Smith, *J. Am. Chem. Soc.* **2004**, 126, 3016-3017.

[16] E. J. Cho, L. Yang, M. Levy, A. D. Ellington, *J. Am. Chem. Soc.* **2005**, 127, 2022-2023.

[17] S. Beyer, P. Nickels, F. C. Simmel, *Nano lett.* **2005**, 5, 719-722.

[18] Z. Deng, Y. Tian, S. Lee, A. E. Ribbe, C. Mao, *Angew. Chem. Int. Ed.* **2005**, 44, 3582-3585.

[19] L. M. Demers, C. A. Mirkin, R. C. Mucic, R. A. Reynolds, R. L. Letsinger, R. Elghanian, G. Viswanadham, *Anal. Chem.* **2000**, 72, 5535-5541.

[20] J. Pyun, T. Kowalewski, K. Matyjaszewski, *Macromol. Rapid Commun.* **2003**, 24, 1043-1059.

[21] L. P. Billen, Y. Li, *Bioorg. Chem.* **2004**, 33, 582-598.

Chapter 8: Conclusions

This thesis research has exploited the use of AuNP/DNA conjugates towards 1) stimuli-responsive nanoassembly and well-controlled 3D nanoassembly, and 2) facile biosensing assays for monitoring DNA functions and relevant biological processes.

As summarized in Figure 8.1, we are able to guide the assembly of AuNPs by species ranging from small charged molecules (nucleotides), to oligonucleotides, and to very long DNA molecules. Specifically, we investigated how surface charges, DNA polymer length and conformations on AuNP surfaces affect AuNP colloidal stability and aggregation. The improved understanding of such factors enables us to control gold nanoparticle assembly by tuning interparticle forces including van der Waals, electrostatic, steric and electrosteric forces. The incorporation of functional DNA (e.g., aptamers and enzymes) that recognize a specific target allows the assembly to be responsive to a certain stimulus. Meanwhile, the distinct colors at different AuNP assembled stages allow us to readily monitor the DNA functions (i.e., DNA aptamer binding and folding, DNA enzyme catalysis) or relevant biological processes (i.e., protein enzymatic manipulation of DNA and nucleotides).

In chapter 2 and 3, the assembly of AuNPs is guided by small charged nucleotides: nucleotides bind to AuNP surface via nucleobase-Au interaction, and negatively charged phosphates stabilize AuNPs via electrostatic repulsion. Therefore, the colloidal stability of the resultant AuNPs attached with a certain type of nucleotide is dependent on 1) the binding affinity of nucleobase to AuNP surface, and 2) the number of phosphate groups carried by nucleotide. In other words, nucleotides with higher binding affinity to AuNP and/or with more phosphate groups provide higher degree of stabilization to AuNPs. This investigation allowed us to monitor protein enzymatic reactions where nucleotides are modified by alkaline phosphatase (chapter 2) and to control the growth of AuNPs using nucleotides as capping ligands (chapter 3).

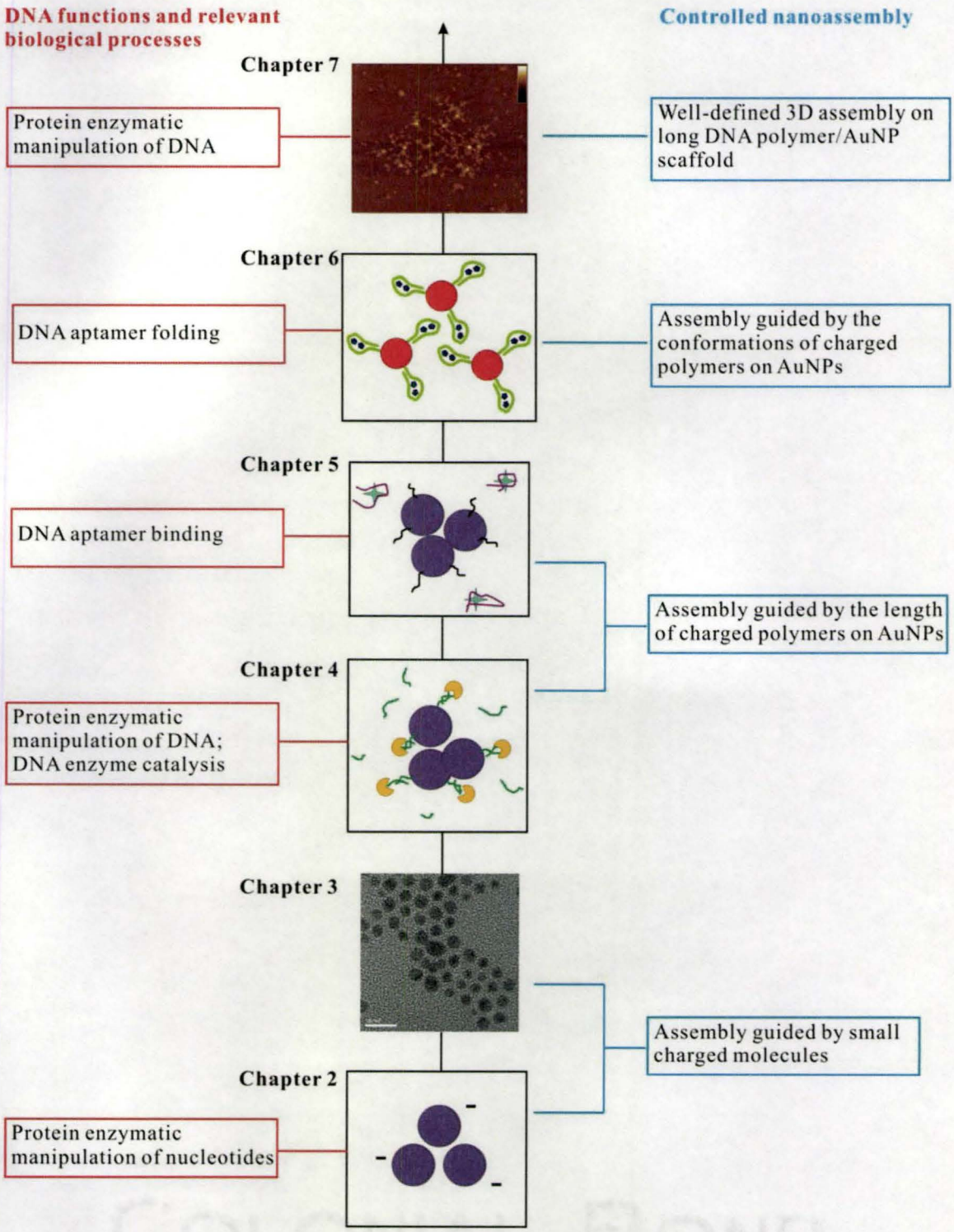

Figure 8.1. *Summary of this thesis work. See the main text for details.*

In chapter 4-6, we examined how surface-tethered DNA polymers affect AuNP colloidal stability and aggregation, and how that can be applied for monitoring DNA functions. We first investigated the DNA polymer length: DNA-modified AuNPs are stabilized electrosterically at a relatively high salt concentration; the remove (or shortening) the DNA molecules by enzymatic cleavage (chapter 4) or the dissociation of DNA aptamers from AuNP surface upon binding to their target (chapter 5) destabilizes AuNPs and results in AuNP aggregation. This can be simply attributed to the loss of negatively-charged polymeric DNA molecules that initially served as colloidal stabilizers.

In chapter 6, we studied how DNA polymer conformational changes influence AuNP colloidal stability. We discovered that AuNPs to which folded aptamer/target complexes are attached are more stable towards salt induced aggregation than those tethered to unfolded aptamers. While the precise mechanism remains largely unknown, it was proposed that the folded aptamers were more extended on the surface than the unfolded (but largely collapsed) aptamers in salt solution. The folded aptamers therefore provide higher stabilization effect on AuNPs from both the electrostatic and steric stabilization points of view.

In Chapter 7, long (typically hundreds of nanometers to microns) ssDNA molecules containing repeating units are generated by protein enzymatic reaction (DNA extension through rolling circle amplification) on AuNP surface. The resultant product provides a 3D-like scaffold that can be subsequently used for periodical assembly of complementary DNA-attached nanospecies. Moreover, the distance between assembled nanospecies can be readily varied by adjusting the length of the circular DNA template. Importantly, this controllable assembly strategy may provide a means to study the physical properties (i.e., interparticle plasmon coupling) of well-organized structures as the position of each individual AuNPs can be well-defined.

This thesis work has largely expanded the use of the "non-crosslinking aggregation" mechanism for the design of AuNP-based colorimetric biosensing assays. As illustrated throughout the thesis, the AuNP aggregation in these assays does not involve any interparticle biorecognition ("inter-particle crosslinking aggregation").

Rather, the AuNP stability and aggregation are modulated by colloidal parameters such as surface charge, the length and conformation of surface-tethered polymers. Meanwhile, we also hope that the new discoveries in this thesis work, particularly the effect of polymer conformations on the colloidal properties, would complement the traditional theories in colloidal and polymer chemistry.

We also expect the general strategies of control colloidal aggregation/dispersion discussed in this thesis can be applied in other AuNP-based sensing platforms, for example, plasmonic light scattering[1] and surface enhanced Raman scattering[2] that exploit interparticle interactions. It is hoped that these principles can facilitate research in nanoassembly fields, such as for the construction of well-defined nanostructures by assembling AuNPs or other types of nano-scaled materials (e.g., quantum dots, nanotubes, nanowires, etc.).

Finally, the colorimetric biosensing assays developed in this thesis work also provide an attractive platform to study biomolecular behaviour (e.g., biorecognition and conformational changes) on the surface, and also to investigate other common DNA (or RNA) structures (e.g., triplex, G-quadruplex, hairpin, i-motif) and protein structures.[3,4] Therefore, these facile biosensing platforms would not only facilitate our understanding of the biological functions of these biomolecules, but also provide guidance in the development of better surface-based biosensing devices (e.g., microarray and nanoparticles).

References

(1) K. Aslan, J. R. Lakowicz, C. D. Geddes. *Curr. Opin. Chem. Biol.* **2005**, 9, 538-544.

(2) R. F. Aroca, R. A. Alvarez-Puebla, N. Pieczonka, S. Sanchez-Cortez, J. V. Garcia-Ramos. *Adv. Colloid. Interface. Sci.* **2005**, 116, 45-61;

(3) S. Chah, M. R. Hammond, R. Zare, *Chem. Bio.* **2005**, 12, 323-328.

(4) D. Murphy, R. Eritja, G. Redmond, *Nucl. Aci. Res* , **2004**, 32, e65.

Appendix: Ph.D. publication list

Journal publications

(1) **Weian Zhao**, M. Monsur Ali, Sergio D. Aguirre, Michael A. Brook* and Yingfu Li*. Paper-based Bioassays Using Gold Nanoparticle Colorimetric Probes. *Anal. Chem.* **2008**, submitted.
(2) **Weian Zhao**, Michael A. Brook* and Yingfu Li*. Design of gold nanoparticle-based colorimetric biosensing assays. *ChemBioChem.* **2008**, in press.
(3) **Weian Zhao**, M. Monsur Ali, Michael A. Brook* and Yingfu Li*. Rolling circle amplification: new applications in nanotechnology and functional nucleic acid-based biodection. *Angew. Chem. Int. Ed.*, **2008**, 47, 6330.
(4) **Weian Zhao**, Jeffrey C. F. Lam, William Chiuman, Michael A. Brook,* Yingfu Li.* Enzymatic cleavage of nucleic acid on gold nanoparticle: a generic platform for facile biosensors. *Small*, **2008**, 4, 810.
(5) **Weian Zhao**, William Chiuman, Jeffrey C. F. Lam, Simon A. McManus, Wei Chen, Yuguo Cui, Michael A. Brook,* Yingfu Li.* DNA aptamer folding on gold nanoparticle: from colloid chemistry to biosensors. *J. Am. Chem. Soc.*, **2008**, 130, 3610.
(6) **Weian Zhao**, William Chiuman, Michael A. Brook,* Yingfu Li.* Simple and rapid colorimetric biosensors based on DNA aptamer and non-crosslinking gold nanoparticle aggregation. *ChemBioChem*, **2007**, 8, 727.
(7) **Weian Zhao**, Ferdinand Gonzaga, Yingfu Li,* Michael A. Brook.* Highly stabilized nucleotide-capped small gold nanoparticles with tunable size. *Adv. Mater.* **2007**, 19, 1766.
(8) **Weian Zhao**, William Chiuman, Jeffrey Lam, Michael A. Brook,* Yingfu Li.* Simple and rapid colorimetric enzyme sensing assays using non-crosslinking gold nanoparticle aggregation. *Chem. Commun.*, **2007**, 3729.
(9) **Weian Zhao**, Yan Gao, Michael A. Brook,* Yingfu Li.* Wrapping single-walled carbon nanotubes with long single-stranded DNA molecules produced by rolling circle amplification. *Chem. Commun.*, **2006**, 3582.
(10) **Weian Zhao**, Yan Gao, Srinivas A. Kandadai, Michael A. Brook,* Yingfu Li.* DNA polymerization on gold nanoparticles through rolling circle amplification: towards novel scaffolds for three-dimensional periodic nanoassemblies. *Angew. Chem. Int. Ed.*, **2006**, 45, 2409.

Presentations

(1) **Weian Zhao**, M. Monsur Ali, Sergio D. Aguirre, Michael A. Brook*, and Yingfu Li.* Biodetection kits using gold nanoparticle-coated paper. McMaster Innovation Showcase, Hamilton, Canada. June 5-6, **2008**. (poster presentation)
(2) **Weian Zhao**, M. Monsur Ali, Sergio D. Aguirre, Michael A. Brook*, and Yingfu Li.* Paper-based bioassays using gold nanoparticle colorimetric probes. Bioactive Paper Conference, Espoo, Finland, June 24-26, **2008**. (oral presentation)

(3) **Weian Zhao**, M. Monsur Ali, Sergio D. Aguirre, Michael A. Brook*, and Yingfu Li.* Paper-based bioassays using gold nanoparticle colorimetric probes. Sentinel: Bioactive paper network, Orangeville, Ontario, Canada, May 5-8, **2008**. (oral presentation)
(4) **Weian Zhao**, Jeffrey Lam, William Chiuman, Michael A. Brook*, Yingfu Li.* A generic colorimetric biosensing assay using surface charge-mediated gold nanoparticle aggregation. MRS (Materials Research Society) fall meeting, Boston, Nov 26-30, **2007**. (oral presentation)
(5) M. Monsur Ali, **Weian Zhao**, Yingfu Li.* Paper-based colorimetric assays. Sentinel Bioactive Paper Network, Edmonton, Nov 1 – 4, **2007.** (poster presentation)
(6) **Weian Zhao**, Jeffrey Lam, William Chiuman, Michael A. Brook*, Yingfu Li.* A generic colorimetric biosensing assay using surface charge-mediated gold nanoparticle aggregation. BioContact 2007, Québec City, Oct 3-5, **2007**. (poster presentation).
(7) M. Monsur Ali, **Weian Zhao**, Shunxing Su, Carlos Filipe, Ebano Ambrosio, Robert Pelton, Yingfu Li.* Detection of target analyte using allosteric deoxyribozyme along with rolling circle amplification: towards development of bioactive paper. Sentinel Bioactive Paper Network, Ottawa, May 22 – 25, **2007**. (poster presentation)
(8) **Weian Zhao**, Yingfu Li, Michael A Brook*, Yan Gao, Srinivas A Kandadai. DNA-gold nanoparticle scaffold for three-dimensional periodic nanoassemblies. MRS (Materials Research Society) Fall Meeting, Boston, MA, Nov 26-Dec 2, **2006**. (oral presentation)
(9) **Weian Zhao**, Yan Gao, Srinivas A. Kandadai, Michael A. Brook,* and Yingfu Li*. DNA polymerization on gold nanoparticles through rolling circle amplification: towards novel scaffolds for three-dimensional periodic nanoassemblies. 89th Canadian Chemistry Conference and Exhibition (CSC), Halifax, May 27-31, **2006**. (oral presentation)
(10) **Weian Zhao**, Elodie Pacard, Carole Chaix, Christian Pichot, Michael A. Brook.* Surface functionalization of silica nanoparticles for direct synthesis of DNA capture oligomers. ACS Central Regional Meeting and 39th Silicon Symposium, Frankenmuth, Michigan, May 16-21, **2006**. (oral presentation)
(11) **Weian Zhao**, Elodie Pacard, Carole Chaix, Christian Pichot and Michael A. Brook*, Controlled silica nanoparticle aggregates for oligonucleotide synthesis, 38th Silicon Symposium, Boulder, Colorado, June **2005**. (poster presentation)
(12) Michael A. Brook, Yang Chen, Ferdinand Gonzaga, Paul Zelisko, Sanela Martic, Amro Ragheb and **Weian Zhao**. NanoChemistry at the interface, Ontario Nano Symposium, **2004**. (poster presentation)

Patents

Stabilized gold nanoparticles and methods of making and using the same. Michael A. Brook, Yingfu Li, **Weian Zhao**, M. Monsur Ali, Sergio D. Aguirre, William Chiuman, Ferdinand Gonzaga. patent application PCT CA2008/000611.

Book Chapters

(1) **Weian Zhao**, Michael A. Brook and Yingfu Li. (invited) Protocols in Nanostructure Design. the Methods in Molecular Biology series by Humana Press. **2008**, in press.